Alterations in Keratin Levels and Modifications in Colorectal Adenomagenesis

Ria Rosser

January 2016

Supervisors: BM Corfe and KS Chapple
Department of Oncology

Thesis submitted to the University of Sheffield for the degree of Doctor of Medicine

Alterations in Keratin Levels and Modifications in Colorectal Adenomagenesis

Table of Contents

Abstract

A cancerized field is an area of abnormal tissue in the vicinity of a cancer but appearing to be macroscopically normal. Identification of these has important clinical implications as abnormal tissues could be left *in situ* following polypectomy or surgical resection, leading to neoplastic recurrence in the same area. Up to 60% of patients develop metachronous adenomas following adenoma excision, the observed high rate of metachronous adenoma formation could be due to field changes analogous to cancerized fields around an adenoma. Keratins are important regulators of colonocyte physiology and their regulatory role is, in part, influenced by post-translational modifications and butyrate exposure. Butyrate has been shown to have a protective effect in the colon to prevent colorectal carcinoma. Alterations in keratin levels have been shown between the cancerized field and normal tissue. The investigation of keratins as a marker for a cancerized field and how they are influenced by butyrate may provide clues in the prevention of and treatment of adenomagenesis and the early stages of carcinogenesis.

This thesis examines the involvement of keratins in adenoma fields and their response to butyrate exposure; the available evidence for these associations is reviewed.

Acknowledgments

I would like to thank every body that has helped and supported me during the research period and the writing of this thesis.

Firstly, I would like to thank my supervisors Dr Bernard Corfe, Mr Keith Chapple and Dr Caroline Evans for their time, patience and invaluable guidance throughout the whole process. I have been very fortunate to work with these incredible people.

Secondly, I would like to thank my colleagues in the laboratory for sharing their expertise, reagents and workspace. I would particularly like to thank Dr Debabrata Majumdar and Miss Joey Chowdry.

Lastly, I would not have been able to complete this research project without the support of my family. Thank you.

List of Figures

List of Tables

Abbreviations

2-D DIGE	Two-dimensional differential gel electrophoresis
ACF	Aberrant crypt foci
AD	Adenoma
APC	Adenomatous polyposis coli
BSA	Bovine serum albumin
CEA	Carcinoembryonic antigen
CO	Contralateral
Colonic segments:	
C	Caecum
A	Ascending colon
HF	Hepatic flexure
T	Transverse
SF	Splenic flexure
D	Descending colon
S	Sigmoid
RSJ	Rectosigmoid junction
R	Rectum
CPG	Cytosine and guanine joined by phosphodiester bond
DNA	Deoxyribonucleic acid
EDTA	Ethylenediaminetetraacetic acid
EMR	Endoscopic mucosal resection
ESD	Endoscopic submucosal dissection
FAP	Familial adenomatous polyposis
Gal-GalNAc	D galactose-beta-[1-->3]-N-acetyl-D-galactosamine
GuHCl	Guanidine hydrochloride
HAD	High butyrate adenoma
HCO	High butyrate contralateral
HDACS	Histone deacetylases
HDB	High detergent buffer
HMS	High butyrate mid-sigmoid
HN	High butyrate normal
HNPCC	Hereditary non-polyposis colorectal cancer
HPLC	High performance liquid chromatography
ICAT	Isotope coded affinity tag
IF	Intermediate filaments/intermediate sized filaments
IHC	Immunohistochemistry
iTRAQ	Isobaric tags for relative and absolute quantitation
K18	Keratin 18
K19	Keratin 19
K8	Keratin 8
KRAS	Kirsten Ras oncogene
LAD	Low butyrate adenoma
LC-MS/MS	Liquid chromatography coupled with tandem mass spectrometry
LCO	Low butyrate contralateral
LDB	Low detergent buffer

LMS	Low butyrate mid-sigmoid
LN	Low butyrate normal
MGMT	O^6-methylguanine-DNA methyltransferase
MMTS	Methyl methanethiosulfonate
MS	Mid-sigmoid
NRP-1	Neuropilin-1
PBS	Phosphate buffered saline
PK	Proteinase K
PKC	Protein kinase C
PS23	Phosphorylation at serine residue 23
PS431	Phosphorylation at serine residue 431
PS73	Phosphorylation at serine residue 73
PTM	Post-translational modification
R0	Index colonoscopy
R1	Repeat colonoscopy 1
R2	Repeat colonoscopy 2
R3	Repeat colonoscopy 3
R4	Repeat colonoscopy 4
R5	Repeat colonoscopy 5
SC	Sodium citrate
SCFA	Short chain fatty acid
SCX	Strong cation exchange
SD	Standard deviation
SFRP	Secreted frizzled-related proteins
SILAC	Stable isotope labelling by amino acids in cell culture
SOP	Standard operating procedure
SNOMED	Systematized Nomenclature of Medicine
STH	Sheffield Teaching Hospitals
SUMO	Small ubiquitin-like modifier
TBS	Tris buffered saline
TBST	Tris buffered saline with tween
TCEP	Tris-(2-carboxyethyl)phosphine
TEAB	Triethylammonium bicarbonate buffer
TNF	Tumour necrosis factor
VEGF	Vascular endothelial growth factor
WHO	World health organisation

Chapter 1

Literature Review

Chapter 1 Literature review

This literature review defines the pathogenesis of colorectal adenomas as a precursor to colorectal cancer and describes the current evidence for field cancerization. This thesis examines the involvement of keratins in adenoma fields and their response to butyrate exposure; the available evidence for these associations is reviewed.

1.1 The History of Adenomatous polyps

Adenomatous polyps are benign tumours widely recognised as the precursor to colorectal cancer (Neugut et al. 1993), evidenced by pathological, clinical and epidemiological observations. Synchronous (two or more tumours occurring at the same time) adenomatous polyps are found in 27% of colorectal cancer resection specimens (Carlsson et al., 1987). Removal of adenomas is associated with a lowered risk of colorectal cancer (Winawer et al., 1993). Familial adenomatous polyposis (FAP) is an inherited disorder of the bowel characterised by hundreds of adenomatous colorectal polyps. The lifetime risk of developing colon cancer in patients with FAP, without intervention is 100% (Hampel and Peltomaki, 2000). For these reasons treatment of adenomas and halting their progression are important approaches in the prevention of colorectal cancer. Despite treatment, patients have a high chance of forming further adenomas, even after removal. Adenomas that form at two different time points in the same patient are termed metachronous adenomas. Current data shows up to 59% of patients develop metachronous adenomatous polyps following removal of a previous polyp (Nava et al., 1987) compared to 16% of patients with no abnormality at index colonoscopy (Neugut et al., 1995). The metachronous incidence rate suggests the presence of one adenoma can influence the formation of another. This theory is supported by numerous studies indicating the multiplicity of adenomas at baseline examination to be a powerful predictor of recurrence (Martinez et al., 2001, Bonithon-Kopp et al., 2004, Noshirwani et al., 2000). Adenoma size greater than 1cm is also a strong predictor of both recurrence (Winawer et al., 1993b) and malignant potential (Otchy et al., 1996).

Other studies have highlighted higher metachronous rates where index adenomas were proximally located within the colon (Martinez et al., 2001, Bonithon-Kopp et al., 2004). The authors (Martinez et al., 2001, Bonithon-Kopp et al., 2004) define the proximal colon as transverse colon up to the caecum and the distal colon as from the rectum to the splenic flexure.

1.1.1 Origins of the Adenoma

Lining the human colon is a sheet of columnar epithelial cells, periodically invaginating to form crypts. There are millions of crypts within the colon and within those crypts are stem cells, capable of regenerating all intestinal cell types (Humphries and Wright, 2008). Differentiated cells produced by the stem cell migrate towards the surface of the crypt and are shed into the lumen. The rapid replacement of colonic epithelium means differentiating cells are replenished every few days and do not have time to accumulate the multiple genetic defects required for malignant transformation during their short lifespan. Therefore, only mutations acquired within the stem cell population would be maintained (Cairns, 1975). A stem cell that has acquired a mutation can establish a monocryptal clone via niche succession; the mechanisms by which this is achieved have been outlined by Leedham and Wright (Leedham and Wright, 2008). Crypts composed of mutated cells expand by crypt fission (Greaves et al., 2006) may lead to a patch of monoclonal related mutated crypts within the epithelium (a cancerized field) (Figure 1).

1.1.1 Origins of the adenoma

Crypt fission
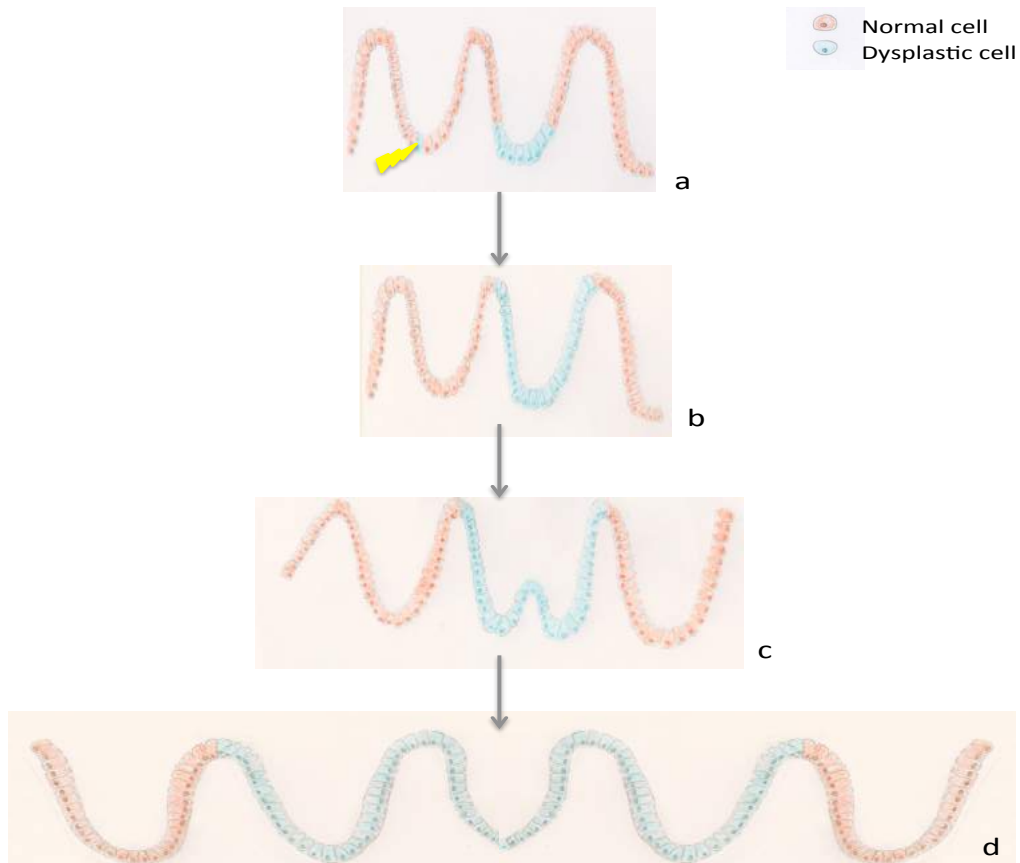
Figure 1. Formation of monoclonal crypts.

A monoclonal field is formed when a stem cell acquires a mutation (yellow arrow) (a), dysplastic cells then colonise a crypt (b). Once the crypt has been replaced by dysplastic cells the crypt undergoes crypt fission to form two monoclonal crypts (c). The fission pattern continues to produce many monoclonal crypts surrounded by normal cells (d).

1.1.1 Origins of the adenoma

If a whole crypt is colonised by dysplastic cells, the earliest detectable precursor lesion of tumour: a monocryptal adenoma, is seen (Nakamura and Kino, 1984). Monocryptal adenomas can only be seen on histological examination, where the adenoma cells of the crypt are seen to be different to normal cells. The manner in which a monocryptal adenoma develops is a controversial subject. Two mechanisms have been proposed:

1. where dysplastic cells spill over the top of the crypt and colonise adjacent crypts (the top-down theory) (Shih et al., 2001) (Figure 2)
2. fission of monocryptal adenomas (the bottom-up theory) to form a field (Preston et al., 2003). (Figures 1 and 3)
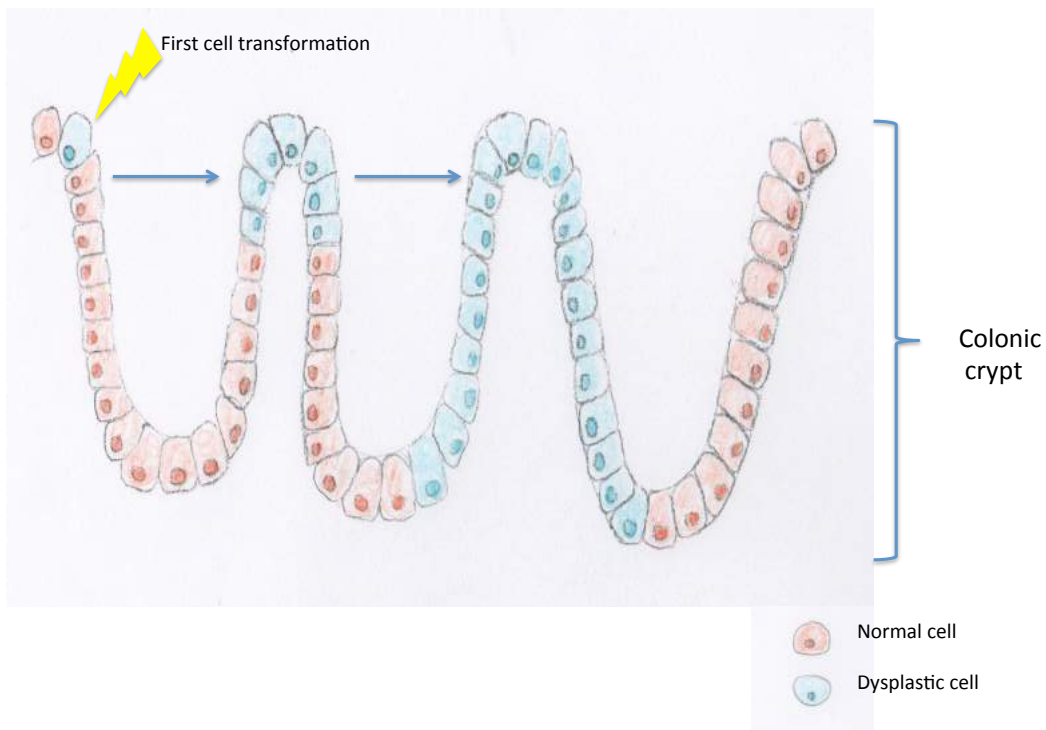
Figure 2. 'Top-down' theory for crypt colonisation.

A normal cell becomes dysplastic (yellow arrow) and colonises the crypt from a 'top-down' fashion.

1.1.1 Origins of the adenoma

Bottom up theory
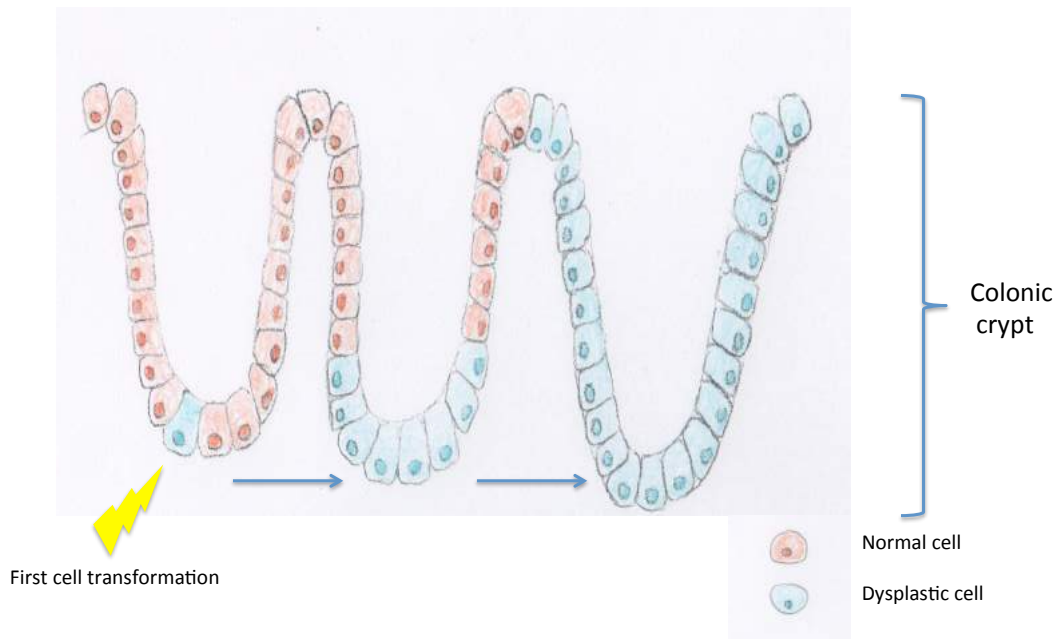
Figure 3. 'Bottom-up' theory for crypt colonisation.

A stem cell becomes dysplastic (yellow arrow) the mutation is maintained and colonises the crypt from the 'bottom-up'.

An expanding lesion of dysplastic crypts (by either of the two mechanisms described above) requires interaction with a second lesion of dysplastic crypts to form a macroscopic polyclonal adenoma.

1.1.2 Adenoma-Carcinogenesis model

A genetic model for the progression of cancer from adenomatous polyps was proposed in 1988 (Vogelstein et al., 1988).
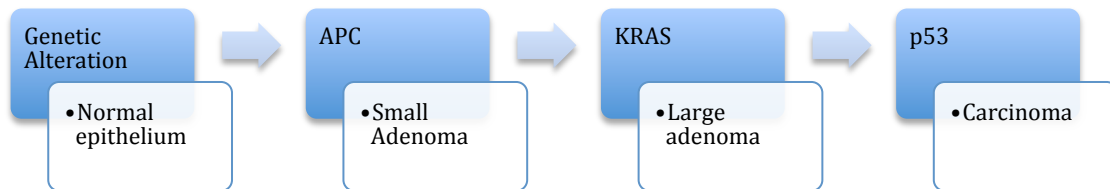
Figure 4. **Genetic Carcinogenesis Model**

Adenomatous polyposis coli (*APC*) mutation is an early event in colorectal adenomagenesis, sufficient for colorectal adenomas to grow to 1cm in diameter (Lamlum et al., 2000). In the absence of functional *APC*, beta catenin (an oncoprotein) accumulates and WNT signalling is inappropriately activated. Aberrant WNT pathway signalling is an early progression event in the development of 90% of colorectal cancers (Fodde et al., 2001). It has been proposed that Kirsten Ras (KRAS) oncogene mutation, next in the sequence, occurs in one cell of the small adenoma and through clonal expansion produces a larger and more dysplastic tumour. Subsequent genetic alterations produce advancing dysplasia until carcinoma formation (Fearon and Vogelstein, 1990). Although a series of sequential genetic changes has been suggested, the authors recognise that the specific order of genetic changes may not be important in tumour progression. For these reasons it has been argued that the multistep model is flawed, as the progression-related genetic changes are inconsistent (Feinberg et al., 2006). Feinburg et al., (2006) also highlight that many studies have linked specific changes in gene expression but with no underlying mutation to account for the expression of changes.

The multistep carcinogenesis model does not address the latency of tumour progression. The prevalence of adenomatous polyps at 50 years of age is 30%

increasing to 50% and 65% at 60 years and 70 years respectively (Bond, 2000). If it takes decades to acquire a mutation to form a benign adenoma then it would be reasonable to assume it would take just as long to acquire the next genetic mutation to continue the sequence. This assumption is based on the observation that rate of point mutation does not seem to be increased in colorectal cancer in comparison to normal tissue (Wang et al., 2002).

It is increasingly clear that genetic alterations are not the only mechanism by which adenomas arise. The advancement in molecular technologies, more recently, has explored the concept of field effect through identification of molecular abnormalities in tissues that appear histologically normal. Due to these developments, alternative pathways to neoplasia that include molecular abnormalities and modified epigenetic changes have been hypothesized (Polley et al., 2006). Identification of such molecular differences is important since they give insight into the early stages of carcinogenesis and may act as a biomarker for early cancer detection and thus prevention.

1.2 Field effects – Theory and Definitions

A field is defined as an area of macroscopically normal tissue, which precedes and predisposes to the development of a cancer (Bernstein et al., 2008). A field effect is the persistence of an abnormal field following resection of a cancerous lesion. Since the field effects concept was introduced in 1953 its interpretation has evolved into the growth of a mutant clone to produce a field of cells predisposed to subsequent tumour growth (Braakhuis et al., 2003). More recently, a modification of the definition has been proposed ' a preconditioning of an area of epithelium to tumour growth either as a result of a clonal proliferation or because of consistent changes to cells in the stromal compartment' (Graham et al., 2011). What remains consistent is that the histological appearance of the pre-neoplastic field may be normal, hyperplastic or dysplastic.

Field effects have important clinical implications as:

i. they give insight into the early stages of cancer progression

ii. these fields may remain, following surgical resection of the primary tumour, giving rise to second primary tumours or local recurrence.

Recently, proteomic techniques have demonstrated that morphologically normal tissues around colorectal cancers and adenomas have acquired molecular abnormalities, particularly in keratin expression (Polley et al., 2006). The histologically normal looking tissue surrounding pathological tissue has been termed field cancerization, field defect or field effect by different research groups.

The study of cancer field effects is well established in head and neck cancer (Braakhuis et al., 2003). Other organ systems that have been studied include oesophagus, stomach, lung, skin, bladder and colon. These organs all contain epithelial cells whose physiological role is to protect that organ from environmental insult. It is thought exposure of carcinogens to these mucosal

membranes causes damage to epithelial cells which proliferate to form a field of genetically altered cells (Dakubo et al., 2007).

1.2.1 Difficulties in Investigating Field Effect changes in Colorectal Cancer

Colorectal cancer is the third most common cancer in the United Kingdom with 35000 new cases diagnosed each year (Cairns et al., 2010). The capability to detect potential cancer risk and prevent progression would be very valuable in this prevalent disease. Despite its frequency, there is a paucity of information in field effects surrounding colorectal cancer in relation to other organ systems. There are a number of reasons for this observation. Field effects were first reported in head and neck cancer and have therefore undergone a longer period of recognition and investigation. It is well known that wide resection of rectal cancers is required to reduce local recurrence rates (Enker et al., 1979). It is possible that routine wide excisions of colorectal cancers have also removed the 'field' and thus a lower local recurrence rate is seen. Anatomical restrictions in head and neck cancers prevent radical resections and thus pre-neoplastic fields can be left behind.

Other organs that have received more attention in field effect investigation include the oropharynx and oesophagus. A possible explanation of this is the recognition of their specific carcinogens and site of exposure. Betel nut chewing can lead to oral cancer presenting as an ulceroproliferative area. The site of cancer and surrounding field can be easily recognised. A similar explanation applies to the oesophagus where acid reflux and Barrett's metaplasia can be easily identified and investigated. Within the colon inherent difficulties exist that hamper the investigation of field effects. There is no specific carcinogen exposure site and the marker of mucosal change (adenomatous polyps) do not always progress to cancer. It has been estimated that 90% of adenomas do not progress to become cancerous (Levine and Ahnen, 2006). Current guidance is that all polyps should be removed unless obviously non- neoplastic and only polyps that are greater than 1cm in size should be tattooed if they are unable to be removed endoscopically (Zafar et al., 2012). As most polyps (potential

adenomas) are removed during incident colonoscopy revisiting the field becomes impossible unless the area was tattooed. The tortuosity and length of the colon coupled with variation in anatomy makes it difficult for the endoscopist to know the exact location of the endoscope, which adds to the difficulty in revisiting the field.

The field effect theory should only be investigated in the absence of known germline mutations otherwise all the tissues of that individual would be regarded as the predisposed field. In colorectal cancer there are several known hereditary syndromes, the two commonest being familial adenomatous polyposis (FAP) which makes up 1% of colorectal cancer presentations (Kinzler and Vogelstein, 1996) and hereditary non-polyposis colorectal cancer (HNPCC) which makes up 6% (Vasen et al., 1991). Due to these reasons, more focus has been placed on the hereditability of colorectal cancer and known genetic mutations rather than the molecular differences that have recently been discovered. The acquisition of such genetic changes, however, may be late changes in the disease process, which will be missed when studying the precancerous field.

Another reason for slow progression in colon cancer field investigation is that many studies have been comparing cancer tissue and using the surrounding normal looking tissue as a control, assuming that is has no changes. As a result, those studies have been unable to compare differences and draw conclusions from them.

1.2.2 Colorectal Field Effects and Clinical Applications

The current treatment for adenomatous polyps is endoscopic removal via colonoscopy. The recommendation for this comes from epidemiological observations that most colonic cancers are preceded by premalignant adenomatous polyps, therefore colonoscopic detection and polypectomy provides an opportunity for cancer prevention (Atkin et al., 2002). However up to 60% of patients develop new adenomas (metachronous occurrence) after

polyp removal. It is unknown why metachronous adenomas occur but development of further adenomas after polypectomy suggests a field, from which they arise, may have been left behind. Addressing a polyp without treating a field may be inadequate in cancer prevention.

There is a paucity of literature regarding field effects around colorectal polyps and cancer. This may be due to the existence and wide acceptance of a known model for colorectal carcinogenesis and heavy reliance on identification of genetic mutations. However the changes of field effects may be more subtle than the theories investigated so far.

It is also unknown where metachronous adenomas occur in the colon, in relation to a previously removed adenoma. This is, however, an important area of investigation since identification of locations of metachronous occurrences could help define how and why adenomas arise. If metachronous adenomas are found to appear in the same location this would strongly support the theory that pre-neoplastic fields are left behind following polypectomy.

The national polyp study found a 70-90% reduction in expected incidence of colorectal cancer in patients undergoing colonoscopy surveillance than a reference population (Winawer et al., 1993a). This study provides evidence that continued surveillance in patients who have had adenomas previously removed is necessary. However, colonoscopy and polypectomy is not without risk with up to 2.7% reported risk of major haemorrhage (Atkin et al., 2002). Other problems associated with colonoscopy include patient discomfort, bowel preparation and the potential of missed polyps. There are also financial implications for continued surveillance, together with inconvenience and continued invasive risk to the patient.

The study and identification of field effects can potentially prevent the need for colonoscopy and its associated complications. If field effects around adenomas are identified then continued colonoscopies and polypectomies alone may not prevent the long term risk of cancer. This is especially important in the case of

large adenomas where many are removed by endoscopic mucosal resection (EMR) and more recently endoscopic submucosal dissection (ESD). EMR and ESD carry risks of perforation (1.3%, 4.9%) (Holt and Bourke, 2012) and bleeding (9.5%, 7%) (Basford et al., 2014) respectively. The reported risk of recurrence for EMR is (15.4%) and for ESD (1.2%) (Tajika et al., 2011), therefore adenomas surrounded by field defects may require wider colonic resection to prevent recurrence and subsequent cancer. The authors conclude that strict colonic surveillance is required to manage recurrence after EMR. This approach confers large financial and time implications not to mention risk to the patient and a risk of missed polyps. Identification of field effects can allow diagnosis and follow up to be tailored to a patient's clinical and pathological need. Identified fields may have to undergo careful examination or radical resection. Despite adequate histological clearance margins the remaining field tissue has an increased risk of developing multiple independent (synchronous or metachronous) cancers.

Understanding field effects is an important approach to cancer treatment. Our current practice may be inadequate in the treatment and prevention of cancer if precancerous fields are left behind. Research into whether fields exist and how they are formed could allow the prevention of cancer in the earliest stages.

1.3 Evidence for field cancerization

The concept of field effects and cancerization has been investigated in many approaches; current studies involving epigenetics, protein events, clonality studies and adenoma progression will be covered in this section.

1.3.1 Epigenetic evidence

Epigenetic inheritance is defined as cellular information, other than the DNA sequence itself, that is heritable during cell division (Feinberg and Tycko, 2004). Pathological epigenetic changes can lead to aberrant activation of growth-promoting genes and aberrant silencing of tumour suppressor genes (Feinberg and Tycko, 2004). Feinburg and Vogelstein (1983) report global epigenetic changes preceding the initial mutations in cancer. DNA methylation (a recognised type of epigenetic alteration implicated in gene disruption) is observed to be altered in a range of tumours examined (Feinberg and Vogelstein, 1983). Feinberg et al., (2006) later proposed these hypomethylation changes must precede the earliest genetic alterations as they are always found, even in benign neoplasms (Feinberg et al., 2006). Unlike genetic changes such as mutations and chromosomal rearrangements, epigenetic changes are reversible. Previous research efforts have been based on DNA sequencing which will miss important epigenetic changes. Examination of the epigenome at a molecular level has identified similar properties between apparently normal field tissue and pathological tissue.

1.3.1.1 DNA methylation studies

Ahuja et al., (1998) studied the association between aging and DNA methylation of promoter associated CpG islands. CpG islands are genomic regions rich in dinucleotides (**C**ytosine and **G**uanine joined by a **p**hosphodiester bond) (Ahuja et al., 1998). Earlier work by the same group identified hypermethylation in promoter CpG islands in all colonic neoplasms that were studied (Issa et al.,

1994). The authors found significant similarities in N33 gene methylation intensity between field and cancer tissue in comparison to normal tissue from disease free patients. Macroscopically normal field tissue and cancer tissue had significantly higher N33 methylation intensities than tissue from patients with no colorectal cancer (Ahuja et al., 1998).

The DNA repair gene O^6-methylguanine-DNA methyltransferase (MGMT) is frequently methylated in colorectal cancer (Shen et al., 2005). Shen et al., (2005) found similar MGMT promoter methylation patterns in cancer tissue and morphologically normal cancer adjacent tissue when compared to normal tissue. Furthermore, the degree of methylation in cancer adjacent tissue was proportional to the proximity to the cancer and was not associated with any tumour DNA or the paired normal mucosa (Shen et al., 2005).

1.3.1.2 Epigenetic inactivation of secreted frizzled-related proteins (SFRP)

Secreted frizzled-related proteins (SFRPs) can inhibit WNT receptor binding to prevent WNT pathway signalling (Finch et al., 1997). Aberrant WNT pathway signalling is an early progression event in the development of 90% of colorectal cancers (Fodde et al., 2001). SFRP expression is silenced when the genes that encode for them are hypermethylated. To link these findings Suzuki et al., (2004) studied the consequences of epigenetic inactivation of SFRP genes (Suzuki et al., 2004). Using HCT116 colorectal cancer cell lines in which the DNA methyltransferase genes are disrupted and the silencing of SFRPs reversed, the authors found no methylation in the peripheral blood lymphocytes and normal colon tissue of healthy individuals but in individuals with colorectal cancer found dense hypermethylation in both tumour tissue and apparently normal mucosa from the same patients. The same authors also reported SFRP methylation in 11 out of 15 samples in abberrant crypt foci (ACF), an early mucosal change which usually lack APC mutations, thus emphasizing the presence of epigenetic changes in fields during very early carcinogenesis and demonstrating that it may often precede genetic changes.

1.3.2 Protein expression and early tissue events

Beyond the histological and molecular levels, fields around colorectal cancer have been found to express altered proteins when compared with non-pathological tissue and display more comparable tissue properties with cancer than normal and distant mucosa.

1.3.2.1 Expression of carcinoembryonic antigen (CEA)

Carcinoembryonic antigen (CEA) is a glycoprotein that is used as a serological tumour marker for colorectal cancer and is also found in colon cancer tissue extracts (Gold and Freedman, 1965). One study evaluated the use of CEA expression as a marker of field defect and to map its topography in relation to colorectal carcinoma (Jothy et al., 1996). Jothy et al., (1996) studied 14 patients with colorectal adenocarcinoma by sampling 5 biopsies from each patient: one of the carcinoma and then four other morphologically normal biopsies at increasing distances from the tumour (adjacent, 1cm, 5cm and 7-10cm). Using immunohistochemistry (IHC) to detect expression of CEA protein, the authors demonstrated statistically significant reduction of staining intensities at increasing distances from the tumour. These results demonstrate a field effect but do not answer why CEA is expressed at high levels around the field of the tumour.

1.3.2.2 Bcl-X_L anti-apoptotic protein expression

Bcl-X_L is an anti-apoptotic protein that inhibits apoptosis by blocking release of cytochrome c from mitochondria. Normally, the release of cytochrome c leads to the activation of caspases, which cause cell death through cleavage of DNA and cytoskeletal proteins. Since the survival of neoplastic cells depends on both cell proliferation and reduced cell death, the role of Bcl-X_L and any associated field change in apoptosis has been examined (Badvie et al., 2006). The authors used immunohistochemistry to identify Bcl-X_L staining intensity (measured as a

labelling index). Using colorectal specimens following surgical resection they took tissue samples from the cancer, 1cm proximal to the cancer and 10cm proximal to the cancer. Tissues from patients without cancer were used as controls. They noted proportional and significant increases in Bcl-X$_L$ labelling indices in mucosa situated at 1cm and 10cm away from the cancer compared to patients without cancer, suggesting that a field of characteristically similar tissue to cancer surrounds the cancer itself.

1.3.2.3 Altered mucin

Mucosa from adenoma and carcinoma tissue and their adjacent tissue have been found to secrete histochemically altered mucin in contrast to normal mucosa (Lanza et al., 1985, Filipe and Branfoot, 1974, Owen and Reid, 1995). It is unknown whether the altered mucin initiates adenoma formation as a result of the presence of neoplasia. It has been shown that D galactose-beta-[1-->3]-N-acetyl-D-galactosamine (Gal-GalNAc) is present in mucin obtained from neoplastic colon cells and normal colon cells within a colon harbouring neoplasia but not in normal cells of normal colons. (Xu et al., 1992). Vucenik et al., developed a test (GO-Schiff test) to detect Gal-GalNAc from mucin samples obtained via the rectum (Vucenik et al., 2001). The authors detected Gal-GalNAc in mucin from patients with cancer and no Gal-GalNAc in mucin from those without cancer with 100% sensitivity and 97% specificity. Interestingly, 60% of patients tested positive for Gal-GalNAc after tumour resection implying the persistence of a field effect after tumour removal.

1.3.2.4 Protein kinase C

Protein kinase C (PKC) is a mediator of trans-membrane signal transduction, with roles in cell growth and differentiation. McGarritty et al., (1994) found PKC activity was significantly greater in normal tissue adjacent to cancer and adenomas in comparison to normal colonic tissue from control patients without pathology. Although PKC activity was more similar between field tissue and

adenoma tissue than normal tissue, the authors noted a large variability in PKC activity thereby limiting its use as a marker for colorectal cancer (McGarrity and Peiffer, 1994).

1.3.2.5 Neuropilin-1 expression

Overexpression of the trans-membrane glycoprotein neuropilin-1 (NRP-1), a receptor for vascular endothelial growth factor (VEGF), is thought to enhance cancer cell survival (Parikh et al., 2004). Yu et al., (2011) found differences in NRP-1 expression between distant bowel mucosa and field mucosa of patients with adenoma (Yu et al., 2011). NRP-1 expression in mucosa distant to adenoma mucosa was inversely related to butyrate (a short chain fatty acid) concentration. In addition, NRP-1 levels decreased with increasing butyrate concentrations. NRP-1 expression in the field was lower and not related to butyrate concentrations. Adenoma samples showed similar lowered NRP-1 expression as the field but the correlation to butyrate became positive, with higher NRP-1 expression at higher butyrate concentrations. This study demonstrates a progressive field change in both NRP-1 expression and butyrate correlation with proximity to the adenoma.

1.3.2.6 Proteomic analysis

Differences in protein expression between tumour mucosa and normal neighbouring mucosa have been previously identified through two-dimensional differential gel electrophoresis (2-D DIGE) and mass spectrometry (MS) (Alfonso et al., 2005, Friedman et al., 2004). These studies were able to demonstrate that these techniques are able to identify tumour specific changes in the proteome between tumour and apparently normal tissues from the same individual i.e. the same genetic background. Polley et al., (2006) used these techniques to investigate differences in protein expression between the normal mucosa of neoplasia free patients and apparently normal field mucosa of those with neoplastic lesions. Changes in protein expression were identified through two

dimensional gel electrophoresis and mass spectrometry (Polley et al., 2006). The significance of their results were twofold: firstly, they found altered protein expression in the macroscopically normal field tissue around adenoma and cancer in comparison to macroscopically normal colon tissue from disease-free patients; secondly, among the 206 significantly altered proteins were keratins. Polley et al., (2006) found keratins (in particular several isoforms of keratin 8) were under-expressed in tumour tissue but overexpressed in the field tissue of adenoma and cancer patients when compared with tissue from healthy patients. Their study provides evidence to support the field effect theory and also suggests that keratins may be implicated in these field changes.

1.3.3 Clonality studies

The polyclonal structure of adenomas may be explained by the presence of field cancerization. Adenomatous polyps arise from monoclonal crypts but have polyclonal structures, composed of at least two somatic lineages (Novelli et al., 1996, Merritt et al., 1997a, Thirlwell et al., 2010). When Novelli et al. (1996) examined the intestinal mucosa of an XO/XY mosaic individual with familial adenomatous polyposis (FAP) they found the normal colonic crypts were composed exclusively of either XO cells or XY cells (and were therefore monoclonal) but at least 76% of the microadenomas in the same patient were composed of XO/XY mixed crypts and were thus polyclonal. Thirlwell et al. (2010) verified similar findings: all polyp tissue was demonstrated to be polyclonal in their FAP patients.

The mechanism of how clonal monocryptal adenomas become polyclonal adenomas is unknown. Two plausible explanations have been proposed:

  i.   Random collision (Novelli et al., 1996)
  ii. Crypt interaction (Thirlwell et al., 2010)

The random collision theory suggests that polyclonality results from chance, whereby two different neoplasms in close proximity overlap to form a mixed tumour. This was proposed as early experiments demonstrated polyclonality in colonic tumours from patients with high numbers of polyps such as FAP. A high density of polyps within a small area makes random collision theory conceivable as crypts expand into each other's spaces. Using models with lower tumour burden, Thliveris et al., (2005) also demonstrated polyclonality within crypts (Thliveris et al., 2005). However, mathematical models have suggested that random collision is an unlikely explanation.(Newton et al., 2006, Thirlwell et al., 2010).

Crypt interaction (where alterations in one crypt can influence its neighbours to develop mutations through intercellular signalling (Ishiguro et al., 2006)) is now thought to be more probable. Thliveris et al. (2011) expand on a concept introduced by Beutler (1984) whereby an initiated clone emerges from the crypt and recruits another clonal population within a defined distance to participate in forming a polyclonal tumour (Beutler, 1984). This distance has been estimated at 68μm, roughly the distance between two adjacent crypts (Thliveris et al., 2011). The authors speculate that release of mitogenic factors from cells within a dysplastic crypt may modify cellular proliferation in the neighbouring crypts. In agreement with this theory are the descriptions of Mueller and Fusenig (2004) who describe stromal cell interactions with tumour epithelial cells, to allow influence of cancer development and progression (Mueller and Fusenig, 2004). Intestinal tumorigenesis can be instigated by stromal signalling in human polyposis syndromes (van den Brink and Offerhaus, 2007). The interaction between stromal cells and epithelial cells, known as morphostasis, acts through intercellular signalling to maintain tissue microarchitecture. Disruption in morphostasis through epithelial adenomatous polyposis coli (APC) gene mutation could affect the local microenvironment and prompt neighbouring crypts to select for an independent epithelial mutation (Thirlwell et al., 2010).

Thirlwell et al., (2010) suggest microadenoma formation may rely on the transformation of neighbouring crypts to overcome morphostatic control of the tissue microenvironment. Graham et al. (2011) also propose that an altered stromal field permits or causes second mutations in the surrounding crypts (Graham et al., 2011). The crypts would be mutually reliant; one single initiatied crypt would have to wait for the mutation of another crypt in close proximity to allow propagation. The altered stromal field is therefore equivalent to the cancerized field from which polyclonal adenomas arise. Crypt interaction would also reinforce the observation that the presence of one or more adenomas increases the likelihood of metachronous adenoma formation.

1.3.4 Metachronous adenoma

Metachronous adenomas refer to adenomas that develop at two different time points. The high incidence of metachronous adenoma has been introduced earlier in this review. Patients who have had adenomas excised have been shown to have up to 60% risk for a new, metachronous adenoma within 4 years of a previous polypectomy (Neugut et al., 1985) (Matek et al., 1985) (Waye and Braunfeld, 1982). A prospective study comparing the rate of metachronous adenomas (termed recurrent in the paper) and incidence of adenomas found the recurrence rate was significantly higher than the incident rate (42% and 16% respectively) (Neugut et al., 1995). This evidence suggests a field defect or cancerized field maybe left behind following polypectomy, leading to a high rate of new adenoma formation. There is also evidence to show the field may be influenced by the presence of adenomas, since metachronous incidence is increased by the size and number of adenomas at baseline (Noshirwani et al., 2000).

One consideration is that adenomas identified to be metachronous (developed later) might actually be synchronous adenomas (present at the same time) that were missed at the original endoscopy. Same day 'back-to-back' colonoscopies have revealed the overall miss rate for adenomas is 24% (Rex et al., 1997). There is also variable use, in literature, of the term 'recurrent' adenoma when authors are describing metachronous adenomas. There are obvious difficulties in proving whether an adenoma really recurs at the same point, whether a metachronous adenoma has developed near the same area or whether adenomas have regrown due to inadequate resection. As a result of these difficulties and inconsistencies, understanding the nature of adenoma growth remains ill defined.

1.3.5 Summary –potential causes of field cancerization

The evidence for field cancerization is summarized in Figure 5. The potential causes are not mutually exclusive, it may even be possible that interactions between mechanisms support field changes.
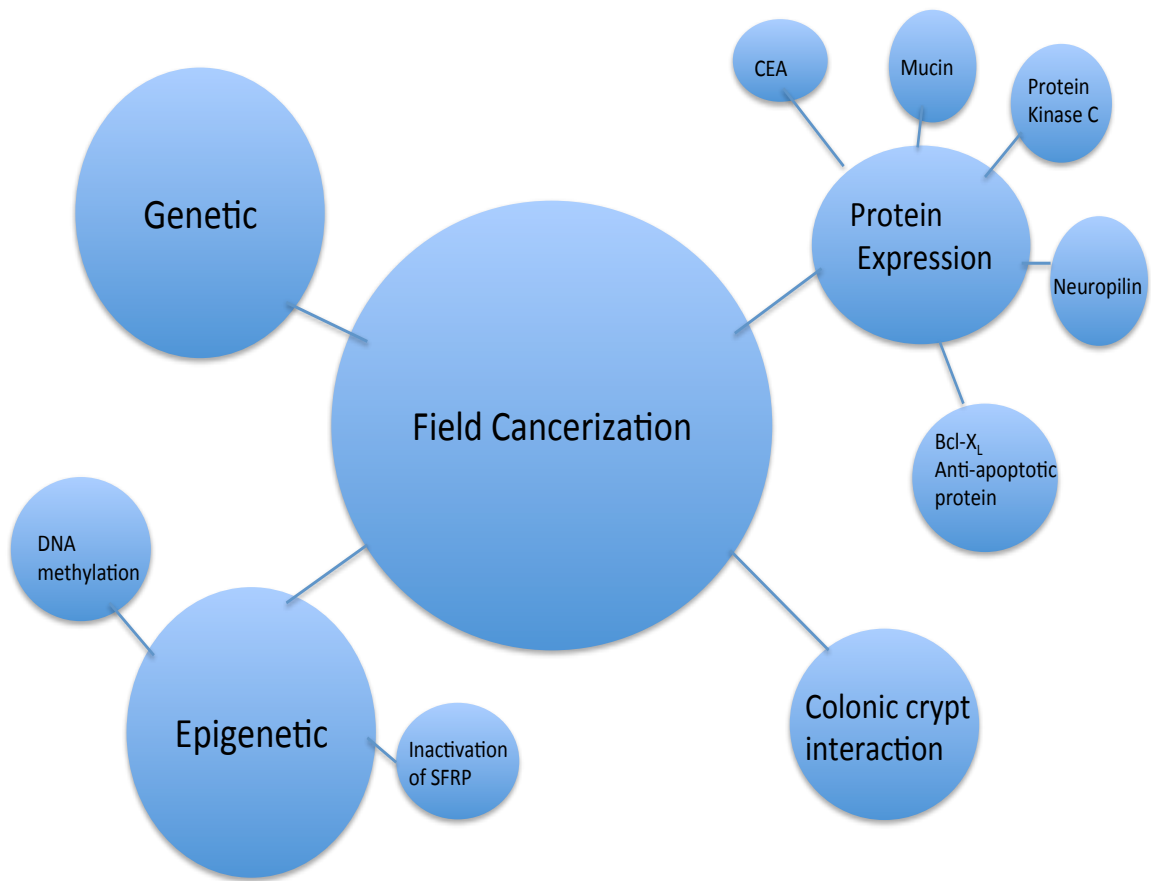
Figure 5. Potential causes of field cancerization.

1.4 Dietary modification of colorectal cancer risk

Epidemiological data suggests 5-10% of colorectal cancer is heritable (Burn et al., 2013). The majority of colorectal cancer is therefore sporadic in origin with genetic and environmental factors playing a role. There is an abundance of data linking dietary and lifestyle factors with colorectal cancer risk (Bingham et al., 2003). Studies indicate DNA damage of colonocytes due to intake of red meat, casein and soy as causative factors of colorectal cancer (Toden et al., 2007, O'Callaghan et al., 2012) and other research suggests low dietary intake of fibre as a contributor to cancer risk and equally a diet high in dietary fibre as protective (Bingham et al., 2003). A wealth of studies has shown that butyrate produced from fermentation of fibre is the molecule responsible for the chemopreventive properties of a fibre-rich diet (McIntyre et al., 1993, Perrin et al., 2001, Bingham et al., 2003). The implication that colorectal cancer may be preventable through dietary modifications is important to understand the mechanisms behind diet-mediated colonic epithelial preservation or damage.

Keratins have been implicated in the strength and stability of colonocytes in intestinal epithelium (Majumdar et al., 2012b) and in turn butyrate has been shown to both influence the properties of keratins and reduce colon cancer risk. The process by which butyrate protects the colon and whether it alters colonocyte structure with respect to keratins is poorly understood. The association between keratin alteration in colonic neoplasia and the field around them in response to butyrate are explored in this thesis. Understanding keratins and how they are influenced by butyrate would allow advances in both prevention and treatment for neoplasia with particular relevance to early changes such as field cancerization.

1.5 Keratins and Butyrate in Colonic Tissue

1.5.1 Keratins

The cytoskeleton of epithelial cells is often referred to as 'scaffolding' for the cell due to its capacity to maintain cell shape. It affords the ability to do this through one of its components, intermediate filaments (Figure 6). Keratins are the largest subgroup of intermediate filament proteins (Majumdar et al., 2012b).
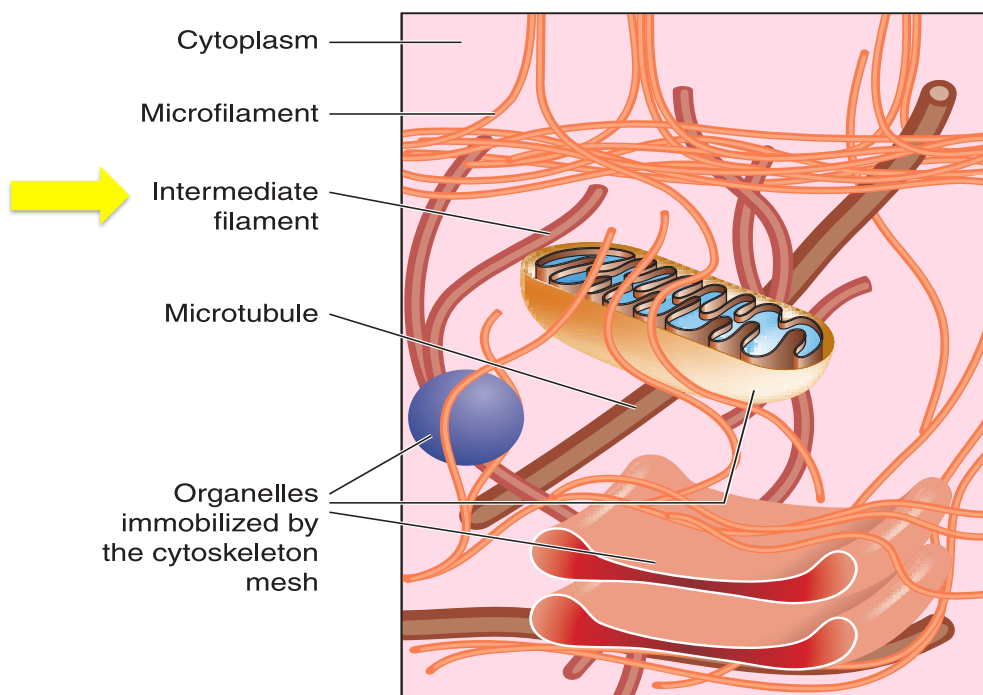
Figure 6. Components of an epithelial cell

(Source: Shutterstock®)

Intermediate filaments are formed from heterodimers of type1 and type 2 keratin. The predominant keratins in colonocytes are type 2 keratin 8 (K8) and type 1 keratin 18 (K18), though keratins K7, K19 and K20 are also found (Moll et al., 1982). Keratins provide mechanical strength to intestinal epithelia and allow colonocytes to resist chemical and mechanical stresses. They also partake in regulatory functions of a cell including cell cycle, cell differentiation and apoptosis (Magin et al., 2007).

In cancer, keratins are extensively used as immunohistochemical markers in diagnostic tumor pathology. Keratin tumour markers have been utilised for bladder, cervix, kidney and liver cell staining and specifically changes in K7, K8, K18, K19 and K20 are used for the colon (Moll et al., 2008). Other studies show keratin changes as a predictor of cancer cell invasion and metastasis (Knosel et al., 2006), as well as in treatment responsiveness (Bauman et al., 1994), indicating a role of keratins as multifunctional regulators of epithelial tumorigenesis.

The importance of K8 in gastrointestinal physiology has been demonstrated in keratin knock-out studies. Baribault et al., (1994) generated K8 knock-out mice and found those surviving to adulthood had high rates of intestinal mucosal inflammation and hyperplasia (Baribault et al., 1994), highlighting that the absence of K8 causes intestinal epithelial cells to become more fragile. Owens et al., (2004) confirmed this association through identification of genetic mutations in K8 and K18 in colonocytes from patients with inflammatory bowel disease (Owens et al., 2004). The authors also studied the effect of K8 mutation on filament assembly through cultured cells. Using electron microscopy, they found wild type K18 and K8 formed smooth, regular filaments of uniform diameter. By contrast, mutant K8 formed shorter, less straight filaments of varying diameter. If deficient intermediate filaments are manufactured as a result of K8 mutation, the 'scaffolding' of colonocytes is compromised. It is possible that less resilient colonocytes are more susceptible to the effects of carcinogens leading to adenoma-carcinogenesis.

Toivola et al., (2004) examined the physiological importance of keratin 8 in electrolyte transport in the colon. Using 1-2 day old K8 knock-out mice (before colonic hyperproliferation and inflammation presents in the colon) Toivola et al., (2004) noted decreased sodium ion absorption and increased chloride ion secretion in K8 knock-out mice in comparison to wild type mice. They concluded that colonic keratins function by regulating electrolyte transport, most likely by targeting ion transporters to their cellular components (Toivola et al., 2004).

There is an increasing body of evidence to show that alterations in keratins are associated with adenomagenesis and carcinogenesis in the colon. Polley et al., (2006) found keratins [in particular several isoforms of keratin 8] were under expressed in tumour tissue but overexpressed in the field tissue of adenoma and cancer patients when compared with tissue from healthy patients. Khan et al., (2011) report similar findings where keratin 8 expression was shown to progressively increase from normal mucosa to the field around and cancer itself (Khan et al., 2011).

1.5.2 Butyrate

High dietary intake of fibre is associated with a reduced risk of colorectal cancer (Bingham et al., 2003). The mechanism for this observation could be due to the action of short chain fatty acids (SCFAs), a fermentation product of fibre. Butyrate is a SCFA and is the preferred source of nutrition for colonocytes (Roediger, 1982). It is known to inhibit proliferation in colonic tumor cells and cell lines but to stimulate proliferation in healthy colonic epithelial cells. This is often referred to as "the butyrate paradox" (Figure 7) (Vanhoutvin et al., 2009).

Butyrate Paradox

Normal Colonocyte
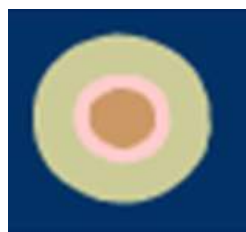
- Nutritional source
- Stimulate proliferation

Colonic tumour cell

- Induce apoptosis
- Inhibit proliferation
- Anti-metastatic effect

Figure 7. Butyrate paradox

The use of butyrate as an anti-cancer agent has been proposed due to its apoptotic effects on cancer cells. Hague et al., (1995) found the SCFAs butyrate, proprionate and acetate were able to induce apoptosis in cancer and adenoma cell lines. Of the three, butyrate was the most effective at inducing apoptosis but rates of apoptosis were diminished against the cancer cell lines in comparison to the adenoma cell lines (Hague et al., 1995). Little is known about the effect of butyrate on the cancerized field.

Ex vivo studies have shown that increased intraluminal levels of butyrate induce a higher rate of apoptosis in colonocytes following exposure to genotoxic agents (Clarke et al., 2012). Butyrate may allow sensitization of colonic cells to damage (Chirakkal et al., 2006) in addition to initiating apoptosis via a number of pathways including TNF-α induction of death receptors and activation of the mitochondrial pathway through up-regulation of pro-apoptotic protein BAK (Pajak et al., 2009, Chirakkal et al., 2006). Tan et al., (2008) described an anti-metastatic effect of butyrate on HCT-116 colorectal cancer cells after 36 hours of butyrate exposure (Tan et al., 2008). This uncovers further pharmacological potentials of butyrate as an anti-neoplastic agent.

Butyrate is commonly regarded as an inhibitor of histone deacetylases (HDACs) but has also been theorised to be a product inhibitor of acetylation (Corfe, 2012). Its influence on gene expression regulation is accomplished through changes in histone acetylation, a post-translational modification (Myzak et al., 2006).

1.5.3 Post-translational modifications of keratins

Protein post-translational modification (PTM) increases the functional diversity of the proteome by addition of functional groups, proteolytic cleavage of regulatory subunits or degradation of entire proteins (Farley and Link, 2009). Keratins can be modified via various PTMs including phosphorylation (Omary et al., 1998), glycosylation (Chou et al., 1992), acetylation (Leech et al., 2008), sumoylation (Snider et al., 2011) and cleavage (Ditzel et al., 2002).

1.5.3.1 Phosphorylation

Phosphorylation is the most researched PTM and its influence on keratins is residue site specific. Several studies have shown that K8 and K18 phosphorylation is elevated upon cell stress (Liao et al., 1995, Ku et al., 1996) and hyperphosphorylation has been associated with the protection of K18 from degradation by caspases (Ku and Omary, 2001) in normal tissue under stress. The keratin PTM profile in cancer, however, is different. Tumour aggressiveness has been linked with dephosphorylation. Mizuuchi et al., (2009) showed colorectal tumour progression related to dephosphorylation of K8 (Mizuuchi et al., 2009). Taken together these studies suggest phosphorylation is chemoprotective in normal tissue but its role is reversed in cancer, where hyperphosphorylation of K8 leads to increased tumour cell survival and inhibition of apoptosis (Arentz et al., 2012, Ku and Omary, 2006). Although the association between butyrate and keratin phosphorylation is incompletely understood, a putative mechanism is via butyrate-induced dephosphorylation of histones (Sealy and Chalkley, 1978).

1.5.3.2 Glycosylation

Glycosylation is known to occur at three residue sites (serine 29, 30 and 48) on K18 (Ku and Omary, 1995). Ku et al., (2010) demonstrated that K18 glycosylation provides a unique protective role in epithelial injury as glycosylation cannot occur in mice overexpressing K18 substitution mutants. In

comparison to wild type mice (with glycosylation) they found non-glycosylated mice were more susceptible to apoptosis and streptozocin-induced liver and pancreatic injury (Ku et al., 2010). It is thought glycosylation promotes phosphorylation and activation of cell-survival kinases (Ku et al., 2010).

1.5.3.3 Acetylation

Keratin 8 is acetylated and the degree of acetylation is butyrate responsive (Leech et al., 2008). Specific sites of acetylation of keratin 8 in response to butyrate have also been identified (Drake et al., 2009). Acetylation of keratin 8 decreases its solubility through filament reorganisation and the formation of tightly associated K8 complexes in non cancer cells (Snider et al., 2013). Increased insolubility may play a role in microtubule and microfilament stabilization (Janke and Bulinski, 2011). This may uncover how butyrate may protect healthy colonocytes through increased cytoskeletal stability following acetylation. An inverse association has been depicted in cancer cells, where K8 becomes disorganised following acetylation due to butyrate exposure (Drake et al., 2009), thus supporting the butyrate paradox theory. Although phosphorylation is known to promote K8 solubility (Omary et al., 1998), in the presence of acetylation, phosphorylation is diminished (Snider et al., 2013).

1.5.3.4 Sumoylation

Sumoylation is a reversible PTM by which a small ubiquitin-like modifier (SUMO) polypeptide is attached or removed (Bergink and Jentsch, 2009). Decreased sumoylation of K8 in colonocytes leads to loss of intestinal stem cells and the subsequent inability to maintain architecture, stability and function of intestinal epithelia (Demarque et al., 2011). Protein sumoylation increases in response to cellular stress (Wilkinson and Henley, 2010). Hypersumoylation encourages keratins to remain in the insoluble compartment, suggesting greater stability through insoluble keratin. (Demarque et al., 2011).

The interaction and influences of phosphorylation, glycosylation, acetylation and sumoylation upon each other are not fully understood. There is evidence that PTM of one keratin influences the PTM of another as hypoglycosylation of keratin 18 leads to hyperphosphorylation of keratin 8 during epithelial cell injury (Snider and Omary, 2014). Since at least one PTM (keratin 8 acetylation) is butyrate responsive, it remains possible that butyrate can cause a cascade of other PTMs that are yet to be discovered.

1.6 Summary

As the evidence for field effects grows, it is becoming clear that removal of colorectal adenomas may not be enough to evade the risk of colorectal cancer. The mechanism by which metachronous adenomas occur is unknown but analysis of the pattern of occurrence may provide clues as to whether field cancerization is involved. This has important clinical implications as current practices in the removal of adenomatous polyps, surgical resection margins and follow up times after polypectomy do not take into account the potential for field effect changes.

Keratins are important regulators of colonocyte physiology and their regulatory role is, in part, influenced by post-translational modifications and butyrate exposure. Alterations in keratin levels have been shown between the cancerized field and normal tissue. The investigation of keratins as a marker for a cancerized field and how they are influenced by butyrate may provide clues in the prevention of and treatment of the early stages of carcinogenesis.

Chapter 2

General Hypotheses and Aims

Chapter 2 General Hypothesis and Aims

2 Hypotheses

- If cancerized fields exist, metachronous adenomas will occur in the region of an incident adenoma.
- Keratin alterations are present in colonic adenoma tissue and the morphologically normal tissue surrounding it when compared with normal colonic tissue of control subjects.
- Butyrate exposure in the colonic lumen alters keratin function in colonocytes.

2.1 Aims and Objectives

2.1.1 To investigate the site of metachronous adenomas relative to index adenoma.

To theorise a likely model responsible for metachronous adenoma occurrence through analysis of the pattern of metachronous adenoma occurrence within the colon. Locations of metachronous adenomas will be determined and compared with that of the index adenoma by retrospective interrogation of colonoscopy records.

2.1.2 To develop a reliable and robust protocol for extraction of intermediate filaments from colonic mucosa.

There is no standard protocol that enables isolation and solubilisation of intermediate filaments from colonic biopsies and subsequent analysis by gel electrophoresis and gel free liquid chromatography coupled with tandem mass spectrometry (LC-MS/MS). A workflow will be developed for fractionation, extraction and solubilisation of intermediate filaments from colorectal biopsies, to permit isobaric tags for relative and absolute quantitation (iTRAQ) proteomic analysis.

2.1.3 To discover whether field changes in keratin levels exist between adenoma, field and distant tissue samples in comparison to normal controls and whether these changes are responsive to butyrate exposure.

Normal, field and adenoma insoluble proteome (controlling for butyrate) will be compared using iTRAQ proteomic workflow. Data obtained from iTRAQ work will be orthogonally validated using Western blot and immunohistochemistry.

Chapter 3

Metachronous Adenomas Occur Primarily at the Same Site with Slight Proximal Drift

Chapter 3 Metachronous Adenomas Occur Primarily at the same site with proximal drift

3.1 Introduction

Adenomatous polyps are widely recognised as the precursor to colorectal cancer (Neugut et al., 1993). Adenoma removal is associated with a lowered risk of colorectal cancer (Winawer et al., 1993b). Despite treatment, adenomas have a high recurrence rate. Current data shows up to 60% of patients develop metachronous adenomatous polyps following removal of a previous polyp (Nava et al., 1987) compared to 16% of patients with no abnormality at index colonoscopy (Neugut et al., 1995). The higher incidence of metachronous adenomas suggests the presence of one adenoma can influence the formation of another. This theory is supported by numerous studies indicating multiplicity and size of adenomas at baseline examination are powerful predictors of recurrence (Martinez et al., 2001, Bonithon-Kopp et al., 2004, Noshirwani et al., 2000, Winawer et al., 1993b). Adenoma histological features (Martinez et al., 2001) and metabolic factors including age, body mass index and fasting blood glucose have also been reported as predictors of adenoma recurrence (Taniguchi et al., 2014). Other studies have highlighted higher metachronous rates where index adenomas were proximally located (Martinez et al., 2001, Bonithon-Kopp et al., 2004). The authors define proximal location of adenomas as those found in the transverse colon, hepatic flexure, ascending colon and caecum. The mechanism by which index adenomas affect subsequent adenoma development is unknown. However, examination of the locations in which they occur may provide insights into potential mechanisms.

This study therefore investigates the anatomical distribution of metachronous adenomas in relation to the site of index adenoma. Data regarding the site of metachronous adenomas formation has important implications for surveillance endoscopy and may also provide clues to the aetiology of metachronous adenomas (Rosser et al, submitted).

3.2 Hypothesis and Aims

3.2.1 Hypothesis

Investigation of metachronous adenoma locations may provide evidence for field effects in colorectal neoplasia. I hypothesize metachronous adenomas arise by one or a combination of the following models:

1. the interaction of two fields.
2. micrometastatic migration of adenoma cells through the epithelium.
3. shedding and subsequent seeding of adenoma cells through the lumen.
4. systemic release of a sensitizing molecule.
5. luminal release of a sensitizing molecule.

3.2.2 Rationale

<u>Model 1</u>
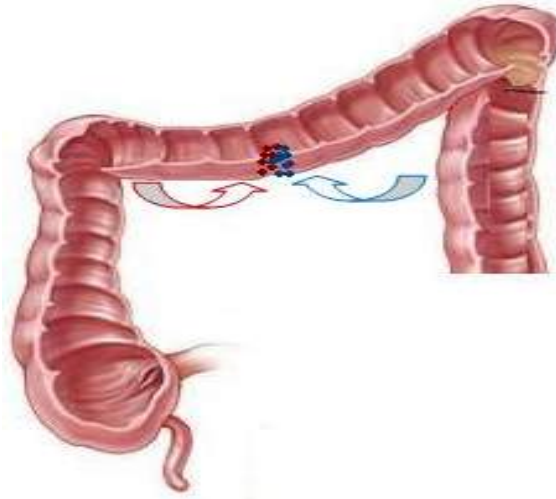
Figure 8. Metachronous adenoma occurs as a result of two fields (red and blue fields) interacting

Adenomatous polyps are polyclonal (Novelli et al., 1996, Merritt et al., 1997, Thirlwell et al., 2010) and it has been hypothesized that they arise due to interaction between two crypts (Thliveris et al., 2011). If this were the case, we would expect metachronous occurrences to appear at the same place, as the field of altered crypts would still exist after polypectomy.

Model 2
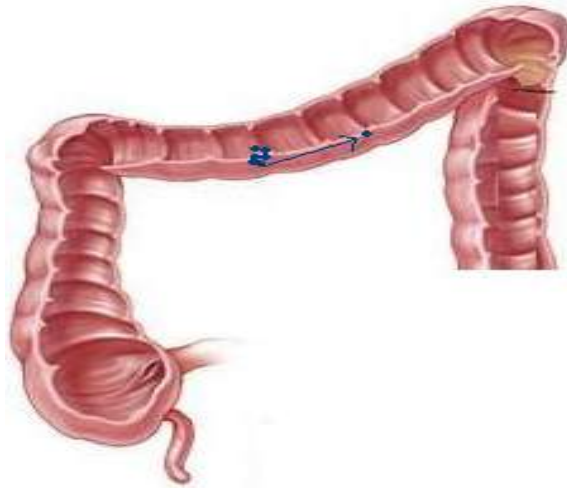
Figure 9. Metachronous adenoma occurs as a result of micrometastatic migration through the epithelium

Epithelial-mesenchymal transition takes place during cancer progression and is necessary for metastasis of epithelial cancers. Colorectal cancer cells at the invasive margin acquire mesenchymal properties such as poor differentiation, high migratory potential, hyperproliferation and loss of cell to cell contact mediated growth inhibition (Thiery, 2002). Similarly, adenoma models could acquire mesenchymal properties to allow intraepithelial migration of adenoma cells through the colonic epithelium to form new adenomas elsewhere. If this were the case, we would also expect recurrences to be in a similar or same region as the incident adenoma and to be composed of similar genetic material to the original lesion.

Model 3
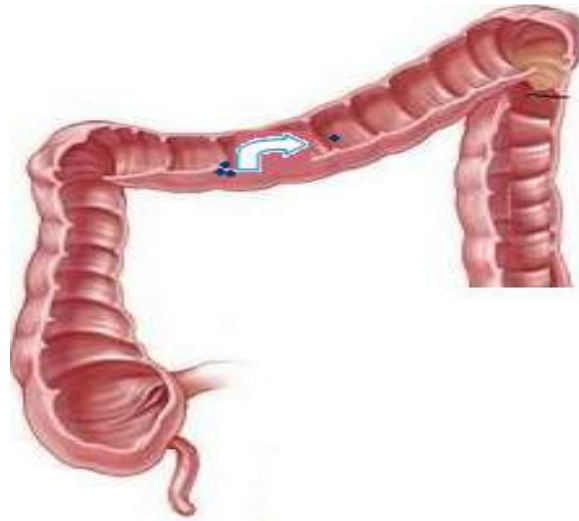
Figure 10. Metachronous adenoma occurs as a result of cell shedding and seeding through the lumen

Exfoliated malignant cells have been found to implant downstream and cause anastomotic recurrence following colon cancer surgery (Gertsch et al., 1992, Umpleby et al., 1984). Similarly, exfoliated adenoma cells could implant and cause recurrence. If this were the case, we would expect the site of recurrence to be distal as the exfoliated cells would be shed and implanted downstream, in line with the direction of the faecal stream. The recurrent adenoma would also have genetic similarities to the original lesion.

Model 4
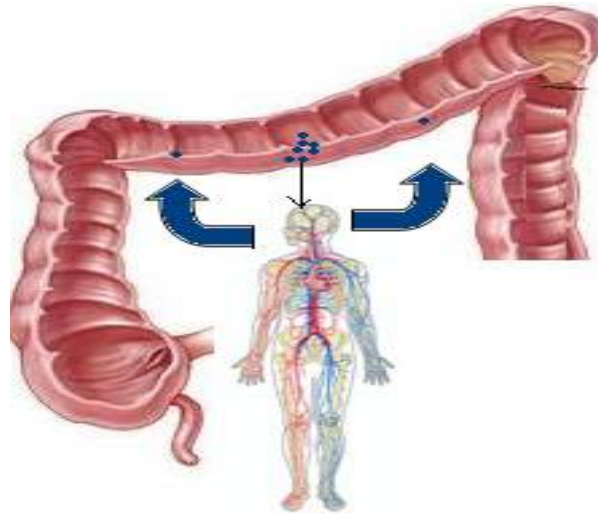
Figure 11. Metachronous adenoma occurs as a result of a sensitizing molecule released systemically

Studies have found modifications in distant tissues can exert changes to the gastrointestinal tract and vice versa. Cho et al., (2008) found that implantation of colon- 26 (CT-26) carcinoma cells subcutaneously in mice altered intestinal endocrine cell counts (Cho et al., 2008). Alternatively, Chen et al., (2012) demonstrated oral inoculation of probiotics resulted in significantly reduced tumour growth at both the dorsolateral flank and colon of mice implanted with CT-26 carcinoma cells (Chen et al., 2012). Furthermore, it is already known that colon cancer cells are capable of secreting carcinoembryonic antigen (CEA) into the circulation (Sack et al., 1988). It is possible, that adenoma cells are also capable of releasing a sensitizing molecule systemically, to encourage adenoma growth elsewhere. If this were the case, the area susceptible to metachronous occurrence may be pancolonic, affecting both the proximal and distal colon. The recurrent lesion may be genetically dissimilar to the original lesion.

Model 5
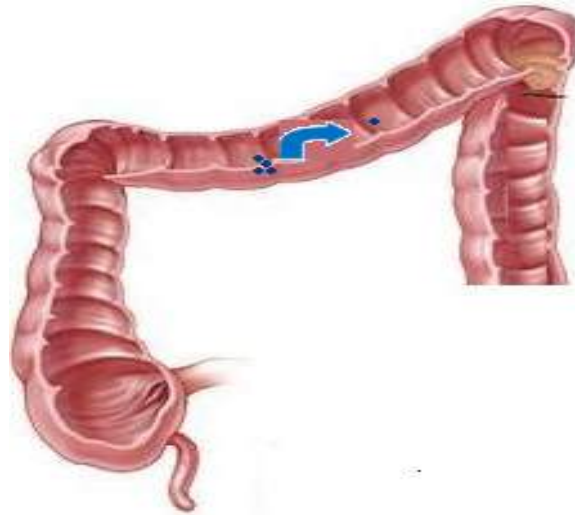
Figure 12. Metachronous adenoma occurs as a result of a sensitizing molecule released into the lumen

Mucosa from adenoma and carcinoma tissue and tissue adjacent to them are known to secrete histochemically altered mucin, in contrast to normal mucosa (Lanza et al., 1985, Filipe and Branfoot, 1974, Owen and Reid, 1995). A sensitizing molecule (such as altered mucin) could be released from adenomatous tissue intraluminally to support or trigger adenoma growth. If this were the case the sites of metachronous occurrence would predominantly be distal to the lesion as the sensitizing molecule is likely to travel downstream, with the proximal colon unaffected. The metachronous site may be proportional to the site of the incident adenoma as concentrations of the sensitizing molecule would be highest around the original lesion. The recurrent lesion would also be genetically dissimilar to the original lesion.

The models described above are not mutually exclusive. It is possible that more than one causative mechanism exists. Study of the locations of metachronous adenoma occurrence following the removal of a previous may give clues as to the model or models likely to be involved.

3.2.3 Aims

Identification of metachronous adenoma occurrence positions, relative to the index adenoma, to determine the likely mechanism or mechanisms for metachronous adenoma formation.

3.3 Method for Data Collection

This study was registered with Sheffield Teaching Hospitals NHS Foundation Trust (STH) reference number 4124 as a service evaluation (Appendix 1).

A prospectively maintained database (Infoflex, Chameleon Information Management Services, UK) was interrogated to identify all colonoscopies performed between January 2001 and August 2011 at STH.

15,121 colonoscopies containing 4759 polyp events were recorded. Patients undergoing more than one colonoscopy and polypectomy were cross-referenced against a histological database to confirm adenoma status. Histology records were accessed via two systems: Integrated Clinical Environment (Sunquest Information Systems, Norwich UK) and iLAB (Apex) (CSC Health, Oxfordshire, UK). In all the cases recorded, patients had undergone a colonoscopy and polypectomy and then a further polypectomy or repeated polypectomies months or years later. A flow chart of data acquisition is shown in Figure 14.

Due to patient confidentiality regulations only event numbers could be retrieved via Infoflex. The event number for each colonoscopy record had to be matched on site (at STH) to the unique patient hospital number in order to access histology records. To ensure patients were not missed a SNOMED (Systematized Nomenclature of Medicine) search was also performed to identify all colorectal adenoma samples processed by STH between January 2001 and August 2011. This identified a further 230 patients with repeat adenoma records, not on the Infoflex list. Colonoscopy records for those 230 patients were retrieved.

The information was collected using a data collection tool (Appendix 2) and collated on an Excel spread sheet. Index colonoscopy was recorded as R0 colonoscopy, repeat colonoscopy was recorded as R1 and so forth (Table 1). Positions of adenomas were recorded according to the colonic segment they

were found: caecum, ascending colon, hepatic flexure, transverse colon, splenic flexure, descending colon, sigmoid colon, rectosigmoid junction and rectum, labelled 1 to 9 respectively (Figure 13). Exclusion criteria were applied (Table 2).
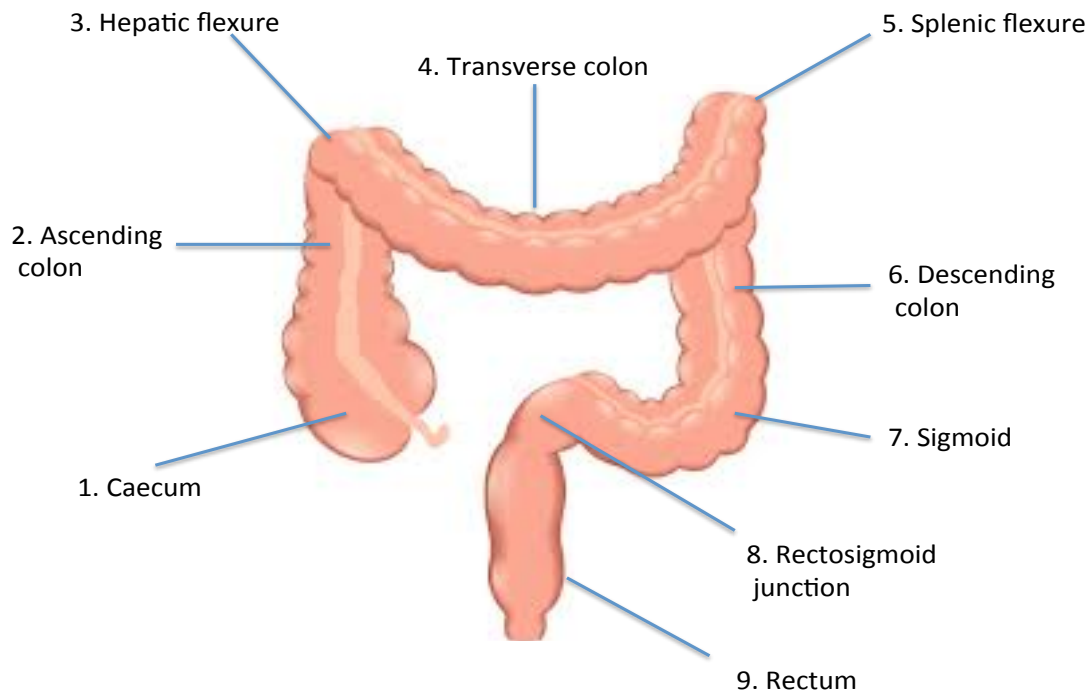
Figure 13. Nine segments of the colon

Positions of adenomas within the nine segments of the colon were recorded according to their locations and labelled 1-9.

Table 1. Colonoscopy numbers and abbreviations

Colonoscopy	Recorded as abbreviation	Colonoscopies in total
Index/incident colonoscopy	R0	1
Repeat colonoscopy 1	R1	2
Repeat colonoscopy 2	R2	3
Repeat colonoscopy 3	R3	4
Repeat colonoscopy 4	R4	5
Repeat colonoscopy 5	R5	6

3.3 Method for Data Collection
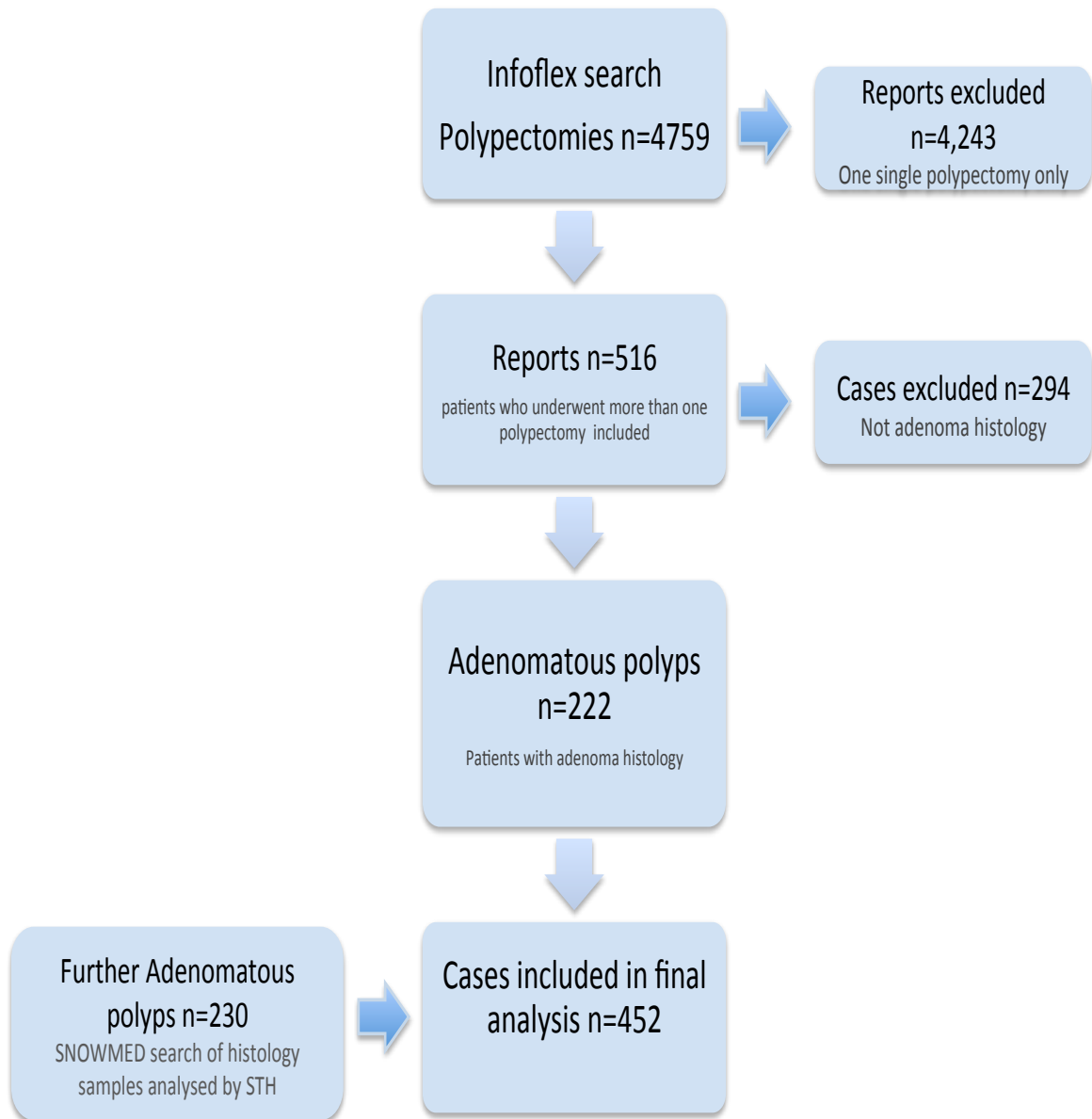
Figure 14. **Flowchart of the method of data acquisition.**

Table 2. Exclusion criteria –pathological diagnoses

Diagnosis
Inflammatory bowel disease (Crohn's Disease and Ulcerative Colitis)
Previous Cancer and Cancer surgery
Familial Adenomatous Polyposis Syndrome
Other Polyposis Syndromes
Hyperplastic Polyps
Hereditary Non-Polyposis Colon Cancer

3.3.1 Problems and solutions for statistical analysis

Some patients developed multiple metachronous adenomas that occurred *both* proximally and distally to the index adenoma. This posed a problem in identification of whether metachronous adenomas were more likely to arise proximally or distally. Equally, some patients had synchronous index adenomas, which created similar analytical problems. Taking these problems into consideration analyses were performed in two ways:

1. using the whole dataset
2. using only patients with one single index adenoma and one single metachronous adenoma.

Analysis 1

To validate the accuracy of our data the cancer distribution percentages within the colon were compared with our own adenoma distribution percentages. Data taken from the R0 colonoscopy/incident colonoscopy (see Table 1) whole dataset analysis 1 was used to calculate the number of adenomas found in each segment of the colon. This calculation was repeated for all the nine segments and compared with data from Cancer Research (UK)[1].

[1]Data from Cancer Research online: http://www.cancerresearchuk.org/cancer-info/cancerstats/types/bowel/incidence/uk-bowel-cancer-incidence-statistics. Last accessed on 18th April 2015.

Analysis 2

The number of adenomas in each segment was calculated for each colonoscopy and these figures were compared between colonoscopies to establish if there was an overall proximal, distal or same site of metachronous occurrence.

Analysis 3

Adenoma segment 'movements' were considered for this analysis. For example: if an index adenoma was found at the caecum at first colonoscopy (R0) and then a metachronous found at the ascending colon at subsequent colonoscopy (R1) this was given a value of -1, for distal movement of one segment. Proximal movements were given a positive value. Since some patients had multiple adenomas at R0, there are more movement events than there are adenomas or patients. For example: if index (R0) adenomas were found at both caecum and ascending and subsequently at R1 another adenoma was found at the caecum, two movement events (0 and +1 respectively) would be recorded. The sum of adenoma movement events was calculated for each movement category (from -8 to +8) between colonoscopies R0 and R1 (where R0 was the index colonoscopy and R1 the next colonoscopy). This was repeated for movements between colonoscopies R1 and R2; R2 and R3 and R3 and R4.

Analysis 1

The percentage of single metachronous adenomas occurring in the same segment or a different segment to the index adenoma was calculated. The difference between adenoma sites was investigated with the one way Chi-squared test.

Analysis 2

The percentage of single metachronous adenomas occurring in either a proximal, distal or the same segment as the index adenoma was calculated. Differences in adenoma recurrence direction were investigated with the one way Chi-squared test.

Analysis 3

How far a metachronous adenoma occurs from the index adenoma was investigated. As a metachronous adenoma following a caecal index adenoma has more potential segment spaces (n=8) to appear distally than for example a sigmoid index adenoma (maximal distal segment space n=2), this creates a bias due to different segment availability. To avoid this bias, only rectal and caecal index adenomas (at the farthest ends) were analysed for metachronous occurrence. This aims to prevent skew as there is no possibility of two way movement.

Analysis 4

The mean number of segments travelled for metachronous adenoma appearing proximal to their index adenoma and similarly for adenomas appearing distal to their index adenoma were calculated. Differences in the number of segments travelled was calculated using one sample t test.

A probability calculation (Appendix 3) was performed to examine whether proximally occurring metachronous adenomas travelled more segments than distally occurring metachronous adenomas according to the segments available to them.

Summary of analyses

Whole Dataset Analysis

Analysis 1 – adenoma distribution within the colon

Analysis 2 – comparison of number of adenomas at each site at each subsequent colonoscopy

Analysis 3 – proximal, distal or no movement for metachronous occurrence

Data

Single Adenoma Analysis

Analysis 1 – percentages of adenomas found in the same or different segment to the index adenoma

Analysis 2 – percentage of adenomas found proximal, distal or in the same segment as the index adenoma

Analysis 3 – distance in segments between a metachronous adenoma and index adenoma at the rectum or caecum

Analysis 4 – Probability calculation of whether proximally or distally occurring metachronous adenomas travelled furthest from the index adenoma, according to the segments available to them.

Figure 15. Summary of analyses

3.4 Results

15,121 colonoscopies containing 4759 polyp events were recorded. 452 patients (156 female and 296 male; median age 75 years [range 32-100]) underwent more than one polypectomy (all polyps histologically confirmed as adenomatous polyps). The median time between colonoscopies was 13 years [range 1 month - 25 years].

3.4.1 Whole dataset - analysis 1

The distribution of adenomas at incident colonoscopy (R0) was comparable to cancer distribution figures published by Cancer Research UK [1] (Figure16). The highest proportion of adenomas (31.1%) were found, as expected, in the rectum.

Transverse colon
5%
7.4%

Hepatic Flexure
3%
3.1%

Splenic Flexure
2%
2.3%

Ascending colon
8%
8.8%

Descending colon
3%
5%

Caecum
14%
9.4%

Sigmoid colon
20%
28%

Other and unspecified sites:
11%

Rectosigmoid junction
7%
5.4%

Rectum
27%
31.1%

- Data from Cancer Research UK[1] in black.
- Data from our analysis in red.
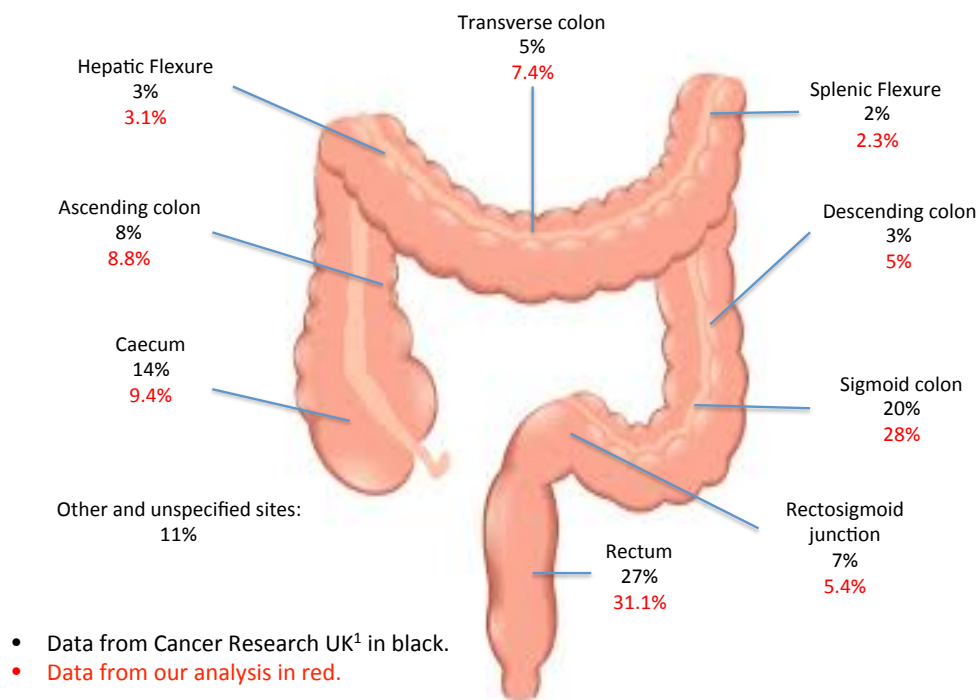
Figure 16. Comparison of percentages of cancer and adenoma per colonic segment.

Figures in black are the percentage of cancers found in each of the indicated colonic segments. The figures in red are calculated from the number of adenomas found at index colonoscopy (R0). The percentages are comparable and support the accuracy of the collected data.

[1]Data from Cancer Research online: http://www.cancerresearchuk.org/cancer-info/cancerstats/types/bowel/incidence/uk-bowel-cancer-incidence-statistics. Last accessed on 18th April 2015.

3.4 Results

3.4.2 Whole dataset - analysis 2

At incident colonoscopy (R0) the majority of adenomas were found in the rectum (n=164) closely followed by sigmoid (n=151). At the next colonoscopy (R1) the majority of adenomas were found again in the sigmoid and rectum. At the third colonoscopy (R2) the majority of adenomas found were maintained at the rectum (n=30) but a secondary peak at the ascending colon (n=29) was seen. In the subsequent colonoscopies (R3, R4 and R5) the majority of adenomas were found in the rectum (Figure 17). This indicates metachronous adenomas appear predominantly in the same colonic segment as the original (index) adenoma.

	C	A	HF	T	SF	D	S	RSJ	R
R0	50	47	17	39	12	27	151	29	164
R1	73	64	16	45	7	29	121	24	95
R2	20	29	6	23	6	5	27	5	30
R3	8	11	2	6	5	1	14	4	18
R4	5	4	2	2	3	2	1	1	7
R5	3	1	0	3	0	1	0	0	5
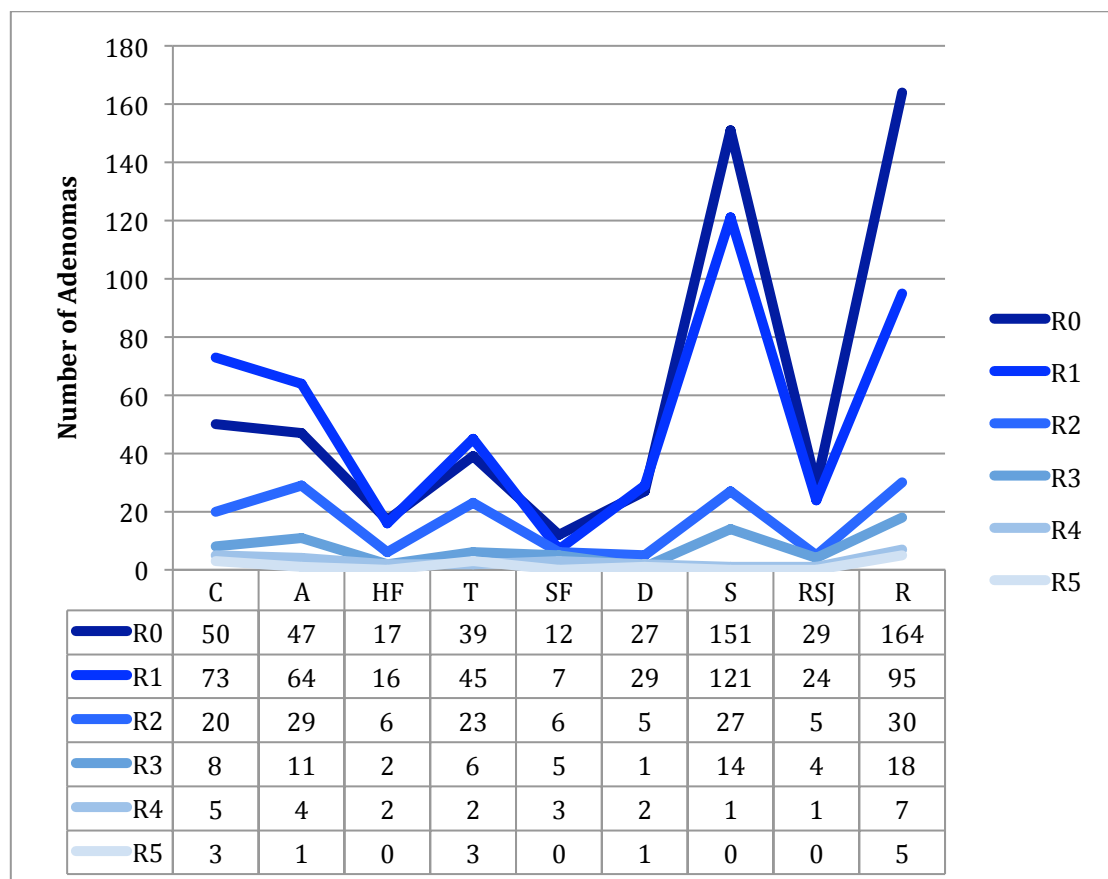
Figure 17. Number of adenomas recorded in each of the nine colonic segments

(Caecum–C, Ascending colon–A, Hepatic Flexure–HF, Transverse colon–T, Splenic flexure–SF, Descending colon-D, Sigmoid-S, Rectosigmoid Junction-RSJ and Rectum-R).

The graphs (lines R0-R5) representing number of adenomas per segment from index colonoscopy (R0) and at each repeat colonoscopy (R1-R5) follow the same trend. The mirroring of the graphs indicates metachronous adenomas are appearing in the same segments at each subsequent colonoscopy.

3.4 Results

3.4.3 Whole dataset - analysis 3

The graphs in Figure 18 all show a peak percentage of adenomas in the 0 movement category. This suggests that the majority of metachronous adenomas do not move segments. However, addition of the sum of percentages in the proximal and distal movement categories reveals the majority of adenomas are not necessarily found in the non movement category (see Table 3.) The total number of segment movements (N) was 601 for R0 to R1; N = 502 for R1 to R2; N= 207 for R2 to R3 and N= 81 for R3 to R4. .

Comparing the index colonoscopy (R0) and the next colonoscopy (R1) it was evident that the least number of metachronous adenomas occurred proximal to the index adenoma (18.6%). 40.2% of metachronous adenomas occurred in the same segment as the index adenoma. The majority (41.2%) occurred in a distal segment to the index adenoma. A similar pattern was seen in the metachronous adenoma occurrence between colonoscopy 2 (R1) and 3 (R2). This pattern was lost between colonoscopies 3 (R2) and 4 (R3) where the metachronous occurrences were evenly distributed between the three categories with a slight proximal drift. In the last two colonoscopies (comparison between R3 and R4), the majority of metachronous occurrences were found in the same segment (51.8%). The bell shaped curve of the graphs in Figure 18 suggests metachronous adenomas were occurring in close proximity to the index position (0 movements).

3.4 Results

Whole dataset – analysis 3

Movement events between R0 to R1

Movement events between

R1 to R2   R2 to R3   R3 to R4
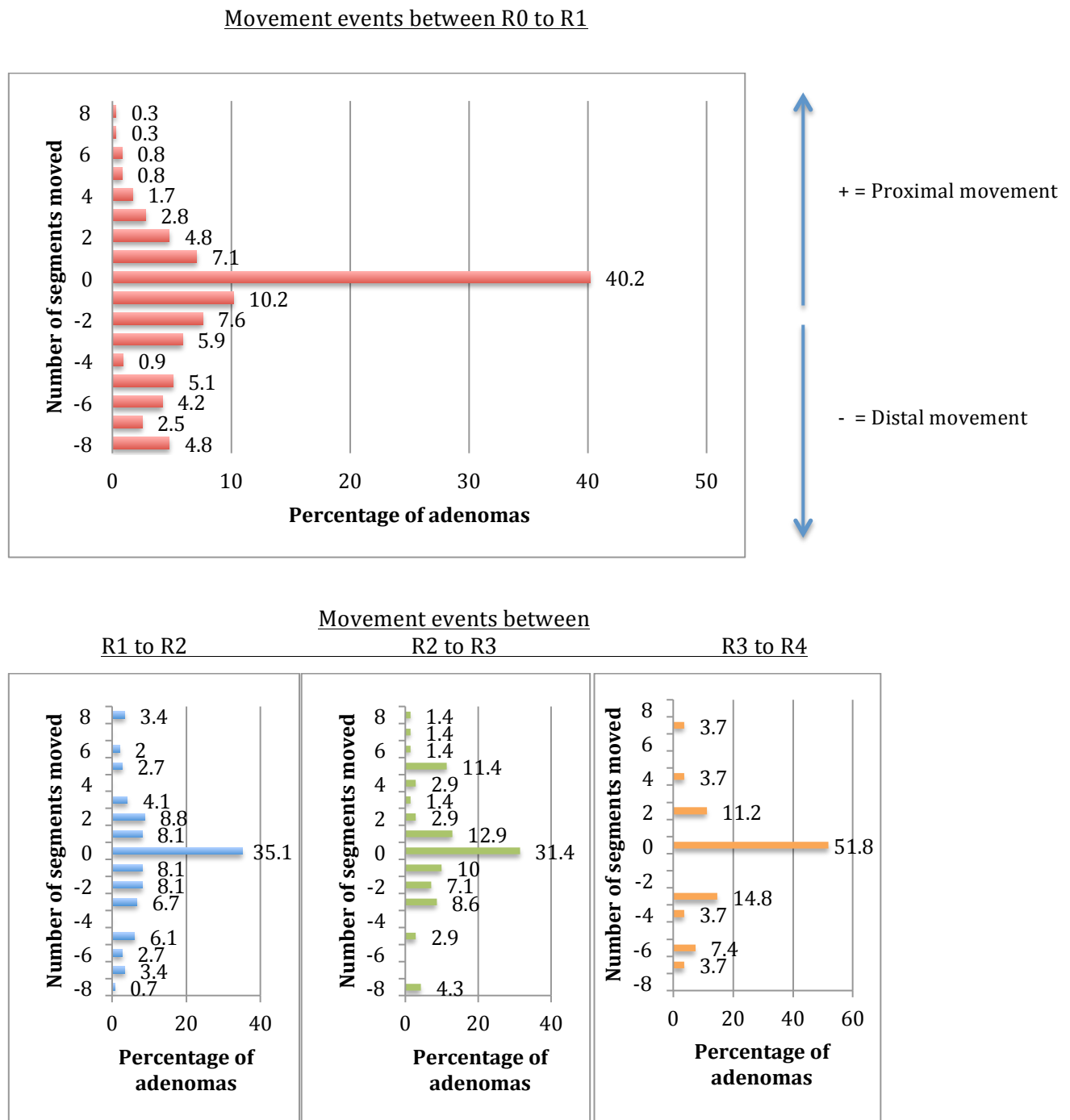
Figure 18. Number of adenomas in each movement category

The number of adenomas in each movement category (-8 to 8) expressed as a percentage of the total of movement events (N) between colonoscopies. All the graphs revealed a peak at 0 segment movement category. The sums of proximal and distal percentages are represented in Table 3.

Table 3. Comparison of the sum of proximal, distal and no movement percentages.

Colonoscopy interval	Proximal (%)	No movement (%)	Distal (%)
R0-R1	18.6	40.2	**41.2**
R1-R2	29.1	35.1	**35.8**
R2-R3	**35.7**	31.4	32.9
R3-R4	18.6	**51.8**	29.6

The data presented in Table 3 is extracted from graphical data in Figure 18. These data shows that at R1 and R2 colonoscopies the majority of adenomas moved distally when the sums of percentages were calculated, although the values of both categories are very similar.

3.4 Results – Single adenoma series

91 patients from the whole dataset were excluded from the following analyses due to either multiple adenomas at index colonoscopy or multiple metachronous adenomas at subsequent colonoscopy.

361 patients (235 male, 126 female, median age [range] 66 [32-91] years) developed a single metachronous adenoma at follow-up colonoscopy. All data below are presented with 95% confidence intervals.

3.4.4 Single adenoma – analysis 1

Metachronous adenomas were more likely to develop in a different segment (61 ± 5%) to that of the index adenoma. 39 ± 5% of metachronous adenomas developed in the same segment as the index adenoma. P< 0.01 one way Chi-squared test.
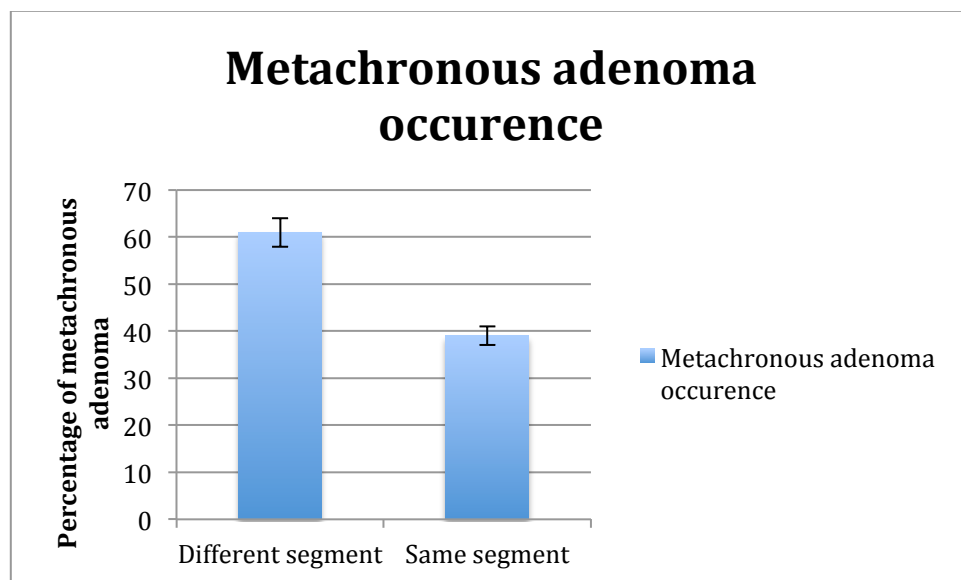
Figure 19. Graph indicating metachronous adenomas were more likely to occur in a different segment than the same segment.

3.4 Results

3.4.5 Single adenoma – analysis 2

Metachronous adenomas were more likely to occur at a site proximal to the index adenoma (41 ± 5%) than either the same segment (39 ± 5%) of a more distal segment (20 ± 5%). P<0.01 one way Chi-squared test.
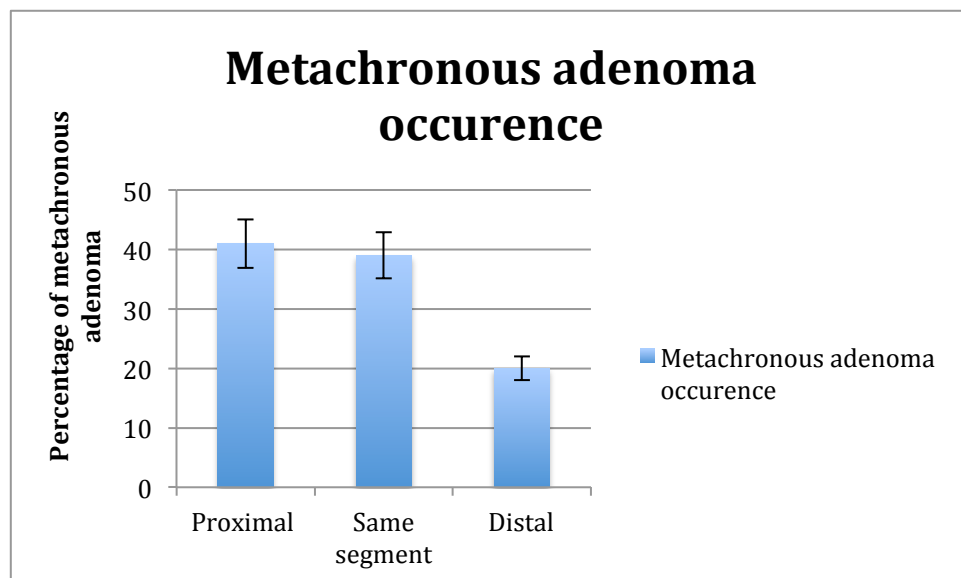
Figure 20. Graph indicating metachronous adenomas were more likely to occur proximal to the index adenoma than either the same segment or distal to the index adenoma.

3.4.6 Single adenoma – analysis 3

Although metachronous adenomas were found to develop at a different segment (analysis 1), the majority developed 2 segments away from the index adenoma. 72 ± 5% of metachronous adenomas developed within two segments of an index rectal adenoma and 73 ± 5% of metachronous adenomas developed within two segments of an index caecal adenoma (Figures 21 and 22). This calculation is corrected for potential segment spaces as an index rectal adenoma cannot move distally and vice versa for caecal adenoma.

3.4 Results
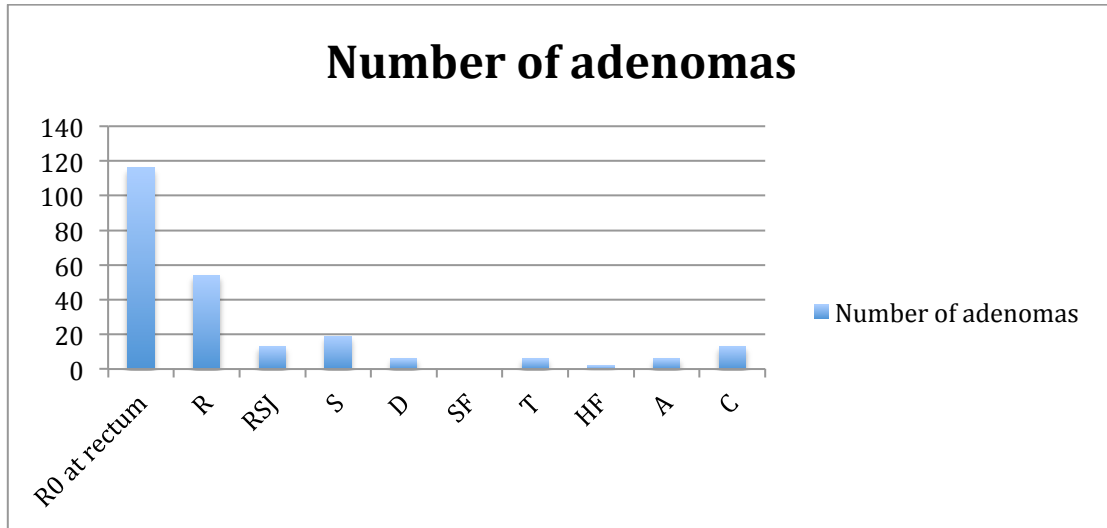
Figure 21. The number and distribution of metachronous adenomas (R1) following the removal of an index adenoma (R0) in the rectum.

72% of metachronous adenomas were found to occur within two segments of the rectum (at the sigmoid, S7 or rectosigmoid junction, RSJ8).
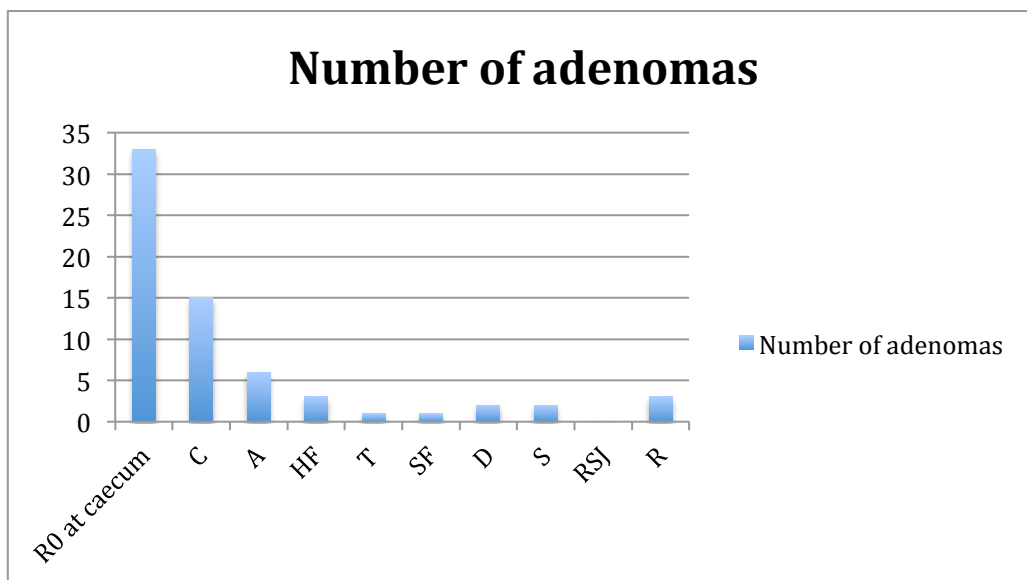
Figure 22. The number and distribution of metachronous adenomas (R1) following the removal of an index adenoma (R0) in the caecum.

73% of metachronous adenomas were found to occur within two segments of the caecum (at the ascending colon, A2 or hepatic flexure, HF3).

3.4 Results

3.4.7 Single adenoma – analysis 4

Proximally-sited metachronous adenomas were more likely to occur in a segment further away (mean [SD] segments travelled 3.5 [2.3]) from the index adenoma than distally-sited metachronous adenomas (2.6 [1.8] segments travelled; $P<0.01$ One sample t test).

Taking into account the available segment movement for each index adenoma: metachronous adenomas that were able to move proximally took 43% of the available travel distance available to them and metachronous adenomas that were able to move distally took 30% of the distance available to them.

3.5 Discussion

3.5.1 Whole data set analysis

Analysis 1 confirms that the data collected is comparable to national cancer statistics; indicating the analyses performed are representative of the general population.

The results from analysis 2 demonstrate metachronous adenomas occur at similar segments, as evidenced by the similarity in graph profiles between colonoscopies. The majority occur in the sigmoid and rectum, as they would be expected to occur (Johnson et al., 1988).

The results from analysis 3 indicate the majority of metachronous adenomas occur in the same segment, or at least close to the index adenoma. The results using these two analytical methods are compatible with a field effect, since adenomas frequently form in the same or similar region. Metachronous adenomas may arise due to the influence of an index adenoma on the field before its removal or alternatively, the field may be inherently predisposed to adenoma formation hence the occurrence of two adenomas at different time points. Results from these analyses do not uncover whether this observation is due to cause or effect.

3.5.2 Single adenoma analysis

The absolute figures from analysis 1 and 2 show more metachronous adenomas develop in a site different to the original adenoma (with a predominance for adenomas to occur proximally) but analysis 3 demonstrates up to 73% of caecal and rectal metachronous adenomas occur within 2 segments of the original adenoma. It is necessary to interpret absolute figures with caution since the interpretation of adenoma location during colonoscopy is not exact. Even with the use of a colonoscopy tracker the locations are still estimated. It is possible that a 2 segment error for estimation exists and thus many adenomas were

actually occurring in the same segment. A colonoscopist can be more confident about the location of the scope at the rectum and caecum. The rectum is the first colonic segment encountered during scope insertion and the caecum has identifiable landmarks that other parts of the colon lack (although it is recognised that endoscopists can still misidentify the caecum) (Adam et al., 2001). The segment error therefore may be minimised at these two locations and thus increasing the accuracy of single adenoma analysis 3.

Analysis 4 aimed to differentiate the characteristics of proximal metachronous adenomas and distal metachronous adenomas to determine which model for metachronous occurrence is more likely. If distally occurring metachronous adenomas were found to occur close to the index adenoma then model 5 would be more likely than model 3 (see Figures 10 and 12).

The observed trend is that of proximal metachronous adenomas occurring further away from the index than distal adenomas. The significance of this trend is multifaceted: if right sided adenomas travelled further, this suggests a wider field, since they could occur more proximally and perhaps a different pathogenesis mechanism to distal adenomas. The second inference is that the intraluminal environment may affect a field as exposure to bowel content is different between the right and left colon (Birkenkamp-Demtroder et al., 2005). An alternative argument is that the observed further travel distance for proximal metachronous adenomas reflects a systemic cause contributing to metachronous occurrence (see Figure 11).

Data from both data sets indicate that metachronous adenomas tend to occur around the same area as the index adenoma, however a very slight distal drift was found in multiple adenoma analyses, whereas a stronger proximal drift was observed in single adenoma analyses.

It is probable the multiple adenoma analyses were not as accurate for proximal and distal occurrence calculation as the single adenoma analyses due to the problems mentioned in 3.3.1. Taken together this data contributes to the

evidence a field effect may exist and that model 1 (field interaction) is the most likely mechanism for metachronous adenoma occurrence. Metachronous occurrence as a consequence of model 2 (micrometastatic migration) remains a possibility but unlikely given that adenomas are benign and therefore, by definition, do not metastasize. Although, one would expect greater distal metachronous occurrences if models 3 and 5 were responsible, this study has demonstrated the reverse. Metachronous adenoma formation due to model 4 (systemic sensitising molecule) is possible but we would expect the results from this study to reveal a stronger pancolonic representation. The proposed models are non-mutually exclusive and non-exhaustive; given the controversy over clonality of normal and neoplastic lesions and the karyotypic variations of adenomas, it is reasonable to propose there may be more than one mechanism for metachronous adenoma formation.

There are limitations to this study. The main limitation is the subjective colonic location according to the colonoscopist. This study did not document whether a tracker was used during the colonoscopy. The study was also retrospective and non-blinded therefore the colonoscopist may be influenced by reading the previous colonoscopy report detailing where previous adenomas were found, leading to a higher 'same segment' occurrence rate.

It has been reported that the likelihood for missed adenomas is greater in the proximal colon than distal colon (Laiyemo et al., 2011). The apparent increased percentage of proximal metachronous adenomas could be due to a high miss rate at index colonoscopy and subsequent detection at the next colonoscopy rather than metachronous occurrence. The miss rate of adenomas of any size has been reported as 22% (van Rijn et al., 2006) therefore up to 22% of our data for index and subsequent colonoscopy (R0 and R1) may be erroneous. The high apparent percentage of proximal metachronous occurrences can also be explained due to the high number of index adenomas in the rectum (as expected); since there is no way for a metachronous adenoma to occur more distally the only options are same segment and proximal occurrence. We aimed to reflect this through the probability calculation and although statistical significance cannot be assigned to

this calculation; it does support the mean segment calculation from analysis 4, which was statistically significant.

The segment sizes of the nine regions of the colon are different, for example the area of the splenic flexure is much smaller than the sigmoid and is therefore likely to have less polyps. This limitation cannot be corrected for but has been noted and must be considered during result interpretation.

The World Health Organisation (WHO) classifies adenomas into tubular (less than 20% villous architecture), tubulovillous and villous histological subtypes (Castells et al., 2009). The probability of high grade dysplasia and malignant transformation increases when polyp size exceeds 1cm or if they have a villous component (Bujanda et al., 2010). There is evidence to show that different histological subtypes follow different carcinogenesis pathways and have different distributions within the colon (Bauer and Papaconstantinou, 2008). Large villous adenomas, with a greater potential for malignant change are more likely to be found in the distal colon (Shussman and Wexner, 2014). Histological subtypes and size of the adenomas were not available for every record and therefore not included in the analysis. A better understanding for the likely cause of metachronous occurrence may be attained with the incorporation of histological subtypes and size in future studies. Adenoma size may be an important factor in relation to model 4 and 5 since adenomas greater than 1cm in size have been shown to influence metachronous adenoma occurrence and malignant change. It is possible that larger adenomas have the ability to secrete greater amounts of sensitizing molecule into the lumen or systemically. This suggestion is strengthened by the observation that 3 or more adenomas (with potentially greater sensitizing molecule secretion ability than one adenoma) are also a risk factor for recurrence (Noshirwani et al., 2000, Saini et al., 2006).

The database of adenoma positions and characteristics generated from this study was submitted for mathematical modelling. Preliminary results have shown metachronous adenoma occurrence from this dataset is not random (Yifan Zhao, personal communication, May 1, 2013). It may be possible to apply

mathematical models to predict positions of future metachronous occurrences. The mathematical modelling has not been performed as part of this MD, but is likely to provide an area for fruitful future research.

The mechanisms by which metachronous adenomas occur is still unknown, although adenoma characteristics, such as size and number associated with recurrence have been identified. A number of studies have identified a higher recurrence rate of adenomas in the proximal colon (Martinez et al., 2001, Laiyemo et al., 2011) however to date there is no published evidence regarding the location in which metachronous adenomas occur in relation to an index adenoma. Investigation of this relationship is unique to this study, the results of which suggest a cancerized field. Likely areas for future metachronous adenoma formation can be targeted during surveillance if a cancerized field has been detected and will determine subsequent treatment.

Keratin dysregulation has previously been described in fields around adenomatous polyps (Polley et al., 2006). In addition, previous studies have used K8 and K18 immunohistochemical staining of lymph nodes as predictors of recurrence in 'node-negative' colorectal cancer (Sasaki et al., 1997). Utilisation of K8 and K18 as predictors of recurrence in colorectal neoplasia is particularly relevant to this thesis. Investigating the locations for metachronous adenoma may enable prediction of recurrence and, equally, successful identification of abnormal K8 and K18 in the pre-adenomatous field could allow prediction of recurrence.

3.6 Summary

3.6.1 Conclusion

- Metachronous adenoma occurrences are likely to be in a similar segment to the index adenoma.
- Development of adenomas in the same area suggests field interaction predisposes to adenoma formation, as fields are left behind following polypectomy.
- Slightly more proximal metachronous adenoma formation emphasises the clinical importance of full colonoscopy (to the caecal pole).

3.6.2 Limitations

- Colonic location is subjective to the colonoscopist, who can only be confident of scope location at the rectum and caecum.
- The colonoscopist was not blinded and thus subject to bias based on previous colonoscopy findings.
- A high miss rate at index colonoscopy can produce inaccurate and high metachronous rates.
- Data was not available for histological subtypes or size of adenomas and therefore could not be adjusted for.

Chapter 4

Development of an integrated workflow for extraction and solubilization of intermediate filaments from colorectal biopsies for proteomic analysis

Chapter 4 Development of an integrated workflow for extraction and solubilization of intermediate filaments from colorectal biopsies for proteomic analysis

4.1 Introduction

Proteomic analysis

Quantitative proteomic methods include isobaric tags for relative and absolute quantification (iTRAQ), stable isotope labelling by amino acids in cell culture (SILAC) and isotope coded affinity tag (ICAT). A mass spectrometry based proteomic technique was chosen to investigate protein differences between cancerized field and normal tissue due to the complexity of proteins in mucosal samples. The way in which keratins differ in a cancerized field is unknown and therefore many peptides were analysed to highlight which keratins deserve focused investigation.

ITRAQ is an isobaric labelling method used in quantitative proteomics by tandem mass spectrometry to determine the amount of peptides from different sources in a single experiment. It uses stable isotope labelled molecules that are covalently bonded to the N-terminus and lysine side chains of peptides (Evans et al., 2012). ITRAQ was employed in this study due to its numerous advantages. It can both identify and quantify thousands of peptides in a relatively short period of time in comparison to 2D gel electrophoresis. In comparison to SILAC, where samples have to labelled *in vivo* or in cell culture, iTRAQ allows labelling of the mucosal samples *ex vivo*, which is imperative for endoscopic-biopsy obtained samples. ITRAQ also has the advantage over SILAC and ICAT in that it can also detect post-translational modifications, which are especially relevant in the study of keratins. The principal advantage over ICAT and SILAC is that many samples can be labelled and analysed simultaneously thereby reducing the amount of mass spectrometry time required for analysis. A disadvantage of iTRAQ in comparison to SILAC is that samples for analysis must be prepared according to a strict multi-step protocol, which is therefore open to processing error.

Intermediate filaments

Intermediate-sized filaments (IF) are among the most insoluble intracellular protein polymer structures (Soellner et al., 1985). Keratins are a major component of IF, of which only 5% are found in the soluble form (Chou et al., 1993). Conventionally, keratins are dissolved in urea (Achtstaetter et al., 1986) but this presents a problem in isobaric tags for relative and absolute quantification (iTRAQ) analysis as urea inhibits proteolytic digestion by trypsin. No IF solubilisation protocols, compatible with iTRAQ processing, have been published. There is therefore an unmet need for a standardized and proven protocol for extraction of insoluble intermediate filaments and preparation for iTRAQ methodologies. This protocol must also enable simultaneous trypsin digestion and preservation of post-translational modifications.

4.2 Aims and Objectives

- To develop a solubilisation protocol for intermediate filaments enabling the analysis of keratins using iTRAQ.
- To demonstrate that the protocol devised produces a final protein yield and protein profiles similar to that of a protocol using urea as the solvent.

This work was undertaken collaboratively and the work described above was carried out with equal contribution. Demonstration of preservation of post-translational modifications was carried out by Debabrata Majumdar, a member of our group.

This work is now published:
Majumdar, D., Rosser, R., Havard, S., Lobo, A. J., Wright, P. C., Evans, C. A. & Corfe, B. M. 2012. An integrated workflow for extraction and solubilization of intermediate filaments from colorectal biopsies for proteomic analysis. *Electrophoresis,* 33**,** 1967-74. (See Appendix 4)

4.3 Materials and Methods

4.3.1 Materials

Low detergent buffer

Low detergent buffer (LDB) was prepared by combining the following:

5mL High Performance Liquid Chromatography (HPLC) grade water;

500µL 10x Phosphate Buffered Saline (PBS);

500µL 1M pH 7.0 3-(N-morpholino)propansulfonic acid (MOPS);

100µL 1M (magnesium chloride) $MgCl_2$;

200µL 100mM ethylene glycol tetra-acetic acid (EGTA) and 150µL 10% (v/v) Triton x-100 in water.

Further HPLC grade water was added to make up the total volume to 10mL.

Phosphatase inhibitor composed of: 100µL phosphatase inhibitor cocktail 2 (P5726); 100µL 2mM sodium β glycerophosphate; 100µL 2mN sodium pyrophosphate decahydrate. 100µL 10mM sodium fluoride was added just before use.

All chemicals were supplied by Sigma Aldrich, Dorset, UK.

High detergent buffer

High detergent buffer (HDB) was prepared by combining the following: 5mL HPLC grade water; 500µL 10xPBS; 500µL 1M pH 7.0 MOPS; 100µL 1M $MgCl_2$; 10µL 100mM Pefabloc (Roche Diagnostics GmbH, Mannheim, Germany); 1mL 10% (v/v) Triton x-100 in water and 2mL 5M NaCl. Further HPLC grade water was added to make up the total volume to 10mL.

Phosphatase inhibitor and 20µL Benzonase Nuclease (Novagen, Merck Chemicals Ltd., Nottingham, UK) were added just before use.

All chemicals (unless otherwise specified) were supplied by Sigma Aldrich, Dorset, UK.

Wash buffer

Wash buffer was prepared by dissolving 40µL 1M MgCl$_2$ and 10µL 100mM Pefabloc (Roche Diagnostics GmbH, Mannheim, Germany) in 19.95ml phosphate buffered saline (PBS).

All chemicals (unless otherwise specified) were supplied by Sigma Aldrich, Dorset, UK.

MCF7 growth media

1640 RPMI media (GIBCO, Invitrogen Paisley, UK) supplemented with heat-deactivated foetal calf serum (Biosera, Sussex, U.K.) and 5% (v/v) Penicillin (10000 units/mL) and streptomycin (10000 µg/mL).

10M Urea

10M urea was prepared by dissolving 6g of urea (Sigma Aldrich, Dorset, UK) in 10ml of distilled water, pipetted into 1mL aliquots and stored at -20°C.

4M Guanidine Hydrochloride

4M guanidine hydrochloride (GuHCl) was prepared by dissolving 0.38g of GuHCl (Sigma Aldrich, Dorset, UK) in triethylammonium bicarbonate buffer (TEAB) at a pH of 8.5 (Sigma Aldrich, Dorset, UK).

4.3.2 Maintenance of MCF7 cells

MCF7 cells (a human breast adenocarcinoma cell line) were used as a source of biological material in method development. MCF7 cells, maintained in-house (originally purchased from ATCC, Middlesex, UK) were cultured in T75 flasks using RPMI growth media. The cells were passaged twice weekly by removing growth medium from the flask and following an in-house protocol for cell culture. Cells were washed in the T75 flask using 10mL phosphate buffered saline (Sigma-Aldrich, Dorset UK) and then incubated with 2.5ml of 0.25% trypsin- 0.53mM EDTA solution (Invitrogen, Paisley, UK) for two minutes at 37°C. The cells were dislodged from the flask and suspended in RPMI growth

media. The cell suspension was centrifuged at 400g (Sanyo, Harrier 18/80 centrifuge). The supernatant was decanted and the remaining cells re-suspended in RPMI growth medium. The suspension was divided into five T75 flasks and the total volume made up to 10mL with RPMI growth medium and returned to the incubator.

4.3.3 Isolation of intermediate filaments from MCF7 cells

Intermediate filaments were isolated from cells which were established at 70-80% confluence. A modified version of the technique used by Achtstaetter et al., was used (Achtstaetter et al., 1986). Growth media was removed from the T75 flask and cells rinsed three times with 3mls wash buffer. 1mL of LDB was added to each flask and swilled for 90 seconds; the buffer was then removed and stored in LoBind Eppendorfs (Eppendorf AG, Hamburg, Germany) to minimise protein loss via binding to the Eppendorf tube. The T75 flasks were incubated on ice for 10 minutes with 1mL of HDB. After 10 minutes 250μL of ice cold sodium chloride (5M) was added to the flask. The resultant wash mixture was pipetted against the flask to detach the monolayer of cells. The cell mixture was aspirated and transferred to Eppendorfs. Eppendorfs were centrifuged at 100000 RCF for 10mins at 4°C. The supernatant (high salt soluble fraction) was pipetted off and aliquoted in Eppendorfs. The remaining pellet of cytoskeletal-intermediate filament within the Eppendorf was labelled and stored for later analysis. All fractions were stored at -80°C until analysis.

4.3.4 Removal of guanidine hydrochloride

When MCF7 intermediate filaments dissolved in 4M GuHCl were mixed with Laemmli buffer (prior to running SDS-PAGE gel) a precipitate was seen. This precipitate was found to interfere with SDS-PAGE gel and Coomassie staining. Efforts to prevent precipitate formation were made by removing GuHCl from the sample once the intermediate filaments were in solution. GuHCl was removed from the dissolved samples using a commercial preparation kit (Pierce® SDS-PAGE Sample Prep Kit (Pierce Biotechnology, Rockford, IL, USA)) according to the manufacturer's protocol.

Guanidine hydrochloride was also removed from colonic samples, once the

intermediate filaments were in solution, using Pierce® SDS-PAGE Sample Prep Kit (Pierce Biotechnology, Rockford, IL, USA) prior to running SDS-PAGE gel and Coomassie stain.

4.3.5 MCF7 – intermediate filament solubility comparison

Coomassie stains were performed to assess whether the protein concentration of intermediate filaments dissolved in GuHCl was comparable to the concentration dissolved in urea. Intermediate filament proteins dissolved in GuHCl were processed using the Pierce®SDS-PAGE Sample Prep Kit. Protein samples eluted in the last step were heated at 95°C for 5 min with non-reducing lane marker (provided with the kit) and loaded onto 12% SDS gels and analysed as previously described by Laemmli (1970). Coomassie stains were performed on SDS-PAGE gels using Instant Blue (Expedeon, Harston, UK). Coomassie band intensities of MCF7 intermediate filaments dissolved in varying concentrations and volumes of urea and GuHCl were compared.

4.3.6 Isolation of intermediate filaments from colonic biopsies

A similar protocol for isolation of intermediate filaments from colonic biopsies was devised based on the protocol for isolating intermediate filaments from MCF7 cells.

Colonic biopsies were homogenised with LDB using Precellys™ 24 (Bertin Technologies, Villeurbanne, France) at 6000 rpm, 30sec, 2 cycles (20sec rest in between cycles). The resulting lysate was removed and centrifuged. The supernatant was stored as fraction 1 (the soluble and extractable membrane protein fraction). The isolation and analysis of fraction 1 was carried out by Lisa Croucher, a member of our group as part of another research project.

The remaining pellet following centrifugation was washed with more LDB and re-suspended in HDB (with Benzonase® Nuclease, (Novagen®, Merck Chemicals Ltd., Nottingham, UK) added at this stage to remove viscous nucleic acids) followed by incubation on ice for 10 minutes. The pellet in HDB solution was centrifuged to yield a supernatant - the high salt soluble protein (fraction 2). The residual pellet was stored as the insoluble cytoskeleton fraction – intermediate

filaments (fraction 3). All fractions were stored in LoBind Eppendorfs (Eppendorf AG, Hamburg, Germany) at -80°C until analysis. Prior to analysis the residual pellet was dissolved in 4M GuHCl.

4.3.7 Colonic biopsy intermediate filament solubility comparison

Protein (from colonic samples) eluted in the last step of Pierce sample prep kit was heated at 95°C for 5 min with non-reducing lane marker and analyzed on 12% SDS-PAGE gels, as previously described in 4.3.5. Coomassie stains were performed using Instant Blue (Expedeon, Harston, UK) for protein detection; band intensity was used as an indicator of protein quantity. Coomassie band intensities of colonic intermediate filaments in varying concentrations and volumes of urea and GuHCl were compared. A proportion of intermediate filament samples were also sonicated (Bioruptor Sonicator, Diagenode, Cambridge, UK) in iced water for 30 seconds for five cycles. Band intensities between sonicated and non-sonicated samples were compared to ascertain whether protein solubilisation and hence yield could be improved following sonication.

4.4 Results

Protein bands were identified around the set molecular weight markers of the manufacturer's lane marker. These proteins were found above 37kDa and above the 50kDa marker. The molecular weight of keratin 8 is 55kDa; keratin 18 is 45kDa and keratin 19 is 40kDa.

The band intensity of Coomassie stains were interpreted as a marker of protein yield (the stronger the band the more protein present). Coomassie stains performed without removal of GuHCl resulted in a precipitate that interfered with SDS-PAGE and reduced band intensities (Figure 23). Removal of GuHCl from solubilized intermediate filaments, using Pierce® prep kit, successfully prevented formation of the visible precipitate and allowed SDS-PAGE gels to be run on both the MCF7 and colonic tissue samples. Band intensities for MCF7 intermediate filaments dissolved in 4M GuHCl were comparable to that of 10M urea (Figure 24). These results enabled a similar protocol to be applied to colonic samples. Coomassie band intensities of colonic intermediate filaments solubilized in 4M GuHCl were stronger than those solubilized in 6M GuHCl (Figure 25). Colonic intermediate filaments dissolved in 4M GuHCl also produced similar band intensities as those dissolved in 10M urea (Figure 25). Efforts to increase protein yield by sonicating samples did not result in stronger band intensities (Figure. 26).

4.4 Results

4.4.1 MCF7 intermediate filament solubility comparison
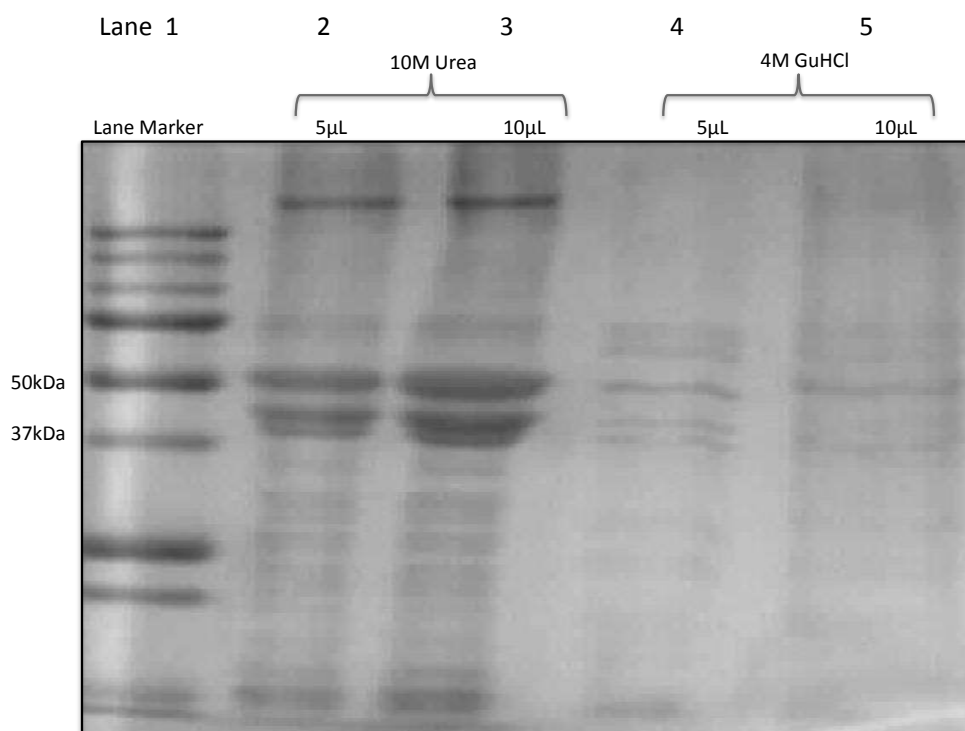
Figure 23. Coomassie stain of MCF7 dissolved in 10M urea and 4M guanidine hydrochloride.

Lane 1 = lane marker indicating molecular weights of proteins

Lane 2 = 5μL of MCF7 sample dissolved in 10M urea.

Lane 3 = 10μL of MCF7 sample dissolved in 10M urea

Lane 4 = 5μL of MCF7 sample dissolved in 4M GuHCl

Lane 5 = 10μL of MCF7 sample dissolved in 4M GuHCl.

The strongest- staining bands seen in lanes 2-5 are around molecular weight markers 37kDa and 50 kDa where keratins 8, 18 and 19 (55kDa, 45kDa and 40kDa respectively) would be expected. The band intensities of lanes 2 and 3 are stronger than lanes 4 and 5 indicating urea is a better solvent than GuHCl for protein identification. The band intensity of lane 3 (10μL of dissolved sample loaded) is stronger than lane 2 indicating more than 5μL of dissolved sample should be loaded for better protein identification. The reduced band intensities in GuHCl samples (lanes 4 and 5) are thought to be due to interference from precipitate formation without Pierce kit clean up.

4.4 Results

4.4.2 MCF7 removal of guanidine hydrochloride
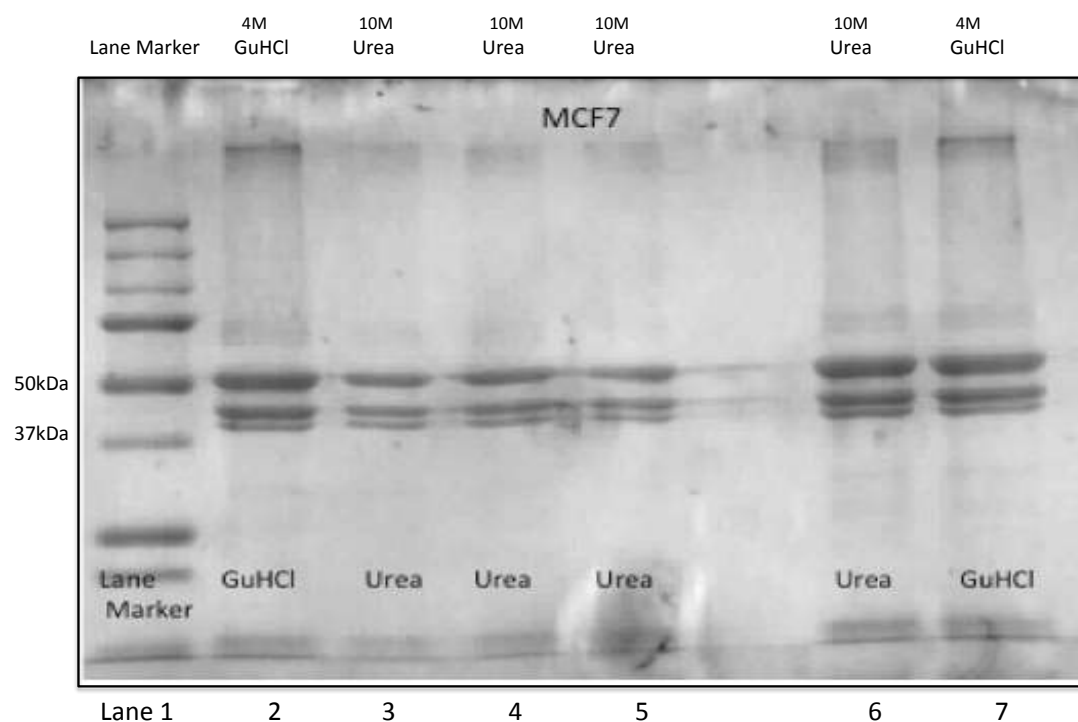
Figure 24. Coomassie stain of MCF7 dissolved in 10M urea and 4M guanidine hydrochloride with Pierce kit clean up.

Lane 1 = lane marker

Lane 2 = 20μL of MCF7 sample dissolved in 4M GuHCl

Lane 3 = 20μL of MCF7 sample dissolved in 10M urea

Lane 4 = 20μL of MCF7 sample dissolved in 10M urea

Lane 5 = 20μL of MCF7 sample dissolved in 10M urea

Lane 6 = 20μL of MCF7 sample dissolved in 10M urea

Lane 7 = 20μL of MCF7 sample dissolved in 4m GuHCl

The same sample was loaded into lanes 3-6 to ensure reproducibility; there were abundant amounts of sample to allow this.

The band intensities of samples dissolved in GuHCl (lanes 2 and 7) are now comparable to the band intensities of samples dissolved in urea (lanes 3-6). Again, as per Figure 23 proteins with the molecular weights where keratin 8, 18 and 19 would be expected are seen. These results indicate removal of GuHCl prevented precipitate formation and thus comparable band intensities to urea were achievable when using GuHCl as a solvent. These results enabled the isolation protocol to be applied to colonic biopsy tissue.

4.4 Results

4.4.3 Colonic biopsy solubility comparison
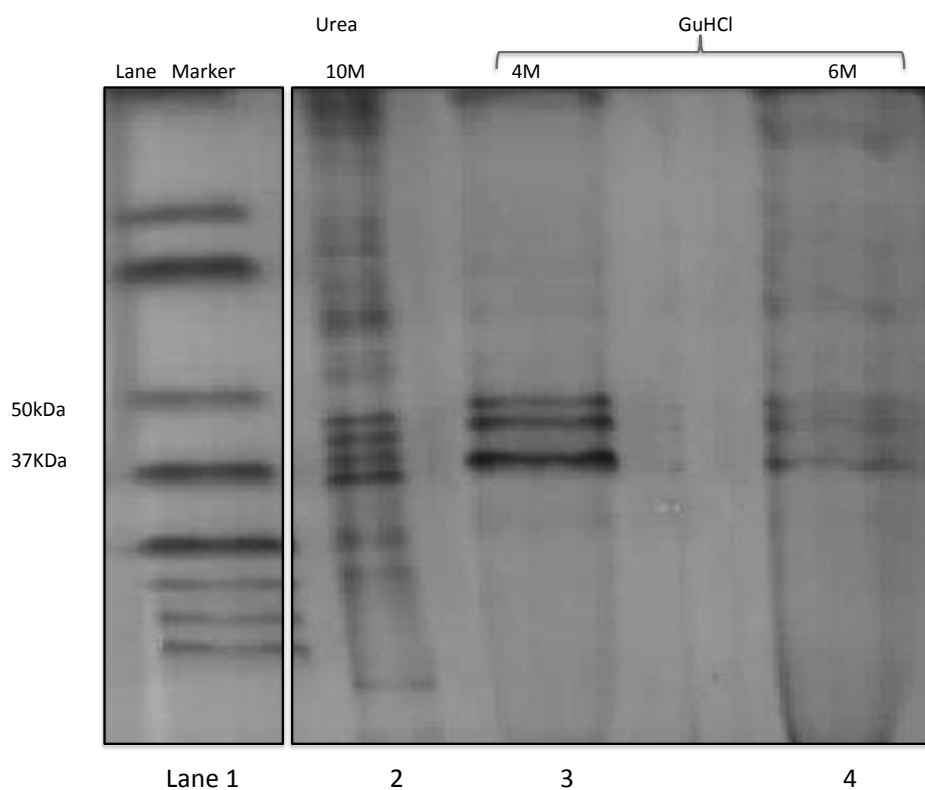
Figure 25. Coomassie stain of colonic biopsies in 6M guanidine hydrochloride.

Coomassie stain of colonic biopsies dissolved in urea and GuHCl revealed similar band intensities to MCF7 cells particularly in the molecular weight region 37-50kDa. Band intensity was not increased by increasing molar concentration of 6M GuHCl.

Lane 1 = lane marker to indicate molecular weights

Lane 2 = colonic biopsy sample dissolved in 10M urea

Lane 3 = colonic biopsy sample dissolved in 4M GuHCl

Lane 4 = colonic biopsy sample dissolved in 6M GuHCl

The strongest band intensity for that molecular weight region was seen in lane 3 (sample dissolved in 4M GuHCl) indicating the higher molar concentrations of GuHCl used in lane 4 are not required for enhanced protein detection. More proteins outside of the molecular weight region of interest were identified in samples dissolved in urea (lane 2) as evidenced by bands seen above and below 55kDa and 37kDa. The proteins of interest (keratins) are thus well represented in 4M GuHCl dissolved samples.

4.4 Results

4.4.4 Colonic biopsy sonication
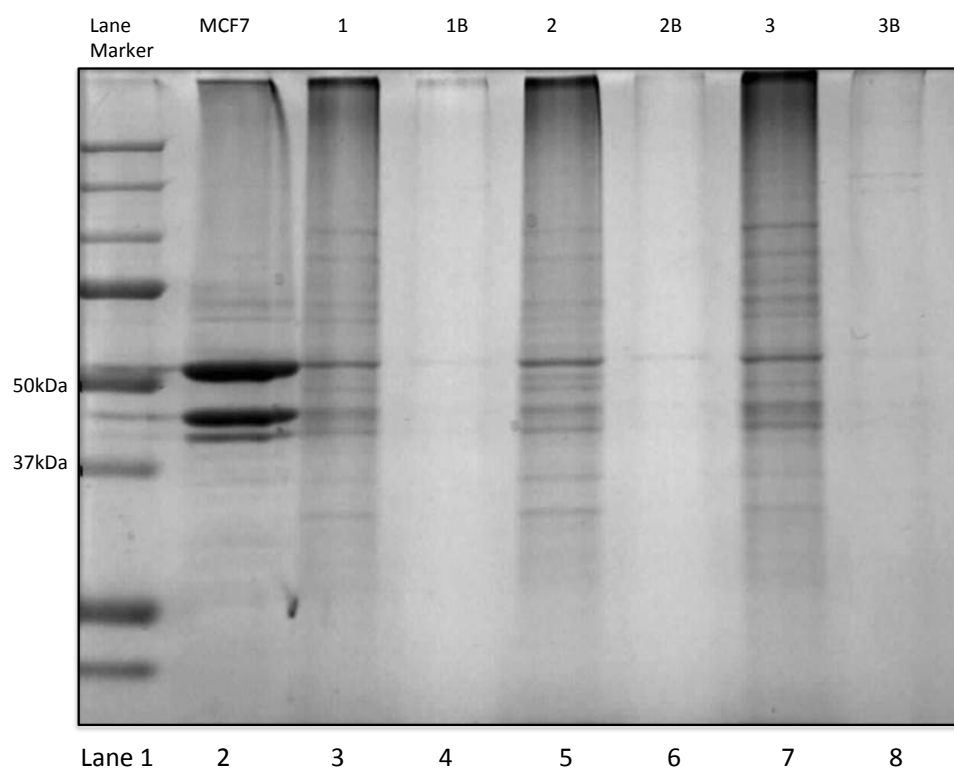
Figure 26. Coomassie stain of colonic biopsies in 4M guanidine hydrochloride with Pierce clean up and sonication.

MCF7 control sample and colonic biopsies were all dissolved in 200μL of 4M GuHCl, labelled MCF7 and samples 1-3, respectively. A further 200μL of 4M GuHCl was added to any undissolved sample material and sonicated, these samples were loaded onto the gel as 1B, 2B and 3B. The band intensity pattern reveals sonication did not improve band intensity.

Lane 1 = lane maker

Lane 2 = MCF7 dissolved in 200μL of 4M GuHCl

Lane 3 = colonic biopsy sample 1 dissolved in 200μL of 4M GuHCl

Lane 4 = colonic biopsy sample 1 sonicated and dissolved in 200μL of 4M GuHCl

Lane 5 = colonic biopsy sample 2 dissolved in 200μL of 4M GuHCl

Lane 6 = colonic biopsy sample 2 sonicated and dissolved in 200μL of 4M GuHCl

Lane 7 = colonic biopsy sample 3 dissolved in 200μL of 4M GuHCl

Lane 8 = colonic biopsy sample 3 sonicated and dissolved in 200μL of 4M GuHCl

4.5 Discussion

A successful protocol was developed for the solubilisation of IF, using 4M Guanidine hydrochloride as the solvent. As previously discussed urea is not iTRAQ compatible as it interferes with trypsin digestion. Guanidine hydrochloride permits trypsin digestion but forms an insoluble precipitate (guanidine dodecylsulphate) by reacting with SDS in Laemmli buffer. Removal of guanidine hydrochloride following solubilisation using a clean up kit enables both SDS page gels and iTRAQ to be performed. Sonication of solubilized and Pierce cleaned colonic biopsy samples did not increase protein yield. These experiments were performed in collaboration with Dr Debrabata Majumdar, up to this point our contribution was equally divided. Dr Majumdar continued the experiments to successfully demonstrate that post-translational modifications were preserved using this protocol by using western immunoblot. The proteins from the colonic biopsy samples dissolved in GuHCl seen at 37 and 50 kDa on Coomassie stain were also demonstrated to be immunoreactive to keratin 8 antibody. This work is now published (Majumdar et al., 2012a), (Appendix 4).

4.6 Summary

1. A protocol was successfully devised to allow solubilisation of colonic biopsies.

2. The protocol devised:
   - uses an iTRAQ compatible solvent - Guanidine hydrochloride
   - requires 'cleaning up' of precipitate guanidine dodecylsulphate
   - produces a similar protein yield and protein profile to that of urea
   - enables the preservation of post-translational modifications

Chapter 5

Application of isobaric Tags for Relative and Absolute Quantification (iTRAQ) proteomics for the detection of molecular changes underlying field effects.

Chapter 5 Application of ITRAQ proteomics for the detection of molecular changes underlying field effects

5.1 Introduction

Previous research into colorectal neoplasia has compared tumour tissue to normal tissue from the same patient, with the assumption that the macroscopically normal tissue is equivalent to that of healthy tissue from disease free patients. Recent investigations in field effects indicate this may be a misguided approach. Numerous studies have shown that the characteristics of tumour tissue are more similar to the field tissue around it than tissue from pathology-free patients. Badvie et al., found anti-apoptotic protein levels were raised in cancer adjacent to normal colonic mucosa and cancer in comparison to mucosa from disease-free colons (p<0.001) (Badvie et al., 2006, Jothy et al., 1996, Shen et al., 2005). Particularly relevant to this study is the overexpression of keratins found in adenoma and field tissue when compared with normal disease-free tissue (Polley et al., 2006).

In addition, work from our group has found an association between butyrate and keratin expression in colorectal cancer (Khan et al., 2011).

To investigate further the association between keratins, butyrate and the cancerized field a proteomic approach was used. 8 plex isobaric tags for relative and absolute quantification (iTRAQ) is a gel free approach that allows simultaneous protein identification and relative quantification of up to eight sample groups. 2-D Gel electrophoresis (2DGE) is a proteomic approach that separates proteins by mass and charge and could have been employed in this study but co-migration of similar proteins may not identify keratin changes and this creates difficulties in reproducing results through 2DGE. Furthermore, iTRAQ is superior to 2-D Gel Electrophoresis (2DGE) for identification of significantly larger protein quantities and is also able to distinguish between proteins with similar biophysical properties (Wu et al., 2006). ITRAQ also has the advantage of allowing cell labelling *ex vivo* and identification of post-translational modifications. The insoluble fraction of a colonocyte after cell lysis is enriched in intermediate filaments and in particular keratins; this fraction has

not been previously examined in isolation in the context of a cancerized field. ITRAQ is particularly useful for identification of peptide differences between tissues when the change is unknown, since iTRAQ has the ability to identify and quantify thousands of peptides simultaneously. In this study the insoluble fraction differences between the cancerized field, adenoma and normal tissue are unknown therefore iTRAQ is especially valuable. The apparent advantage of identifying thousands of peptides also highlights the need for validation experiments after iTRAQ to ensure the changes are not a chance occurrence.

5.2 Hypothesis and Aims

5.2.1 Hypotheses

- Keratins in adenoma tissue and the field around it are overexpressed when compared to normal tissue.
- Levels of keratin expression are butyrate dependent.

5.2.2 Aims

- To identify protein, particularly keratin and other intermediate filament-related changes in relation to adenoma proximity.
- To explore the relationship between colonic keratin expression and luminal butyrate concentration.

5.3 Materials and Methods

5.3.1 Materials

<u>Colonic biopsy material</u>

Archived colonic biopsy material from a previous study (FACT) in our group was used (Corfe et al., 2009). Briefly, endoscopic colorectal mucosal biopsies (≈5mg) were obtained during colonoscopy lists at Sheffield Teaching Hospitals NHS Trust. Ethics committee approval was obtained from the North Sheffield Research Ethics Committee (Reference number: 06/Q2308/93).
A biopsy strategy was followed for each patient (Table 4).

Table 4. Biopsy strategy

Diagnosis	Biopsy position (abbreviation)	Other samples
Normal	2 x mid-sigmoid (N)	Stool for Butyrate Biopsy for IHC
Adenoma	2 x mid-sigmoid (MS)	Stool for Butyrate Biopsy for IHC
	2 x contralateral wall (CO)	Biopsy for IHC
	2 x adenoma (AD)	Biopsy for IHC

16 subjects in total were included in this study. Biopsies from 8 patients with histologically confirmed adenomatous polyps were used. In patients with adenomas two biopsies were taken from the adenoma itself (AD); from the macroscopically normal mucosa on the contralateral wall to the adenoma (CO) and from the mid sigmoid colon (MS). Biopsy material from 8 patients with no lesions or other pathology within the colon was also included. For these subjects a single biopsy from the mid sigmoid colon was taken. For biopsy locations see Figure 27.

Faecal butyrate levels

The subjects, from which biopsies were taken, also provided a stool sample as part of the FACT study for assessment of faecal short chain fatty acid (SCFA) levels. Faecal butyrate levels were determined from the stool sample. Biopsy positions and the mean faceal butyrate level from which the biopsies were taken are shown in Table 5. The faecal butyrate levels recorded by the FACT study were used in this study to determine how patient samples were pooled (see 5.3.2.2.)
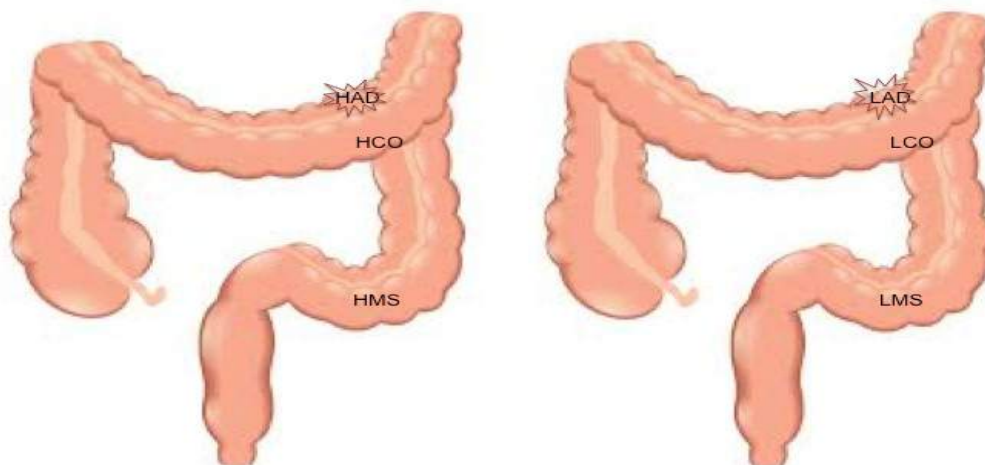
Figure 27. Biopsy locations in the colon

HAD = high butyrate adenoma, HCO = high butyrate contralateral and HMS = high butyrate mid-sigmoid. LAD = low butyrate adenoma, LCO low butyrate contralateral and LMS = low butyrate mid-sigmoid.

Table 5. Biopsy positions and butyrate levels

Diagnosis	Biopsy position	Butyrate Status	Mean faecal Butyrate concentration mM
Normal	Mid-sigmoid	High	20.5
	Mid-sigmoid		14.5
	Mid-sigmoid		13.9
	Mid-sigmoid		13.7
Adenoma	Adenoma, contralateral wall and mid-sigmoid	High	16.0
	Adenoma, contralateral wall and mid-sigmoid		13.2
	Adenoma, contralateral wall and mid-sigmoid		9.5
	Adenoma, contralateral wall and mid-sigmoid		8.8
Normal	Mid-sigmoid	Low	1.3
	Mid-sigmoid		1.0
	Mid-sigmoid		0.9
	Mid-sigmoid		0.7
Adenoma	Adenoma, contralateral wall and mid-sigmoid	Low	1.4
	Adenoma, contralateral wall and mid-sigmoid		1.0
	Adenoma, contralateral wall and mid-sigmoid		0.8
	Adenoma, contralateral wall and mid-sigmoid		0.6

Biopsy positions and the mean faecal butyrate (mM) environment from which the biopsies were taken. Faecal butyrate concentration was considered low at below 8mM and considered high at above 8mM.

All colonic biopsies had previously undergone homogenisation in low detergent buffer (LDB) using Precellys™24 at 6000rpm, 30 sec, 2 cycles, followed by removal of soluble and extractable membrane proteins (work performed by Lisa Croucher). Samples were processed from this pellet form according to the protocol described in section 4.3.6.

Intermediate filament isolation buffers

High detergent buffer (HDB), low detergent buffer (LDB) and 4M guanidine hydrochloride (GuHCl) were prepared as described in Chapter 4.

ITRAQ sample preparation solutions:

Tris-(2-carboxyethyl)phosphine(reducing agent – to break protein disulphide bonds)

Tris-(2-carboxyethyl)phosphine (TCEP) (Thermo Fisher Scientific, Rockford, IL, USA).

Methyl methanethiosulfonate(alklylating agent – to block cysteine)

Methyl methanethiosulfonate (MMTS) (Thermo Fisher Scientific, Rockford, IL, USA).

Trypsin (enzyme for protein digestion into peptides)

Trypsin Proteomics Grade (Sigma Aldrich, Dorset, UK)

iTRAQ buffers

Volumes as described in methods - all HPLC grade and purchased from Thermo Fisher Scientific, Rockford, IL, USA.

5.3.2 Workflow prior to iTRAQ
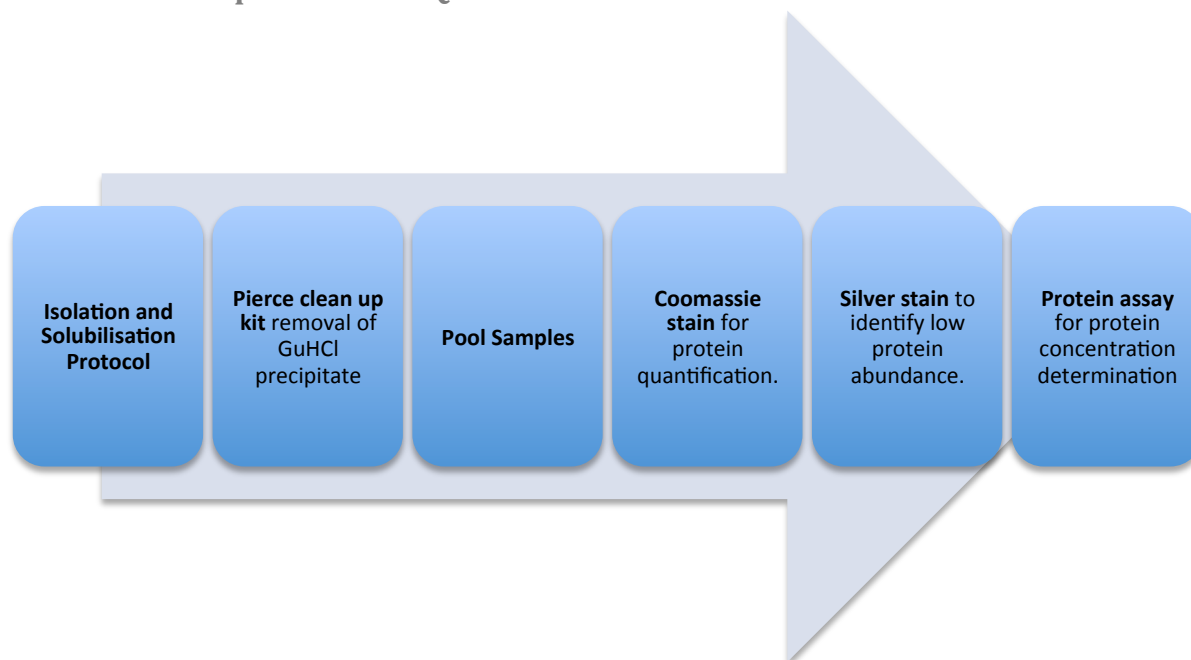
Figure 28. Workflow undertaken prior to iTRAQ analysis

5.3.2.1 Isolation and solubilisation protocol and Pierce clean up.

Samples were processed individually from pellet form according to the protocol described in Chapter 4.3.6. Following the isolation protocol samples were dissolved in 10μL 4M GuHCl and cleaned using a commercial preparation kit Pierce® SDS- PAGE Sample Prep Kit (Pierce Biotechnology, Rockford, IL, USA) according to the manufacturer's protocol.

5.3.2.2 Sample pooling

Following Pierce clean up the eluted protein samples were pooled together according to biopsy site and butyrate concentration. For example, 4 adenoma samples from the highest butyrate environment (highest butyrate concentration) were pooled together and 4 adenoma samples from the lowest butyrate environment were pooled together. Samples from the lowest butyrate environment in the whole archive were selected as 'low butyrate'. The mean faecal concentration of butyrate of the low butyrate group was below 2mM. Accordingly, samples with the highest mean butyrate levels in the whole archive were selected as 'high butyrate'. The mean faecal butyrate concentration for the high butyrate group was above 8mM. This was repeated for biopsies from the contralateral wall, mid-sigmoid and normal samples (Table 6). The pools

represent biopsy samples from highest and lowest butyrate concentrations and have been assigned to either high butyrate or low butyrate status. Half the volume of each pool was kept for validation experiments using western immunoblot.

Table 6. Pooled sample abbreviations and iTRAQ label

Biopsy site	High Butyrate		Low Butyrate	
	Abbreviation	iTRAQ label	Abbreviation	iTRAQ label
Adenoma	HAD	121	LAD	116
Contralateral	HCO	117	LCO	113
Mid-sigmoid	HMS	119	LMS	115
Normal	HN	118	LN	114

5.3.2.3 SDS PAGE and coomassie stain

Coomassie staining was performed to ensure adequate protein quantities were available for iTRAQ analysis. Results from Coomassie stains obtained in Chapter 4 were used as the standard to replicate.

2 μL of pooled protein samples were heated at 95°C for 5 min with a non-reducing buffer (provided with the Pierce kit) and loaded onto 12% SDS-PAGE non-reducing gels with 4% acrylamide stacker made and ran according to the protocol described by Laemmli (1970) (Laemmli, 1970). Coomassie stain was performed using Instant Blue (Expedeon, Harston, UK).

5.3.2.4 SDS PAGE and silver stain

SDS PAGE gel was run as described in 5.3.2.3. Silver stain was performed using Bio-Rad Silver Stain Kit (Hemel Hempsted, UK) using a modified protocol for 1.5mm polyacrylamide gel described by Chevallet et al., (2006) (Chevallet et al., 2006). The gel was immersed in reagents as described below (the volumes listed are suitable for performing Silver Stain in a 21cm x 21 cm x 5cm receptacle).

Reagent	Volume	Time
Fixative	40% methanol/10% acetic acid	400ml	60min
Fixative	10% ethanol/5% acetic acid	400ml	30min
Fixative	10% ethanol/5% acetic acid	400ml	30min
Oxidizer	Provided with kit	200ml	10min
Deionized water		400ml	10min
Deionized water		400ml	10min
Deionized water		400ml	10min
Silver Reagent	Provided with kit	200ml	30min
Deionized Water		400ml	2min
Developer	Provided with kit	200ml	Develop until solution turns yellow
Developer	Provided with kit	200ml	5min
Developer	Provided with kit	200ml	5min
Stop	5% acetic acid	400ml	5min

Figure 29. Modified protocol for Silver stain for 1.5 mm polyacrylamide gel.

116

5.3.2.5 Protein assay of colonic tissue samples

To determine exact protein concentrations protein assays were performed in triplicate on a 32 well plate using FLx 800™ multi detection micro plate reader; wavelength setting 595, 450 (Biotek, Bedfordshire, UK). Bovine serum albumin (BSA) stock solution was prepared by dissolving 15μg of BSA in 1ml of distilled water. Concentration standards (0, 0.3, 0.6, 1.2, 1.5, 1.8 and 2.1) were made by diluting BSA stock solution. 80μL of each standard and 20μL of Bio-Rad solution (Bio-Rad protein assay, Hemel Hempsted UK) was pipetted into each well. To avoid sample depletion samples were diluted to 1 in 10 prior to assay: 1.5μL of each colonic sample was diluted in 13.5μL of TEAB to make a 15μL volume of sample. 5μL of diluted sample was pipetted into individual wells, and 20μL of Bio-Rad solution and 75μL of distilled water were added to each well to make up the total volume to 100μL.

To account for the 1 in 10 dilution, prior to assay, protein concentration calculations were multiplied by a factor of 10.

5.3.3 ITRAQ

Sample preparation and peptide labelling

Sample volumes were calculated to standardise each sample to 60µg. Due to varying protein concentrations, the total volumes for each sample were variable. Samples were diluted to the equivalent of 2M GuHCl by adding the same volume of TEAB as the sample itself. Samples were reduced using TCEP (used at 1µL for every 10µL of sample) heated for 1 hour at 60°C and alkylated using MMTS (used at 1µL for every 20µL of sample). Samples were then trypsin digested at 1 in 20 ratio (3µg trypsin to 60µg sample) at 37°C overnight. Peptides were labelled according to the protocol outlined by Applied Biosystems (Framingham, MA, USA) and combined into a LoBind Eppendorf.

iTRAQ was performed using a standard operating procedure (S.O.P) see Appendix 5. An illustrated workflow of the iTRAQ process is shown in Figure 30.
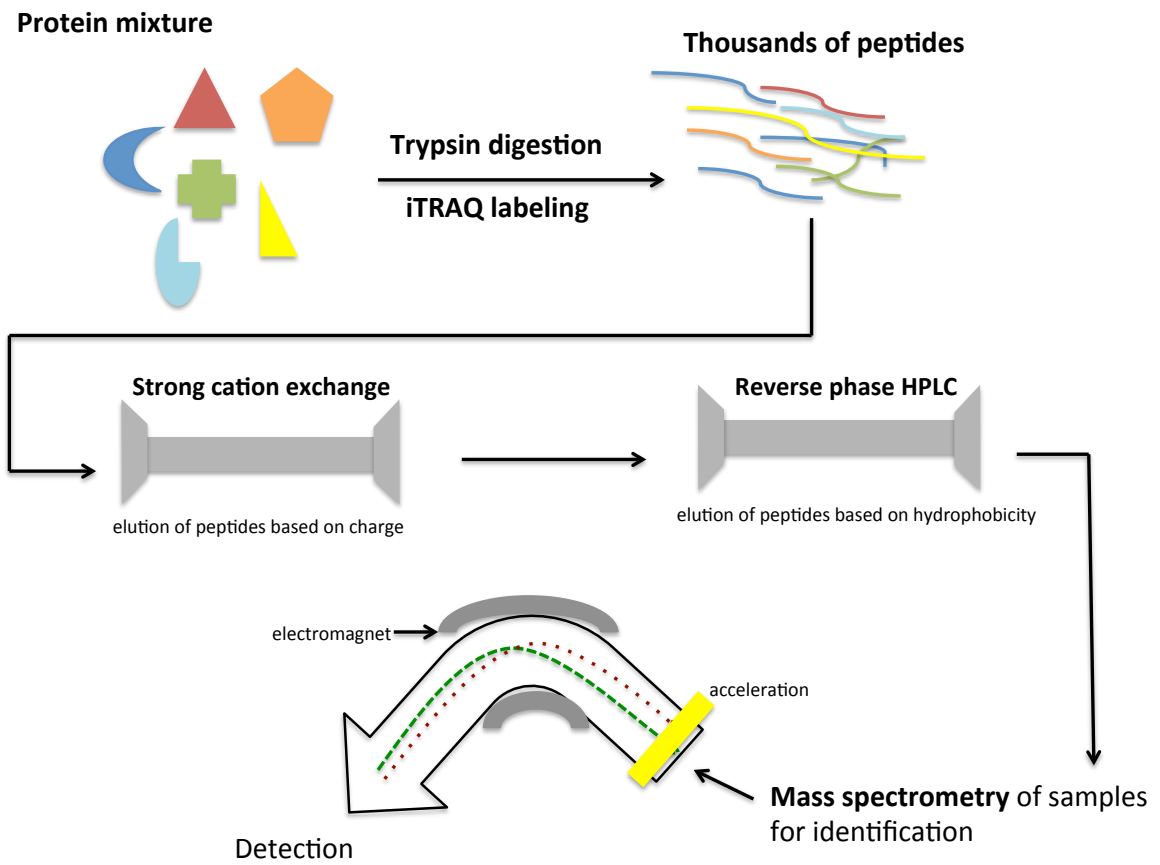
Figure 30. Illustrated iTRAQ proteomic workflow

5.3.4 Statistical analysis

Analysis of the relative abundance ratio between phenotypes was carried out using the significance testing algorithm, Signifiquant (S. Y. Ow et al., 2009). Quantification was obtained at a 95% confidence level from proteins identified by two or more peptides. An increased abundance of protein is signified by fold changes above a factor of 1 and a decrease in the abundance of proteins is indicated by fold changes below a factor of 1.

Hierarchical clustering and Principal Component Analysis was performed by Josselin Noirel (a member of our group) using Mathematic 7.0.0 for Mac. Data was grouped based on the degree of similarity between the samples.

5.3.5 Venn diagram plots

Identification of protein changes mediated by lesion proximity controlling for butyrate

Protein fold changes between macroscopically normal (MS, CO or N) and lesional (AD) samples were calculated individually (within their butyrate groups) and plotted on a Venn diagram using GeneVenn (2006)[1]. Thus protein fold changes between HAD and HCO; HAD and HMS; HAD and HN were identified and plotted on GeneVenn (2006) and a separate Venn diagram was plotted for the low butyrate group.

Identification of protein changes mediated by butyrate controlling for lesion proximity

Protein fold changes between high butyrate normal (HN) and adenoma (HAD) samples were plotted against low butyrate normal (LN) and adenoma (LAD) samples using GeneVenn (2006) to relate protein fold changes of LN and HN in comparison to their adenoma equivalents. Further plots were made for HMS and HAD compared with LMS and LAD and HCO and HAD compared with LCO and LAD.

---

[1] http://simbioinf.com/mcbc/applications/genevenn/genevenn.htm

5.4 Results

5.4.1 Coomassie stain - quality control

2 µL of pooled samples were loaded in each lane. Coomassie stain of the pooled samples (Figure 31) revealed faint band intensities in comparison to the results achieved in Chapter 4. No identifiable protein bands were seen where the proteins of interest (around 37 and 55kDa) would normally be expected. No conclusions regarding protein differences between pooled samples can be drawn from this experiment due to the lack of identifiable bands. Therefore, to ensure the presence of protein within the pooled samples Silver stain was used for its increased sensitivity as a colorimetric method for detection of total protein.
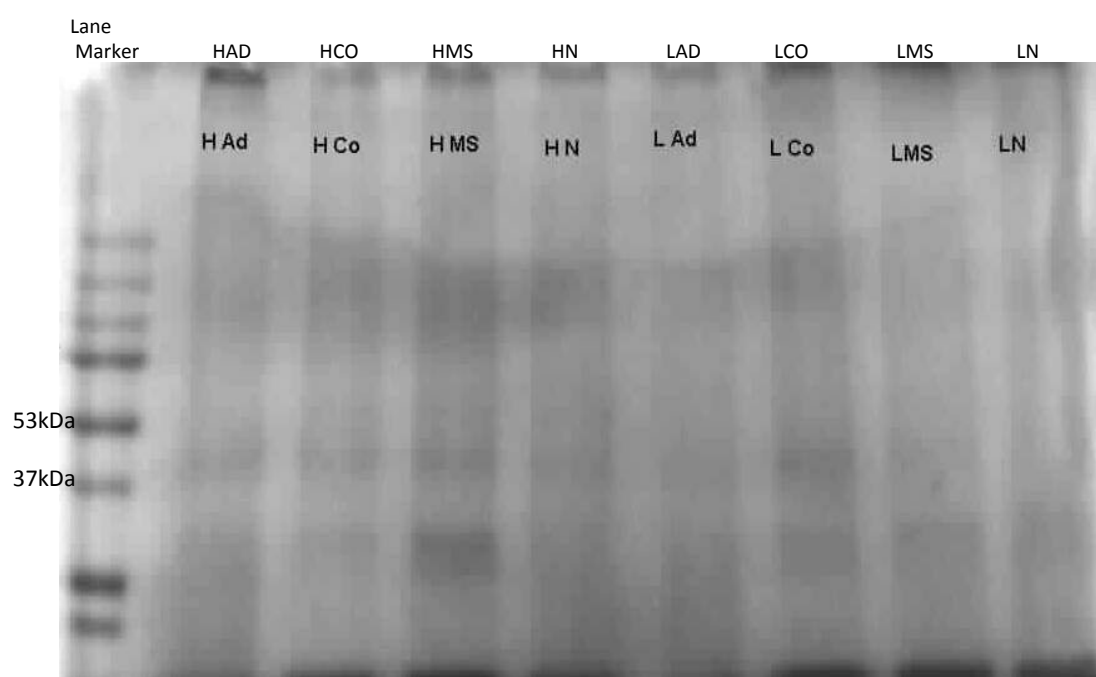
Figure 31. Coomassie stain of pooled samples

Coomassie stain revealed faint band intensities, suggesting inadequate protein.

HAD – high butyrate adenoma, HCO - high butyrate contralateral wall, HMS – high butyrate mid-sigmoid, HN – high butyrate normal, LAD – low butyrate adenoma, LCO – low butyrate contralateral, LMS – low butyrate mid-sigmoid and LN – low butyrate normal.

5.4 Results

5.4.2 Silver stain – quality control

Silver stain revealed negative staining (note very dark image on Figure 32). According to the manufacturers guide, this was due to overload of protein, suggesting adequate amounts of protein were loaded on to the gel. Results from this experiment imply protein quantities may be sufficient to proceed to iTRAQ analysis. Due to the poor quality staining, protein assay was performed to verify if protein quantities were sufficient.
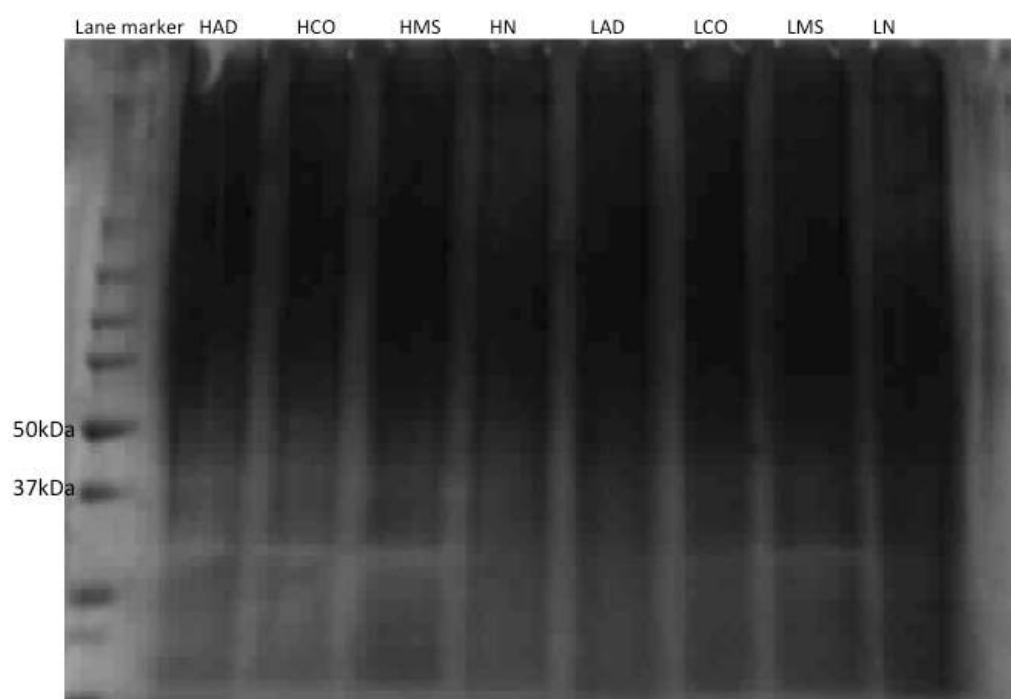
Figure 32. Silver stain of pooled samples

Silver stain revealed negative staining, possibly due to protein overload.

HAD – high butyrate adenoma, HCO - high butyrate contralateral wall, HMS – high butyrate mid-sigmoid, HN – high butyrate normal, LAD – low butyrate adenoma, LCO – low butyrate contralateral, LMS – low butyrate mid-sigmoid and LN – low butyrate normal.

5.4 Results

5.4.3 Protein assay – quality control

Protein assay of pooled samples revealed protein concentrations between 2.9μg/μL and 8.6μg/μL (Table 7). 25μg protein for each sample is required for iTRAQ analysis; these results show sufficient protein quantities are available for iTRAQ processing.

Table 7. Protein concentration and total protein of pooled samples.

Pooled sample	Protein concentration μg/μL	Total protein in 24μL
HAD	2.9	69.6
HCO	4.8	115.2
HMS	3.8	91.2
HN	8.0	192.4
LAD	3.0	72.0
LCO	8.6	206.4
LMS	5.8	139.2
LN	4.2	100.8

5.4 Results

5.4.4 iTRAQ fold change with respect to adenoma proximity

It is possible to make numerous iTRAQ comaparisons from simple individual pooled samples such as HAD compared with HCO (HAD vs HCO) or more complicated multiple comparisons such as differences between HAD and HCO compared with HN, LN, LCO (HAD & HCO vs HN, LN, LCO). For this study comparisons were kept simple such that meaningful differences in proteins could be identified.

Tissue from patients with adenoma pathology (HAD, HCO, HMS) demonstrated higher keratin 8 levels in comparison to normal tissue (HN) from pathology-free patients, irrespective of butyrate status (Table 8). The fold change of K8 progressively decreased with distance away from the adenoma. A similar trend was seen in keratin 18 samples. A statistically non-significant lower fold change was noted in the low butyrate mid-sigmoid sample for K18 (Table 9). K18 fold change also decreased with distance away from the adenoma. No fold change trend was seen for keratin 19. Pathological samples (HAD, HMS, HCO and LAD, LMS, LCO) all had higher keratin 8 and 18 levels in comparison to their respective normal samples (HN and LN) (Figure 33).

Table 8. Fold change in comparison to high butyrate normal sample.

High Butyrate	Adenoma	Contralateral	Mid-sigmoid
Keratin 8	1.22	1.12	1.10
Keratin 18	2.87	1.30	1.00*
Keratin 19	0.84*	0.88	0.45*

P< 0.01
* not significant

Table 9. Fold change in comparison to low butyrate normal sample.

Low Butyrate	Adenoma	Contralateral	Mid-sigmoid
Keratin 8	1.25	1.85	1.31
Keratin 18	1.46	1.42	0.71*
Keratin 19	0.82*	1.40	1.86*

P<0.01
* not significant

5.4 Results –iTRAQ
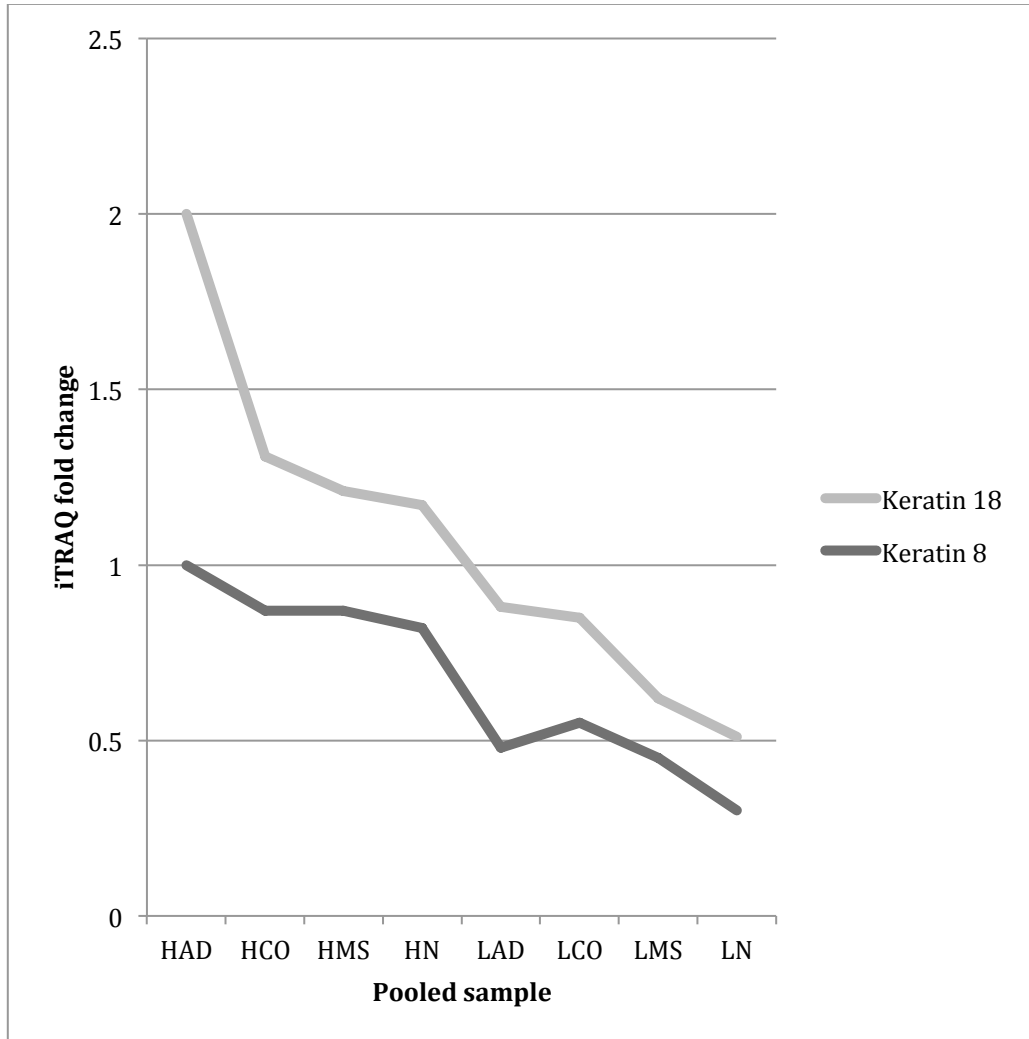
Figure 33. Graph of fold changes in keratin 8 and 18 levels

All samples were compared to high adenoma sample. Keratin 19 not shown since 4 of 6 results were not significant.

5.4 Results

5.4.5 iTRAQ fold change with respect to butyrate status

Fold change comparisons of all samples compared to high butyrate adenoma sample revealed higher keratin levels for both K8 and K18 in high butyrate samples in comparison to low butyrate samples (Figure 33). When samples were matched individually to compare butyrate status all samples from high butyrate environments were found to have higher keratin 8, 18 and 19 levels than their low butyrate equivalents (Table 10).

Table 10. ITRAQ fold change between samples matched for biopsy site

Keratin	HAD vs LAD	HCO vs LCO	HMS vs LMS	HN vs LN
K8	2.06 fold higher in HAD	1.49 fold higher in HCO	1.80 fold higher in HMS	2.53 fold higher in HN
K18	2.48 fold higher in HAD	1.36 fold higher in HCO*	1.81 fold higher in HMS	1.51 fold higher in HN
K19	1.64 fold higher in HAD	1.17 fold higher in HCO*	1.37 fold higher in HMS*	1.94 fold higher in HN

iTRAQ fold change between samples matched for biopsy site indicates the effect of butyrate on keratins.

P value < 0.01 for all fold changes except fold changes indicated with * were not significant

5.4 Results-iTRAQ

5.4.6 Hierarchical Cluster Analysis

Hierarchical cluster analyses were performed (Figures 34 and 35) using proteins identified by four or more peptides. Samples were clustered based on the similarity of the protein expression profiles in log2 of the iTRAQ ratios. The dendogram (Figure 34) indicates the relationship between samples; the shorter the branch length the greater the degree of similarity. It is apparent from this dendogram that samples from a high butyrate status cluster together, implying global levels of butyrate may exert stronger influences on the similarity of proteins than that of field effects.
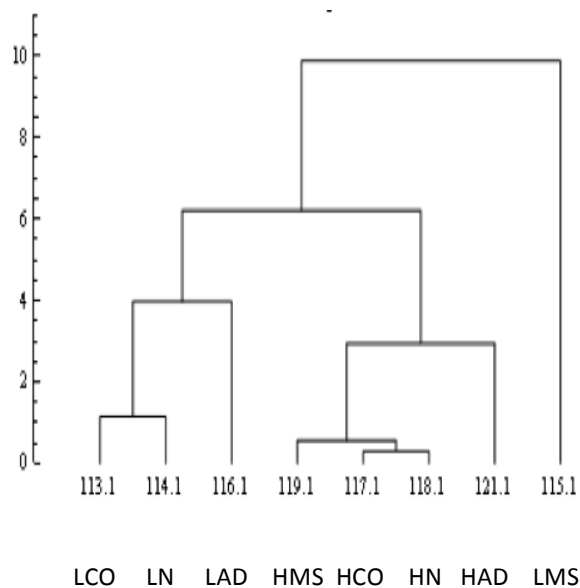
Figure 34. Dendogram of cluster analysis of biopsy samples

Clustering is based on branch points and branch lengths. iTRAQ labels were directly entered as data was to create the dendogram sample. The numerical labels correspond to the samples as follows: 113=LCO, 114=LN, 116=LAD, 119=HMS, 117=HCO, 118-HN, 121=HAD and 115=LMS. Samples LCO, LN and LAD form a co-cluster with LCO and LN forming a sub-cluster away form LAD. Samples HMS, HCO, HN and HAD form a co-cluster with HMS, HCO and HN forming a sub-cluster away from HAD.

5.4 Results- iTRAQ

5.4.7 Principal Component Analysis

Cluster analysis revealed the biopsies grouping together according to butyrate status. High butyrate samples gathered away from the low butyrate samples suggesting that butyrate status exerts a stronger influence over the characteristics of the biopsy than field effects.
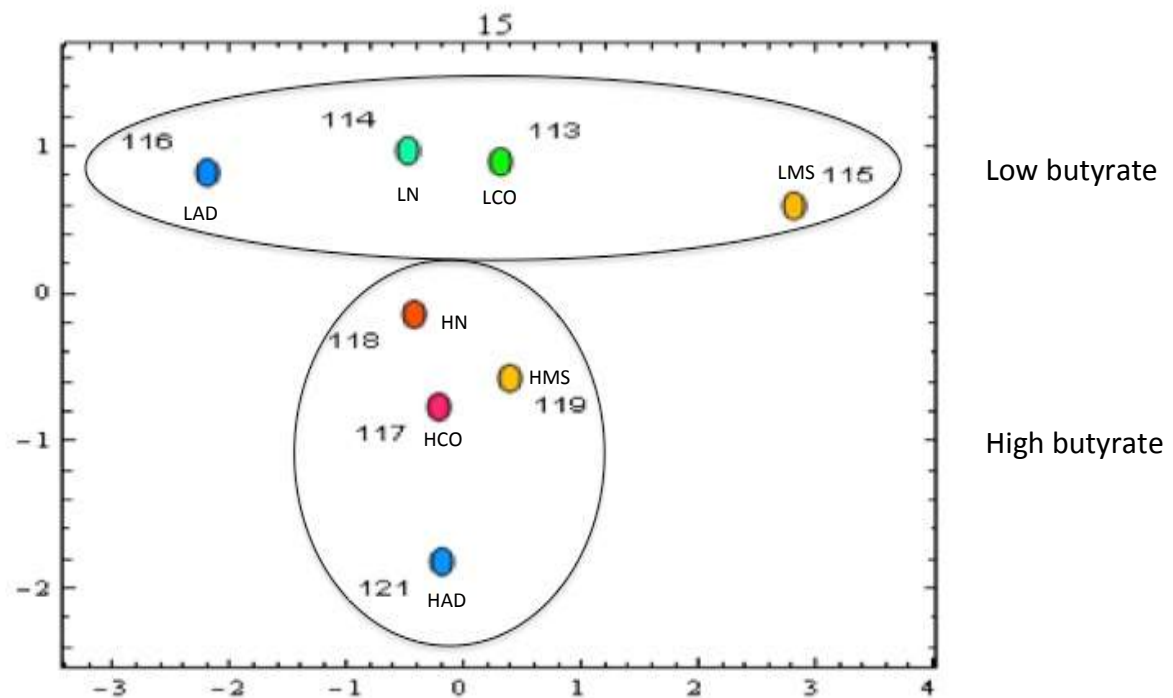
Figure 35. Cluster analysis of biopsy samples

Samples are seen clustering according to butyrate status.

Low butyrate samples: 116 LAD; 114 LN; 113 LCO and 115 LMS clustered away from high butyrate samples: 118 HN; 119 HMS; 117 HCO and 121 HAD, these results suggest the global influence of butyrate exerts a stronger influence over protein expression than field effects.

5.4.8 Identification of keratins and other proteins using iTRAQ

Since iTRAQ is capable of identifying and quantifying thousands of peptides simultaneously, proteins other than keratins were identified during analysis. This study specifies keratins as the proteins of interest but acknowledgment of the other proteins identified must be declared to further other studies and future directions for investigation. Exploring the protein profiles between samples allows them to be categorised according to similarities and may demonstrate a field effect. Detailed analysis of the proteins identified and their relationships were not carried out as part of this study. The full index of peptides identified is listed in Appendix 6.

5.4.9 Identification of protein changes mediated by lesion proximity controlling for butyrate

High butyrate

A Venn diagram of the high butyrate samples (Figure 36) illustrates the fold changes in proteins between HAD and macroscopically normal HN, HMS, HCO. Protein fold changes that are common to either HN, HMS and HCO compared with adenoma appear in overlapped circles. Protein fold changes that are unique to HN, HMS or HCO when compared with HAD appear in non overlapped circles. For example: the green circle illustrates 22 (5 +6 +9+ 2) total protein fold changes between HCO and HAD. Five protein fold changes between HAD and HCO are unique to HCO. Six protein fold changes between HAD and HCO are common with the protein fold changes found between HAD with HN. Nine protein fold changes are common to all histologically normal sample sites (HN, HMS and HCO) when compared with HAD. Two protein fold changes between HAD and HCO are common to the fold changes identified between HAD and HMS. The highest number of unique protein fold changes (non overlapped circles) were found between HCO and HAD (N=5) and suggests decrease in sample similarity with lesion distance HMS and HAD (N=2) and HN and HAD (N=2).

The protein profiles indicate HCO samples are more similar to HAD samples than either HMS or HN samples.

Low butyrate

A Venn diagram of the low butyrate samples (Figure 37) illustrates protein fold changes between LN, LMS, LCO compared with LAD. As before, the non-overlapped areas denote protein fold changes compared with adenoma site that are unique to that biopsy site (LN, LMS or LCO).

The greatest number of unique protein fold changes was between LAD and LMS (N=5). The number of unique protein fold changes was equal between LAD and LCO and LAD and LN (N=2). In the low butyrate environment protein profiles appear to have the greatest similarity between LAD and LMS. If field effects are exerted by lesion proximity we would expect LAD and LCO to share the greatest number of shared protein fold changes with numbers progressively decreasing from LMS to LN as per the high butyrate group. The results reveal field effect protein changes are not influenced by lesion proximity in the low butyrate environment.

5.4 Results - Identification of protein changes controlling for butyrate
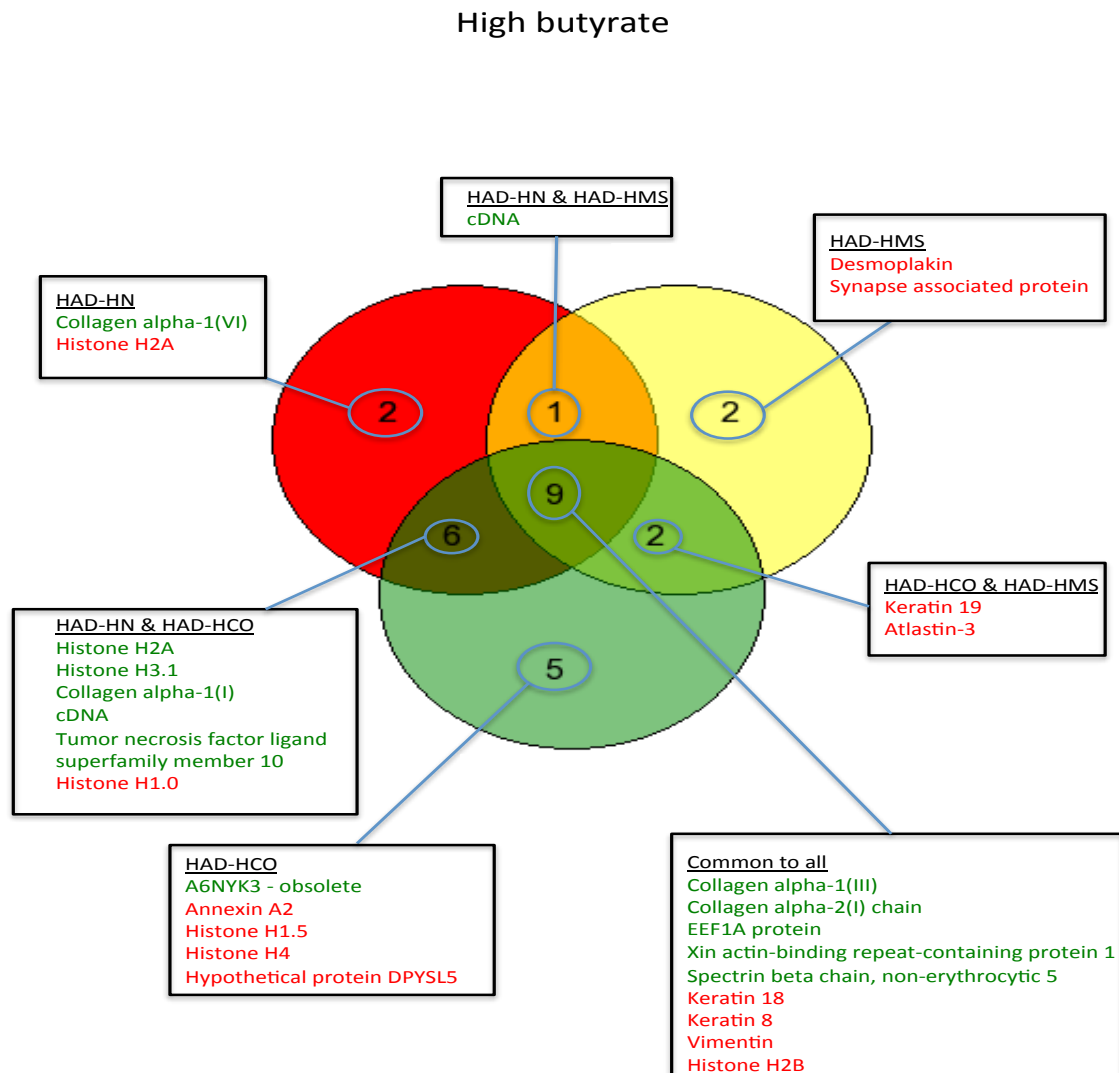
High butyrate

Figure 36. Venn diagram of protein fold changes in comparison to adenoma in high butyrate.

HCO, HN and HMS is compared to HAD. Up-regulated proteins are expressed in bold/green and down regulated proteins are expressed in red.

- 22 protein fold changes found in total between HAD and HCO (green circle)
- 18 protein fold changes found in total between HAD and HN (red circle)
- 14 protein fold changes found in total between HAD and HMS (yellow circle)
- 5 protein fold changes unique to HAD and HCO only and not found in other samples (non overlapped green)
- 2 protein fold changes unique to HAD and HN only and not found in other samples (non overlapped red)
- 2 protein fold changes unique HAD and HMS only and not found in other samples (non overlapped yellow)
- 9 protein fold changes are common to all samples
- other overlapping areas indicate protein fold changes common to those samples.

5.4 Results - Identification of protein changes controlling for butyrate
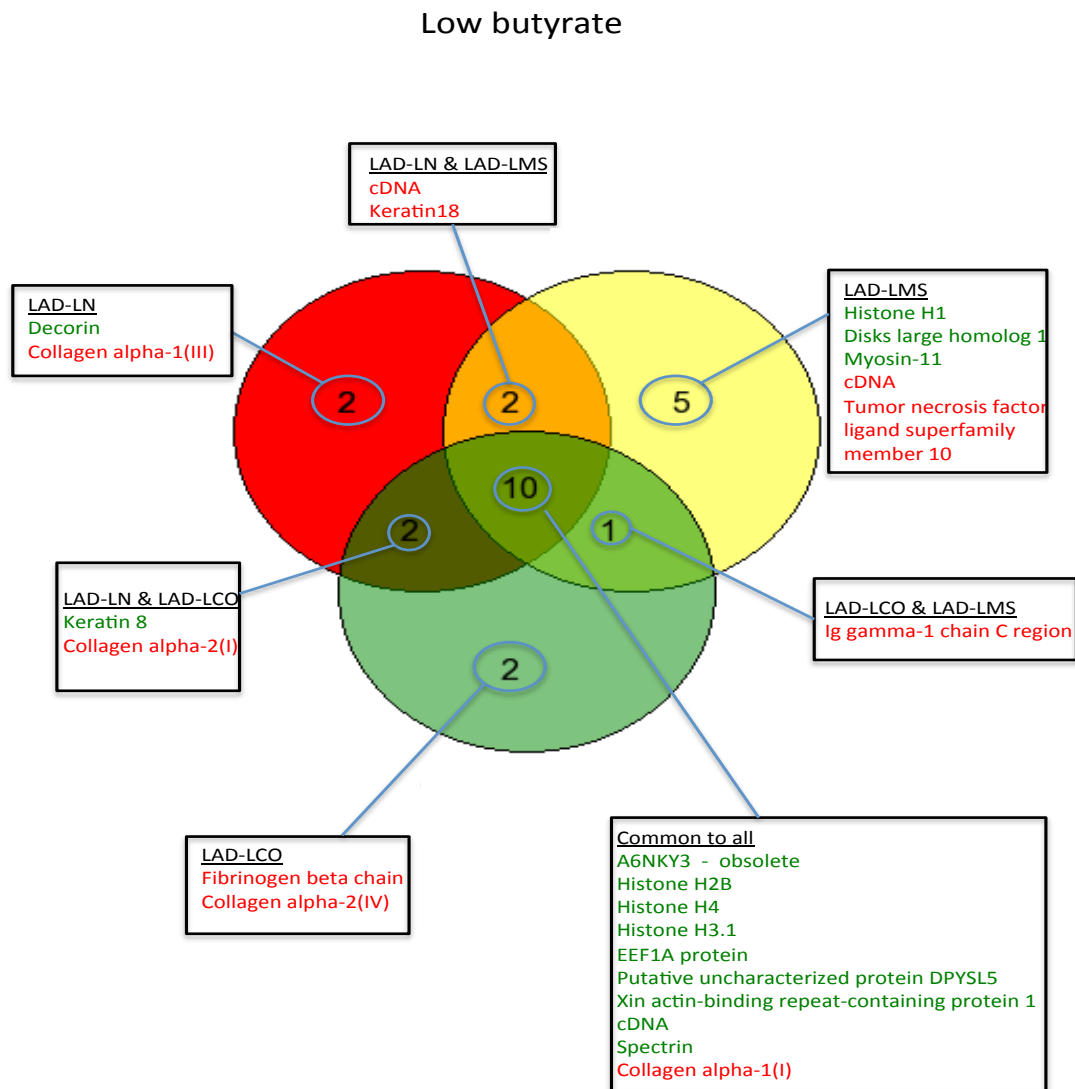
Low butyrate

Figure 37. Venn diagram of protein fold changes in comparison to adenoma in low butyrate.

LCO, LN and LMS are compared to LAD. Up-regulated proteins are expressed in bold/green and down regulated proteins are expressed in red.

- 2 protein fold changes found in total between LAD and LCO only and not found in other samples (non overlapped green)
- 2 protein fold changes found in total between LAD and LN only and not found in other samples (non overlapped red)
- 5 protein fold changes found in total between LAD and LMS only and not found in other samples (non overlapped yellow)
- 10 protein fold changes are common to all samples
- Other overlapped areas indicate protein fold changes common to those samples.

5.4.10 Identification of protein changes mediated by butyrate controlling for lesion proximity

Venn diagrams comparing protein fold changes of HAD-HN to LAD-LN (Figure 38); HAD-HMS to LAD-LMS (Figure 39) and HAD-HCO to LAD-LCO (Figure 40) are shown.

In normal samples compared with adenoma (Figure 38) normal samples in the high butyrate environment (HN) were found to have more unique protein fold changes (N=7) in common with the adenoma sample (HAD) than in the low butyrate samples (N=5).

In mid-sigmoid samples (Figure 39) the reverse association was found, there were more unique protein fold changes in the low butyrate samples (LAD-LMS) (N=11) than in the high butyrate samples (N=7).

In contralateral samples (Figure 40) more unique protein fold changes were found between in the high butyrate samples (N=11) than low butyrate samples (N=4).

When the three figures (38 to 40) are interpreted together it can be shown that a progressive increase in common protein fold changes occurs with proximity to the adenoma samples (Table 11) in the high butyrate samples. A progressive configuration could not be demonstrated in the low butyrate samples (Table 12). In general keratins were up-regulated in high butyrate environments – the only anomaly was K19 (fold changes of which were demonstrated to be insignificant). Vimentin was the only protein universally up-regulated across high butyrate groups. Atlastin-3 was found to be up-regulated in high butyrate environments but only in pathological sites (contralateral and mid-sigmoid).

The full list of proteins identified is listed in Appendix 6.

5.4 Results – Protein fold changes controlling for lesion proximity
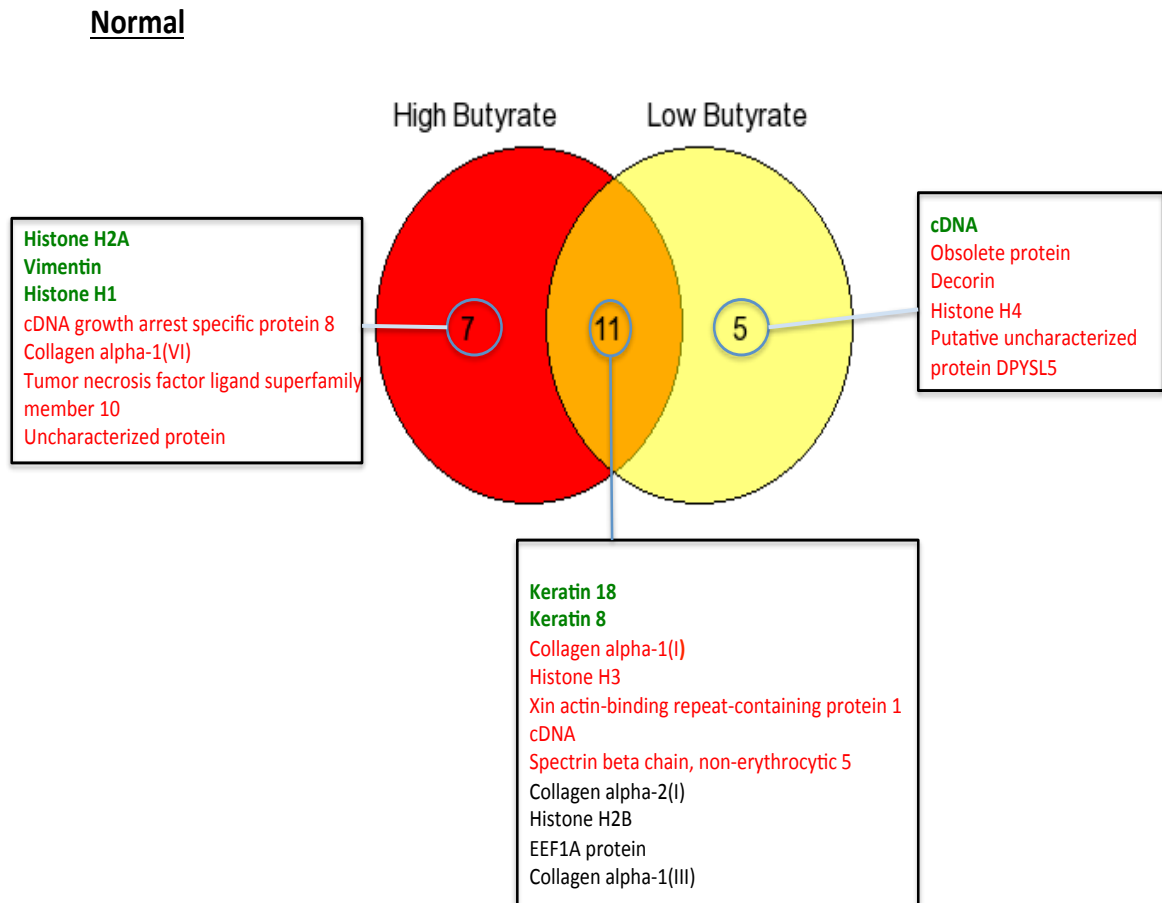
Normal

Figure 38. Venn diagrams of protein fold changes between adenoma and normal samples.

Normal = HAD-HN (red circle) compared with LAD-LN (yellow circle), protein fold changes common to both groups indicated by orange circle.

Up-regulated proteins in bold/green; down-regulated in red and differentially regulated in black.

5.4 Results

Midsigmoid
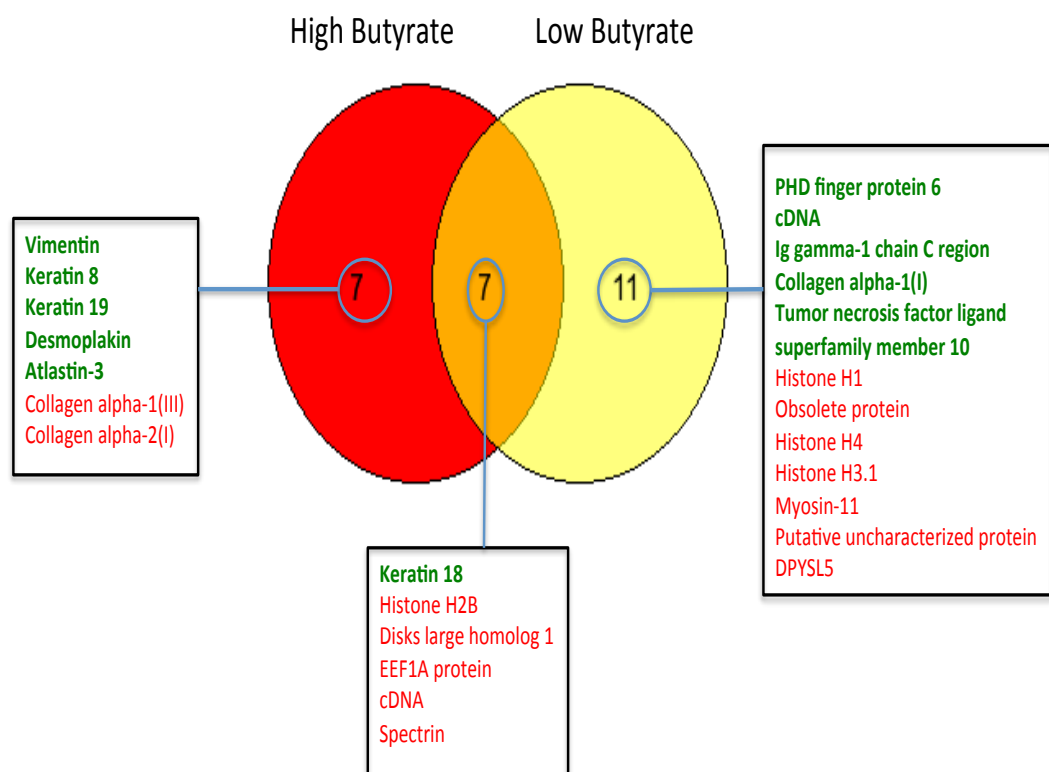
Figure 39. Venn diagrams of protein fold changes between adenoma and mid-sigmoid samples.

Mid-sigmoid = HAD-HMS (red circle) compared with LAD-LMS (yellow circle), protein fold changes common to both groups indicated by orange circle.

Up-regulated proteins in bold/green; down-regulated in red and differentially regulated in black.

5.4 Results

Contralateral

High Butyrate **Low Butyrate**

Vimentin
Keratin 18
Annexin A2
Atlastin-3
Histone H1
Histone H1.5
Histone H2A
cDNA
Collagen alpha-1(III)
Keratin 19
Tumor necrosis factor ligand superfamily member 10

11   11   4

Fibrinogen beta chain, isoform CRA
Ig gamma-1 chain C region
Collagen alpha-2(IV)
cDNA

Xin actin-binding repeat-containing protein 1
Spectrin
Histone H3
EEF1A protein
Obsolete protein
Collagen alpha-1(I)
Keratin 8
Collagen alpha-2(I)
Histone H2B
Histone H4
Putative uncharacterized protein

Figure 40. Venn diagram of protein fold changes between adenoma and contralateral samples.

Contralateral = HAD-HCO (red circle) compared with LAD-LCO (yellow circle), protein fold changes common to both groups indicated by orange circle.

Up-regulated proteins in bold/green; down-regulated in red and differentially regulated in black.

5.4 Results

Table 11. Numbers of protein fold changes identified using Venn diagram in high butyrate samples

Fold change comparison groups	Number of total protein fold changes	Number of unique protein fold changes	Number of protein fold change shared with low butyrate equivalent
HAD-HN	18	7	11
HAD-HMS	14	7	7
HAD-HCO	22	11	11

Numbers of protein fold changes identified using Venn diagram in high butyrate samples demonstrating a progressive increase in protein fold changes similarities from HN to HCO (second column).

Table 12. Numbers of protein fold changes identified using Venn diagram in low butyrate samples

Fold change comparison groups	Number of total protein fold changes	Number of unique protein fold changes	Number of protein fold change shared with high butyrate equivalent
LAD-LN	16	5	11
LAD-LMS	18	11	7
LAD-LCO	15	4	11

Numbers of protein fold changes identified using Venn diagram in low butyrate samples. A progressive pattern to adenoma proximity was not demonstrated.

5.5 Discussion

Workflow

A workflow was developed to enable extraction of intermediate filaments from colonic mucosal biopsies for analysis using iTRAQ. Several experimental methods were applied (coomassie stain, silver stain and protein assay) to ensure the Pierce clean up process preserved sufficient amounts of protein to enable iTRAQ anaylsis.

Keratin changes in relation to adenoma proximity

Using iTRAQ, higher K8 and K18 levels were identified in adenoma and field samples than in normal samples from pathology-free colons. This is consistent with the current literature since Polley et al., found increased K8 level in adenoma tissue in comparison to normal mucosa but reduced level of K8 in cancer tissue in comparison to normal mucosa (Polley et al., 2006). These observations may be due to efforts to stabilise colonocytes via keratins as the cell architecture is damaged during adenomagenesis, however the efforts are overcome and K8 drops as the normal colonocyte architecture is destroyed in malignant transformation.

This study demonstrated a field effect in both keratin expression and protein fold change profiles with proximity to the adenoma, in the high butyrate environment. K8 and K18 levels progressively increased from HMS, HCO to HAD according to closeness to the adenoma. This fits with other studies identifying progressive tissue likenesses as samples approach an adenoma (Polley et al., 2006, McGarrity and Peiffer, 1994, Yu et al., 2011). A progressive field effect was not exhibited in the low butyrate environment. The observed incongruity in high and low butyrate sample behaviour could be due to variations in the extension of a field; it is possible that a cancerized field extends beyond the mid-sigmoid area sampled in the low butyrate environment. It is also possible that fields are influenced by butyrate, which this study demonstrates is associated with up-regulation of K8 and K18.

A progressive field effect in fold change was demonstrated in the high butyrate environment but not the low butyrate environment. HAD and HCO samples had more protein fold changes unique to them than when HAD was compared with HMS and HN. Five protein fold changes were identified to be common to HAD and HCO only and not identified in any other samples, suggesting the protein profiles from HAD and HCO sites are more similar than HN and HMS.

The number of unique protein fold changes (used as a proxy marker of similarity) was found to reduce with distance away from the adenoma.
This supports field changes mediated by lesion proximity, as HCO is closest in proximity to HAD and therefore should be most similar in protein profile. Nine protein fold changes were found to be common to all samples, within these proteins were K8 and K18 suggesting identification of K8 and K18 alone is too subtle to identify field effects. Quantifying K8 and K18 expression is a more useful marker of field cancerization. Taken together these results suggests field cancerization is at play since macroscopically normal tissues close to the adenoma are more similar in their protein profile than tissues further away.

Many of the K19 fold change comparisons against normal were not significant, however, it was evident the association was reversed in comparison to K8 and K18. In the high butyrate environment K19 was reduced in pathological samples (HAD, HCO and HMS) as compared to normal (HN). It has been shown that cellular proliferation of neoplastic tissue is related to low expression of K19 (Stammberger and Baczako, 1999). This finding is relevant as adenoma tissue from the low butyrate group also contained less K19 in comparison to other tissues in its group. K19 may not follow the same pattern of co–expressed K8 and K18 because different keratins are altered at different stages of adenomcarcinogenesis and particularly via PTMs (discussed in Chapter 6).

Relationship between keratin expression and butyrate concentration

This study demonstrated that K8, K18 and K19 expression is greater in samples from high butyrate environments than low butyrate equivalents. Previous studies have shown K8 expression is reduced in cancer tissue (Polley et al., 2006) and the reduction in K8 expression is more prominent in cancer tissue from high butyrate environments (Khan et al., 2011); taken with the results of this study, it suggests that butyrate encourages K8 expression in normal tissue up to adenomagenesis but does not exert the same influence over cancer tissue. Once malignant change takes over K8 becomes altered, as demonstrated by the isoforms in this study (Figure 41) and reported by others (Ditzel et al., 2002) (Polley et al., 2006). Butyrate may stimulate K8 expression in order to enhance cytoskeletal stability to prevent malignant change in a cancerized field. Alternatively, butyrate may stimulate cells to express K8 following chemotoxic challenges in order to enhance cytoskeletal stability. Evidence from K8$^{-/-}$ mice studies demonstrates that K8 is essential for apoptosis in colonocytes (Habtezion et al., 2011). Butyrate is also recognised to influence the rate of apoptosis in genotoxically challenged cells (Clarke et al., 2012). This implies butyrate may exert its chemoprotective properties through the modification or sensitization of K8 to influence faulty colonocytes to undergo apoptosis. An area for further investigation is the relationship of K8 levels on rates of apoptosis.

My demonstration of the influence of butyrate concentration on K18 and K19 also correlates with the current literature (Couchie et al., 2002, Wakabayashi et al., 2005).

In addition, butyrate was also seen to influence proteins other than keratins. Exclusively seen in the high butyrate group was up-regulation of tumour necrosis factor (TNF) and down-regulation of annexin A2 in HN and HCO samples compared with HAD. High levels of TNF are known to have anti-cancer properties (Balkwill, 2002) and annexin A2 has important roles in cancer cell migration, invasion, adhesion and angiogenesis processes, which are essential for cancer metastasis (Lokman et al., 2011). Vimentin is known to maintain cellular integrity and provide resistance against stress, although over-expression and methylation is associated with cancer (Satelli and Li, 2011). Universal up-

regulation of vimentin in the high butyrate environment (Figures 38 to 40) suggests butyrate may also exert cell stability in non-cancerous tissue through vimentin. The evidence presented suggests the frequently cited protective effect of butyrate is multifaceted and calls for further investigation of butyrate's influence on other proteins and its role on the modification of PTMs of keratins.

A limitation of the iTRAQ methodology is the pooling of the samples before protein assay. Bias may have arisen due to greater protein quantities of one sample over another.

5.6 Summary

- An iTRAQ work flow was successfully developed for analysis of the insoluble fraction of colonic mucosal biopsies.

- Pathological samples: adenoma, contralateral and mid-sigmoid tissue have increased K8 and K18 in comparison to normal tissue in both high and low butyrate environments.

- K8 and K18 fold changes increased with proximity to adenoma in high butyrate environments.

- K8, K18 and K19 fold changes were universally greater in biopsies from high butyrate environments when compared to their low butyrate counterparts.

- HCA and PCA analysis show butyrate may exert a stronger global effect over protein similarities between biopsies than proximity to adenoma.

- Protein fold change profiles suggest field cancerization in high butyrate environments but not low butyrate environments.

Chapter 6

Field Effects – Orthogonal Validation: Western
Immunoblot and Post-Translational Modifications

Chapter 6 Field Effects - Orthogonal Validation: Western Immunblot and Post-Translational Modifications

6.1 Introduction

Data from chapter 5 demonstrated significant differences in keratin levels between biopsy sites and between butyrate environments. Independent orthogonal validation of these results using western blot will be explored in this chapter.

Post-translational modifications (PTMs) modulate the function of proteins that are not directly coded for by genes (Cho, 2007). Phosphorylation of K8 and K18 results in increased solubilisation and cellular distribution (Ku et al., 1998, Liao et al., 1995) and can be mediated by cell stress (Liao et al., 1995). Hyperphosphorylation in K8 has also been shown to reduce apoptosis (Arentz et al., 2012) and enhance migration of epithelial tumour cells (Busch et al., 2012). Conversely, dephosphorylation of K8 in colorectal cancer has been associated with tumour progression (Mizuuchi et al., 2009). The role of phosphorylation is complex with evidence to show it is site-specific to the keratin (Omary et al., 1998).

K8 has been identified as acetylated and the degree of acetylation is increased with butyrate exposure (Leech et al., 2008) and during mitosis (Khan et al., 2011). In contrast to phosphorylation, acetylation is shown to decrease K8 solubility by forming tightly associated K8 complexes (Snider et al., 2013). Alterations in solubility and structure may indicate acetylation extends its role in stabilization of other cytoskeletal proteins (Janke and Bulinski, 2011) in addition to intermediate filaments.

Furthermore, acetylation of K8 results in a reciprocal reduction of phosphorylation (Snider et al., 2013). This finding suggests a possible mechanism by which butyrate exerts its cancer prevention properties; through

increasing acetylation resulting in decreased phosphorylation and increased apoptosis. The function of acetylation on K8 is not fully understood but evidence indicates its role may be as significant as phosphorylation.

Ditzel et al., found N terminally truncated forms of K8 and K18 in cancerous colonic mucosa (Ditzel et al., 2002). This could demonstrate a pathological PTM that has not yet been demonstrated in adenoma tissue.

Vimentin is a type 3 intermediate filament protein expressed in epithelial cancers and associated with poor prognosis and invasiveness (McInroy and Maatta, 2007). Since vimentin was identified (using iTRAQ) as a protein common to all the high butyrate colonic biopsy samples, it would be valuable to determine whether its presence and quantity is dependent on colonic tissue samples using western immunoblot.

6.2 Hypothesis and Aims

Hypotheses:

- Vimentin could be a useful marker of field cancerization.
- Pathological samples exhibit different PTMs in comparison to normal samples and the PTMs are butyrate-responsive.

Aims:

- To validate, by a second independent method, results obtained by iTRAQ.
- To identify and quantify K8, K18, K19 and vimentin using western blot and densitometry in association with adenoma proximity and butyrate exposure.
- To identify K8 PTMs (phosphorylation, acetylation and N terminus cleavage) in association to adenoma proximity and butyrate exposure.

6.3 Materials and Methods

6.3.1 Materials

12% SDS-PAGE gel

12 % polyacrylamide gels were made according to protocol described by Laemmli (Laemmli, 1970).

Resolve: 2.6mL distilled water, 1.8mL 1M Tris pH 8.8, 2.8mL Acrylamide, 37.5μL 10% APS, 75μL 10% SDS, 9μL TEMED.

Stacker: 3mL distilled water, 1.25mL 0.5M Tris pH 6.8, 0.6mL Acrylamide, 100μL 10% APS, 100μL 10% SDS, 20μL TEMED.

Tris Glycine SDS-PAGE run buffer (x10)

Run buffer was made according to the manufacturers instructions (National Diagnostics, Hessle, UK.)

Tris Glycine electroblotting buffer (x10)

Transfer buffer was made according to the manufacturer's instructions (National diagnostics, Hessle, UK.)

Primary antibodies

1. Keratin 8 (ab9023, Abcam, Cambridge, UK) used at dilution 1:1000 (5μL in 5mL 5% milk).

2. Keratin 8 PS431 (ab59434, Abcam, Cambridge, UK)) - detects keratin 8 phosphorylated at Serine 431 dilution used at 1: 10000 (1μL in 10mL 1% BSA).

3. Keratin 8 PS73 (ab32579, Abcam, Cambridge, UK) detects keratin 8 phosphorylated at Serine 73 dilution used at 1: 10000 (1μL in 10mL 1% BSA).

4. Keratin 8 PS23 (ab76584, Abcam, Cambridge, UK) detects keratin 8 phosphorylated at Serine 23 dilution used at 1: 10000 (1μL in 10mL 1% BSA).

5. Keratin 8 N terminus – (raised in-house) detects keratin 8 truncated at the N terminus used at dilution 1: 1000 (5µL in 5mL 5% milk).

6. Keratin 8 Acetyl Lysine 10 – (raised in-house) detects keratin 8 acetylated at lysine 10 used at 1: 1000 (5µL in 5mL 5% milk).

7. Keratin 8 Acetyl Lysine 482 - (raised in-house) detects keratin 8 acetylated at lysine 482 used at 1: 500 (10µL in 5mL 5% milk).

8. Keratin 18 (ab668, Abcam, Cambridge, UK) used at 1: 1000 (5µL in 5mL 5% milk).

9. Keratin 19 (ab7754, Abcam, Cambridge, UK) used at 1: 1000 (5µL in 5mL 5% milk).

10. Vimentin (MAB3400, Millipore Corporation, USA) used at 1: 500 (10µL in 5mL 5% milk).

Antibodies raised in-house were done so with the help of Eurogentec, Southampton, UK.

Secondary Antibodies

1. Polyclonal goat anti-mouse - P0447 (Dako, Cambridge, UK) used at 1:2000 (5µL in 10mL 5% milk).

2. Polyclonal goat anti-rabbit - P0448 (Dako, Cambridge, UK) used at 1: 2000 (5µL in 10mL 5% milk or 1% BSA according to primary antibody).

6.3.2 Methods

Pooled samples reserved as described Chapter 5 were thawed and used for western immunoblot validation. These samples were identical to those analyzed in the iTRAQ process.

12% polyacrylamide gels were prepared and run using a modified protocol described by Laemmli (1970). Briefly, volumes equivalent to 30μg protein (MCF7, HAD, HCO, HMS, HN, LAD, LCO, LMS and LN) were heated to 95°C for 5 minutes with 5x sample buffer (Pierce, Thermo Scientific, USA) and loaded onto 10 well gels. SDS PAGE gels were run at 100mV for 90 minutes. Proteins were transferred to polyvinylidene fluoride membrane (Millipore Corporation, USA), blocked in 5% non-fat dried milk or 1% BSA, washed in tris buffered saline (TBS) with 5% tween (Sigma, USA) (TBST) and incubated in primary antibody at room temperature for one hour (Table 13). Membranes were washed 3 times in TBST and incubated in secondary antibody (Table 13) for one hour at room temperature followed by further washes in TBST. Membranes were treated with ECL solutions (Immunoblon™ Western Chemiluminescent HRP substrate: HRP substrate peroxide solution and HRP substrate Luminol Reagent, Millipore Corporation, USA) for chemiluminescence detection of protein bands. Membranes were imaged using Chemigenius Bio-Imaging System (Syngene, Cambridge, UK).

Due to sample volume constraints, not enough SDS-PAGE gels and hence membranes could be produced for each antibody to be applied to separate membranes. Membranes had to be stripped using western blot stripping buffer (Thermo scientific, Rockford, IL, USA), re-imaged (following ECL) to ensure adequate stripping and re-probed (Table 14). If negative results for post-translational modifications occurred following western blot, membranes were stripped and re-probed for keratin 8 to ensure keratin 8 proteins were still present on the membrane.

Densitometry (to quantify western immunoblot results) was performed using GeneTools software (Syngene, Cambridge, UK).

Table 13. Primary antibodies and corresponding secondary antibody used for western immunoblot.

Primary antibody	Secondary antibody
Keratin 8	Anti mouse in milk
Keratin 8 PS431	Anti rabbit in BSA
Keratin 8 PS73	Anti rabbit in BSA
Keratin 8 PS23	Anti rabbit in BSA
Keratin 8 N terminus	Anti mouse in milk
Keratin 8 Acetyl lysine 10	Anti rabbit in milk
Keratin 8 Acetyl lysine 482	Anti rabbit in milk
Keratin 18	Anti mouse in milk
Keratin 19	Anti mouse in milk
Vimentin	Anti mouse in milk

Table 14. Antibodies used in first western immunoblot and after stripping.

Membrane number	Primary antibody	Primary antibody (after stripping)	Reprobe for K8
1	Keratin 8	K19	
2	Keratin 18	Vimentin	
3	Keratin 8 N terminus	Acetyl Lysine 10	Keratin 8
4	Keratin 8 Acetyl Lysine 10	Acetyl Lysine 482	Keratin 8
5	Keratin 8 PS73	Keratin 8 PS431	
6	Keratin 8 PS23	Keratin 8	

6.4 Results

6.4.1 Western blot K8 and K18

Western immunoblot for K8 and K18 are shown in Figure 41 and densitometry values of the immunoblots are shown in Table 15. Densitometry values were greater in the high butyrate samples for both K8 and K18. Lower molecular weight forms of both K8 and K18 were seen in the MCF7 control sample and in the HAD and LAD samples.
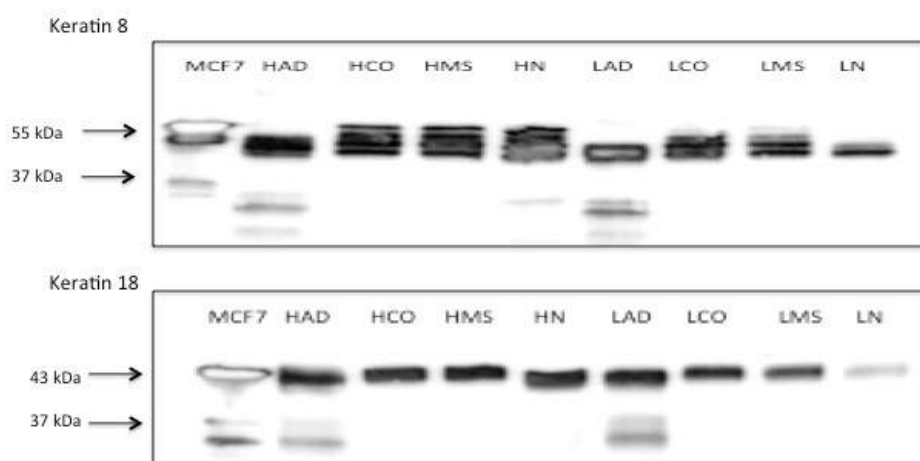
Figure 41. Western immunoblot showing immunoreactive bands for K8 and K18

Note lower molecular weight isoforms of K8 and K18 in HAD and LAD samples.

Table 15. K8 and 18 densitometry values using HAD as the relative comparison.

Antibody	HAD	HCO	HMS	HN	LAD	LCO	LMS	LN
8	1	1.19	1.16	1	0.65	0.89	0.8	0.49
18	1	0.87	0.93	0.99	1	0.76	0.62	0.23

6.4 Results

6.4.2 K8 comparison to iTRAQ results

Keratin 8

The findings of the iTRAQ data set and densitometry for K8 correlate as indicated by the line graphs (Fig. 42). The pathological samples (AD, CO and MS) exhibited greater fold changes and densitometry when compared with normal controls (N) within their butyrate groups.

Keratin 8

	HAD	HCO	HMS	HN	LAD	LCO	LMS	LN
Densitometry	1	1.19	1.16	1.01	0.65	0.89	0.8	0.49
iTRAQ	1	0.87	0.87	0.82	0.48	0.55	0.45	0.3
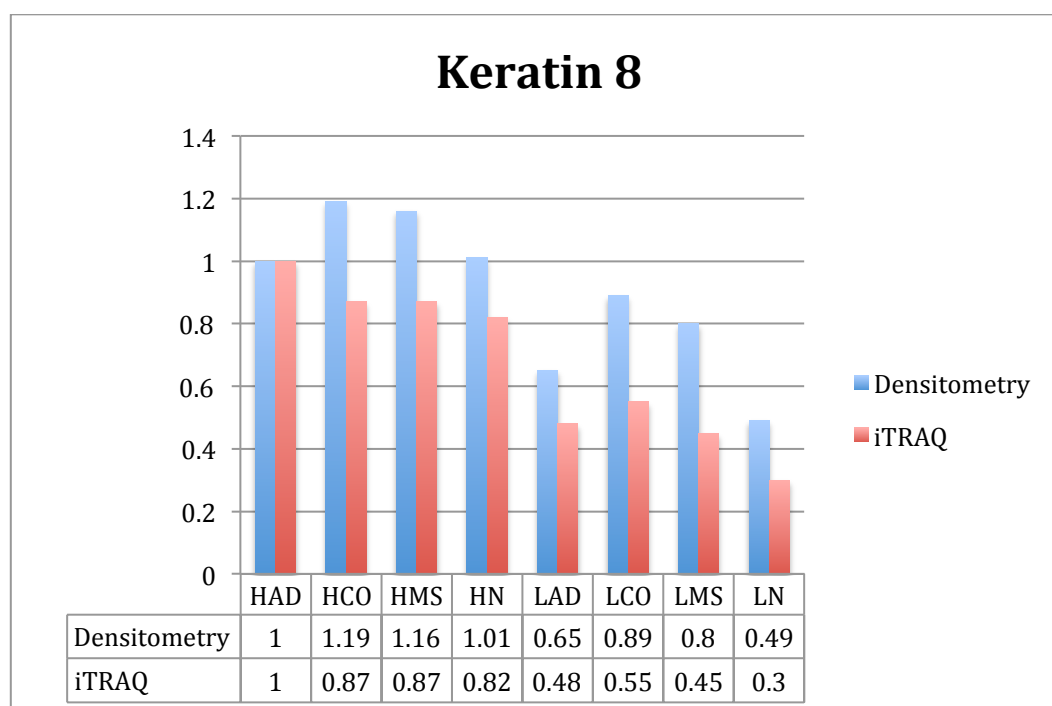
Figure 42. Graph comparing iTRAQ fold change with densitometry for K8

Both densitometry and iTRAQ fold changes calculated using HAD as the reference sample. An anomaly was seen at HCO where densitometry values increased from HAD whereas HCO fold changes decreased from HAD, however, overall mirroring of the graphs indicate densitometry values validate iTRAQ fold changes.

6.4 Results

6.4.3 K18 comparison to iTRAQ results

Keratin 18

Selected densitometry readings from western blot followed the findings of the
iTRAQ data set for K18 (Figure 43) but not all. As per the iTRAQ data set non
adenoma samples exhibited lower densitometry readings than the adenoma
samples for both high and low butyrate. A field effect (decrease in keratin 18
densitometry with distance from adenoma) was not demonstrated, however, the
general trend of densitometry follows iTRAQ as shown by the mimicking of the
graphs.

Keratin 18

	HAD	HCO	HMS	HN	LAD	LCO	LMS	LN
Densitometry	1	0.87	0.93	0.99	1	0.76	0.62	0.23
iTRAQ	1	0.44	0.34	0.35	0.4	0.3	0.17	0.21
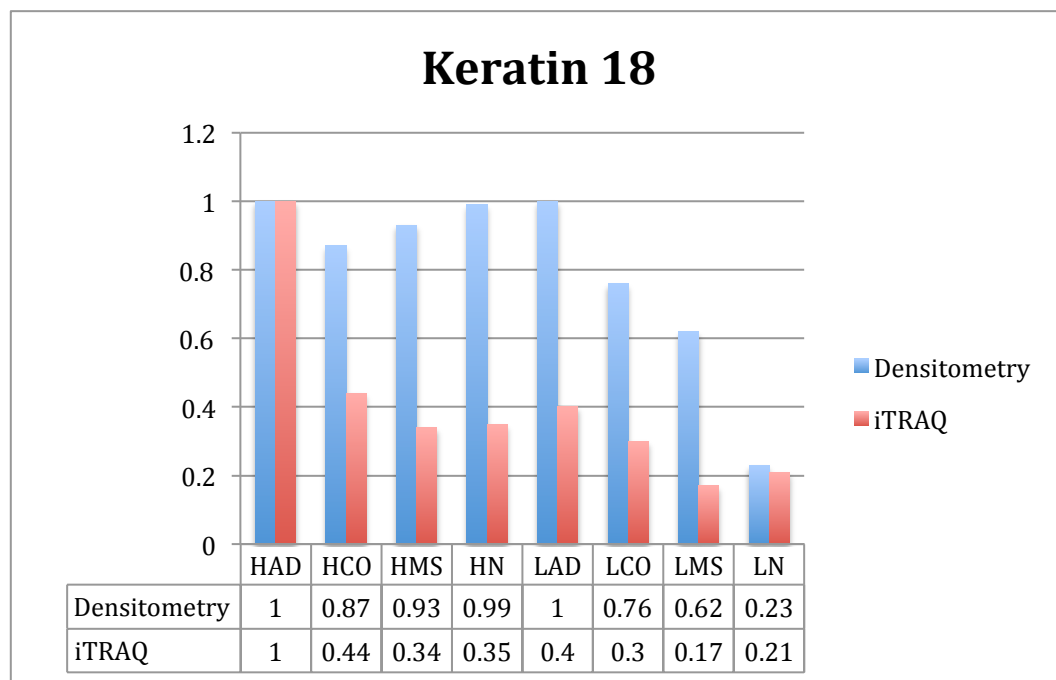
Figure 43. Graph comparing of iTRAQ fold change with densitometry for K18

Using HAD as the reference sample; there is a decrease in K18 expression from HAD to HCO in
both iTRAQ fold change and densitometry. There is a further decrease in K18 with distance from
adenoma in HMS and HN in iTRAQ fold changes but this pattern is not replicated in densitometry.
In LAD the same decrease in iTRAQ fold change and densitometry of K18 is seen from LAD to LCO
this pattern continues in densitometry with distance from adenoma but is lost in iTRAQ fold
change beyond LCO.

6.4 Results

6.4.4 Western blot K19 and vimentin

Keratin 19

Immunoreactive bands were demonstrated for keratin 19 in HAD and LAD samples only (Figure 44). For densitometry HAD was used as the reference sample, however, other than LAD, readings could not be obtained for the remaining sample types (Table 16).

Immunoreactive bands could not be identified for vimentin in HAD and LN. The band imprint of LCO suggests a transfer problem (possible air bubble) from gel to membrane. In the vimentin membrane HCO was used as the reference for densitometry and no readings were obtained for HAD and LN (Figure 44).

6.4 Results

6.4.4 Western blot K19 and Vimentin
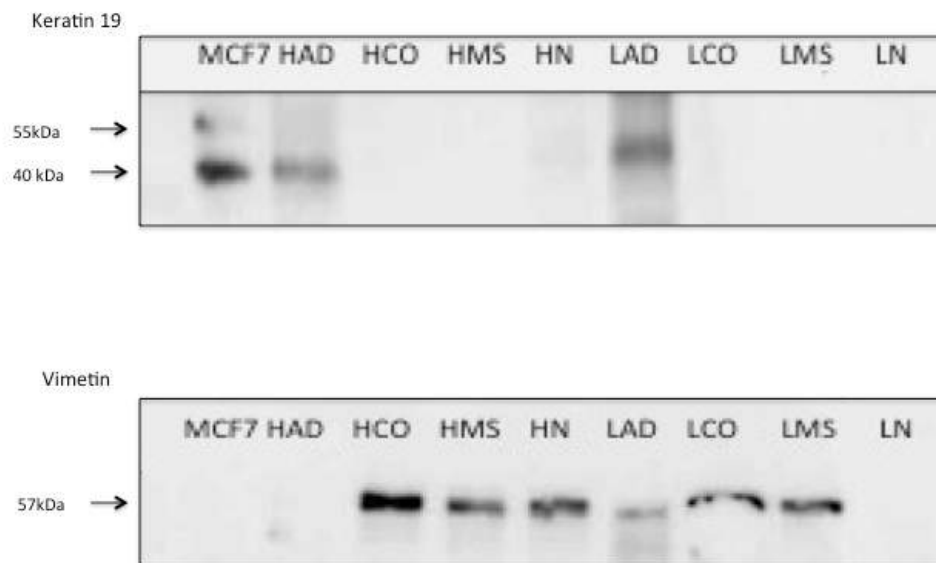
Figure 44. Western immunoblot showing immunoreactive bands for K19 and vimentin.

Immunoreactive bands could not be identified in K19 for HCO, HMS, HN, LCO, LMS or LN therefore densitometry readings could not be obtained. Immunoreactive bands for HAD and LN were not demonstrated for Vimentin therefore densitometry readings could not be obtained for those samples.

Table 16. K19 densitometry values using HAD as the relative comparison.

Antibody	HAD	HCO	HMS	HN	LAD	LCO	LMS	LN
19	1	-	-	-	1.19	-	-	-
Vimetin	-	1	0.86	0.87	0.80	0.83	0.88	-

6.4. Results

6.4.5 K19 comparison to iTRAQ results

Keratin 19

Immunoreactive bands for K19 were very weak and densitometry readings were not sufficient to compare with iTRAQ findings (Figure 45). Densitometry was performed to standardise all the comparisons but in the case of K19 it is of little value since immunoreactive bands are only visible in the HAD and LAD samples (Figure 44).

Keratin 19

	HAD	HCO	HMS	HN	LAD	LCO	LMS	LN
Densitometry	1				1.19			
iTRAQ	1	0.99	0.96	1.19	0.6	0.79	1.21	0.58
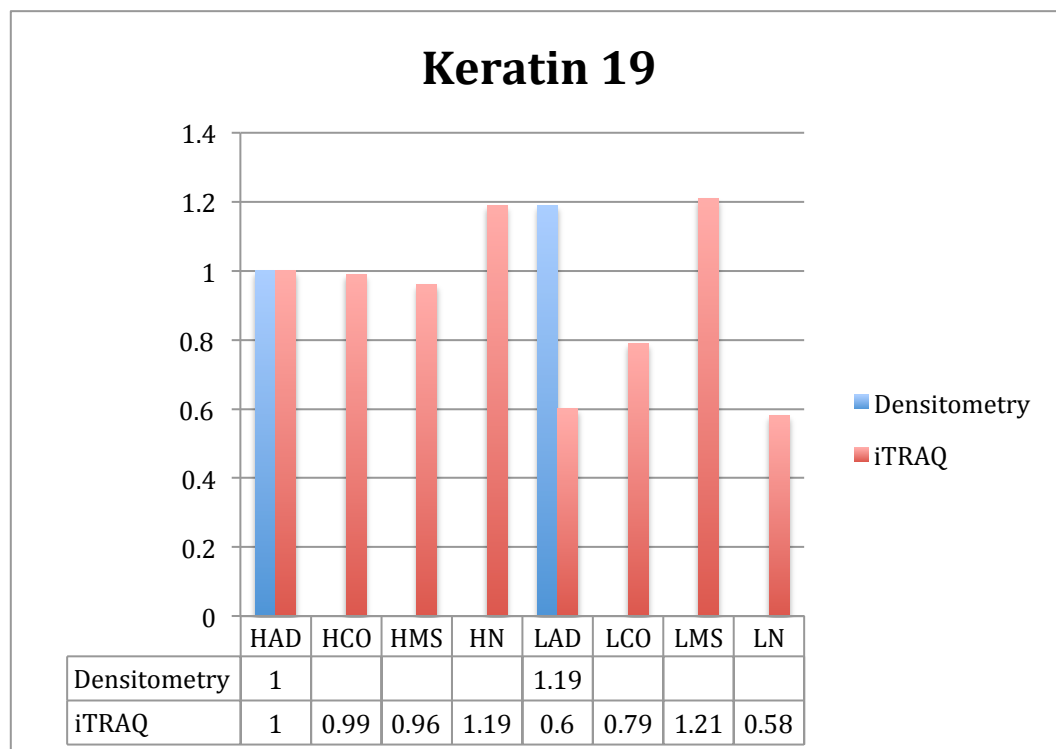
Figure 45. Graph of iTRAQ fold change for K19

Densitometry readings were not sufficient to compare with iTRAQ findings.

6.4 Results

6.4.6 Vimentin comparison to iTRAQ results

Vimentin

Western blotting was suboptimal for vimentin and is reflected in the immunoreactive bands (Figure 44) readings for HAD and LN could not be obtained. A number of densitometry readings followed the iTRAQ findings (Figure 46) both densitometry and iTRAQ fold changes revealed a decrease in vimentin from HCO and HMS and an increase in vimentin from LAD to LCO.

Vimentin

	HAD	HCO	HMS	HN	LAD	LCO	LMS	LN
Densitometry		1	0.86	0.87	0.8	0.83	0.88	
iTRAQ	1	0.68	0.56	0.56	0.56	0.66	0.56	0.55
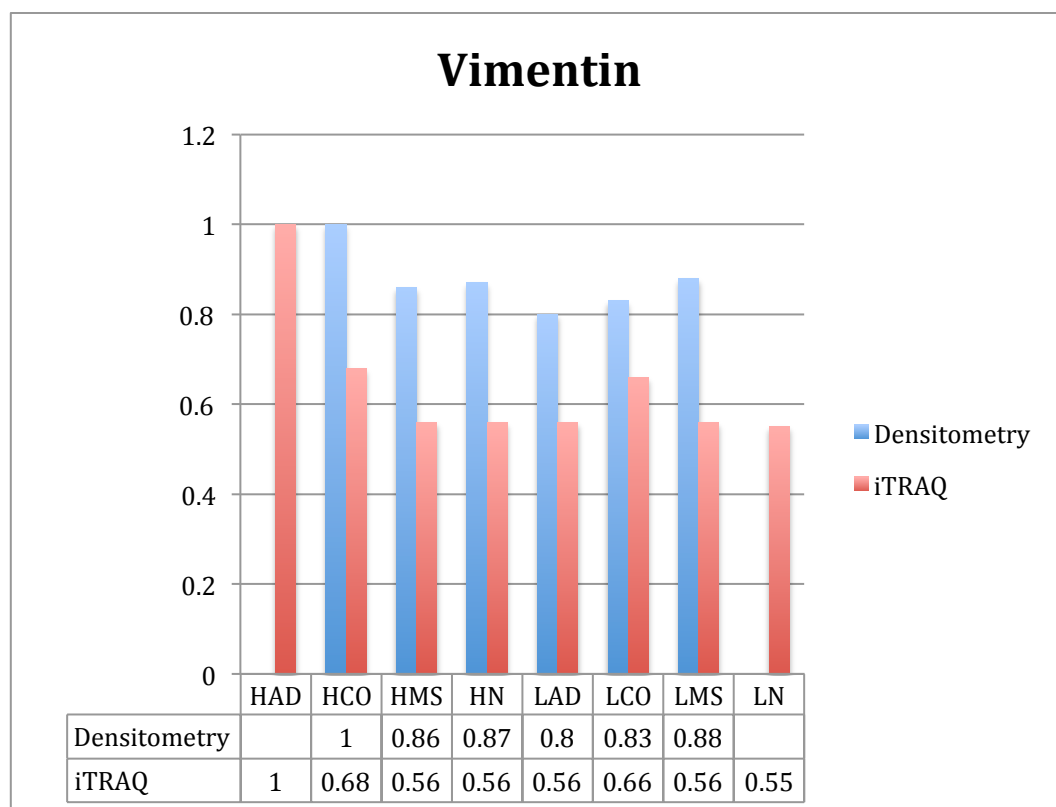
Figure 46. Comparison of iTRAQ fold change and densitometry for vimentin.

Densitometry readings could not be obtained for all samples but there are areas in the graphs that mirror each other showing relative validation of the iTRAQ findings.

6.4 Results

6.4.7 Western blot of K8 phosphorylation

Keratin 8 Phosphorylation

All samples demonstrated phosphorylation at serine residues: 23, 73 and 431, however some immunoreactive bands were weak (Figure 47).

Densitometry of PS23 immunoreactive bands indicate adenoma samples (of both high and low butyrate environments) have reduced phosphorylation on serine 23 compared to other sample groups (Table 17).

Weak immunoreactive bands were seen for PS73. In this case, the densitometry values did not indicate a reduction in phosphorylation of adenoma samples as seen with PS23 and PS431.

The reverse serine phosphorylation pattern of PS23 was seen for PS431, where immunoreactive bands for adenoma samples were similar or stronger than other sample groups.
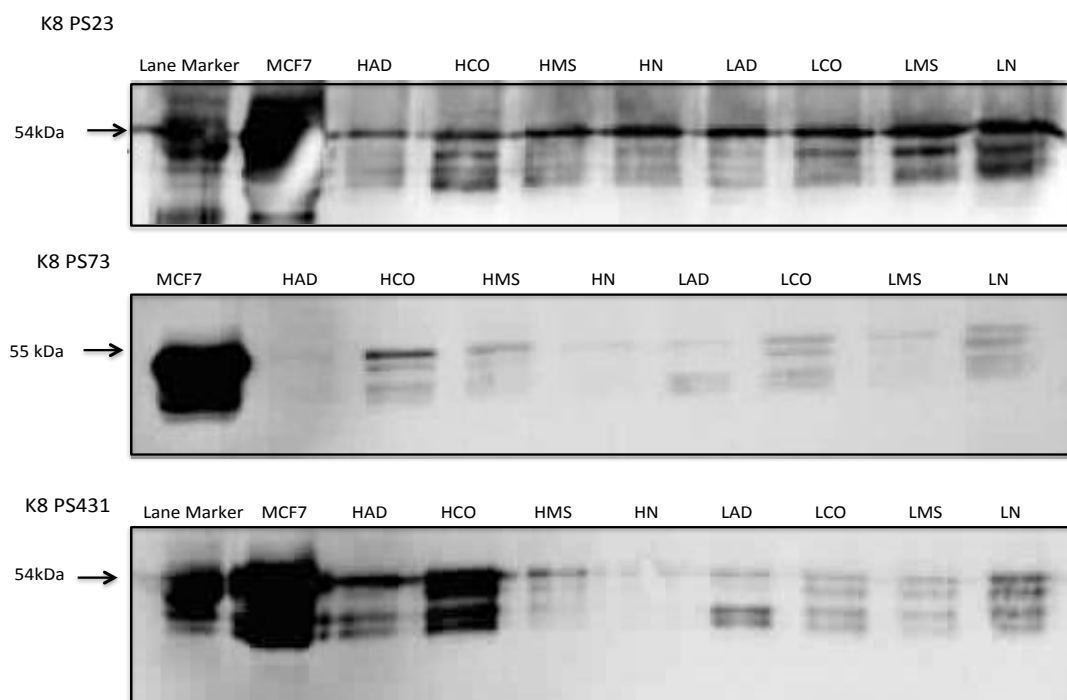
Figure 47. Western immunoblot showing immunoreactive bands for K8 phosphorylated at serine residues: 23 (PS23); 73 (PS73); 431 (PS431)

Table 17. Phosphorylation densitometry values using HAD as the relative comparison

Antibody	HAD	HCO	HMS	HN	LAD	LCO	LMS	LN
PS23	1	1.45	1.38	1.38	1.15	1.43	1.55	1.58
PS73	1	1.07	1.02	0.64	0.93	1.02	0.85	1.04
PS431	1	1.01	0.96	0.45	0.97	0.81	0.64	0.99

6.4 Results

6.4.8 Western blot K8 N terminus and acetylation

An immunoreactive band representing K8 truncated at the N terminus was visible for the MCF7 sample but conclusive immunoreactive bands could not be demonstrated for our sample set (Figure 48). Immunoreactive bands could not be demonstrated for acetyl lysine 10 and acetyl lysing 482. To ensure adequate K8 was transferred onto the membranes, the membranes were stripped and incubated with K8 antibody. Both stripped and re-probed membranes confirmed the presence of K8.
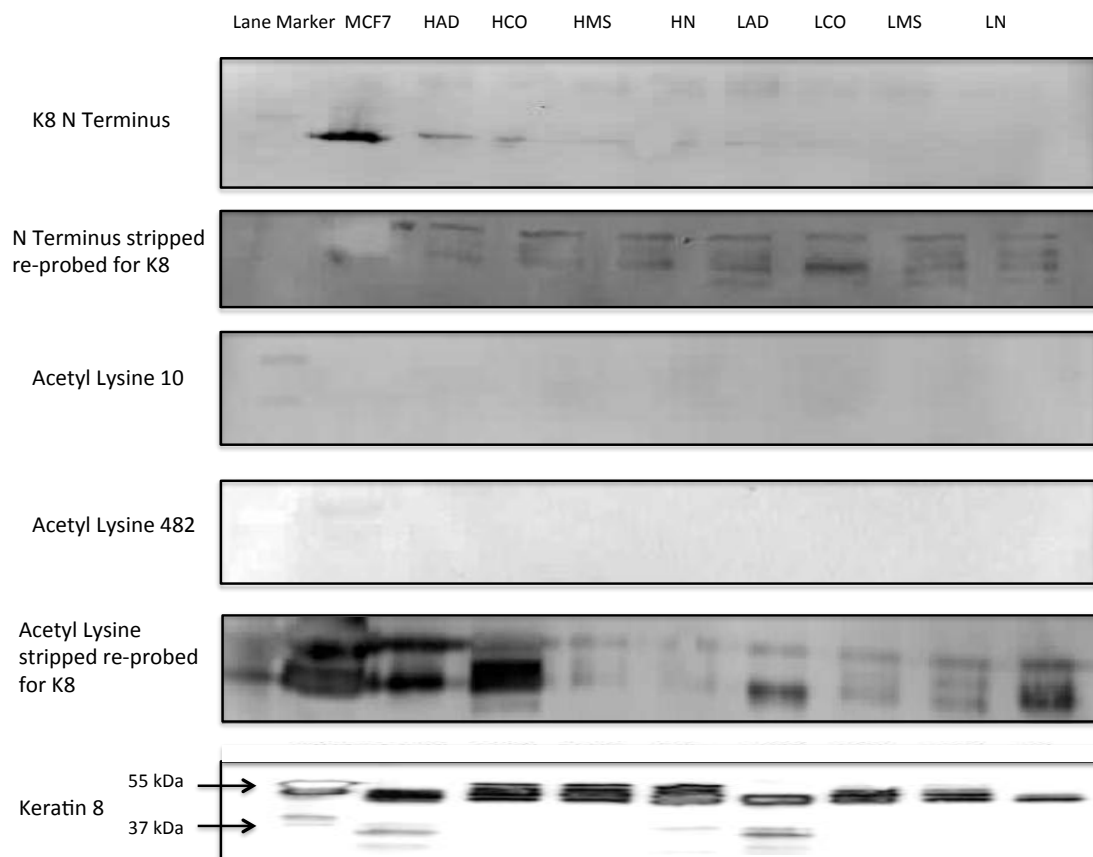
Figure 48. Western immunoblot using K8 N terminus antibody, Acetyl lysine 10 and Acetyl lysine 482 and K8 for comparison

No immnuoreactive bands could be demonstrated. To demonstrate the presence of K8, membranes were stripped and re-probed with K8 antibody, which confirmed the presence of K8.

6.5 Discussion

Keratins and Vimentin

Western blot analysis was able to validate the iTRAQ findings for both K8 and K18. Stronger immunoreactive bands for K8 and K18 were confirmed in the high butyrate samples as compared to the low butyrate samples and also in the pathological tissue when compared to the normal. If densitometry values are used as a proxy for expression these results support the iTRAQ expression data for K8 and K18.

K19 and vimentin western blots did not follow iTRAQ findings; suboptimal protein levels following membrane stripping may be partly responsible for this. Due to shortages in sample availability some membranes had to be reused and experiments could not be repeated. Some iTRAQ fold changes for K19 were not significant therefore comparisons with densitometry were of limited value. Investigation of vimentin was a deviation from the original aim but it was chosen for validation as the results from chapter 5 indicate vimentin as a protein that was consistently up-regulated in the high butyrate environment. This observation was not seen in western blot since high butyrate samples did not exhibit stronger immunoreactive bands. If larger sample volumes were available this would have obviated the need for membrane stripping and may have produced better results. iTRAQ fold changes of vimentin were only matched by one peptide therefore the significance of vimentin to this study may not be as great as originally thought. However, there is evidence of increased vimentin in the cancerized field of breast tissue (Trujillo et al., 2011), suggesting this as an area of future investigation in the colon.

Post-translational modifications

Keratin 8 appeared to be less phosphorylated at serine 23 in adenoma samples than other samples. On the contrary, Arentz et al., found increased phosphorylation at serine 23, 73 and 431 in cancer samples compared with matched normal controls (Arentz et al., 2012). The reason for the discrepancy could be two fold: our results were derived from adenoma tissue rather than cancer; secondly we concentrated wholly on the insoluble form of K8, whereas Arentz et al. investigated both forms together. Increased phosphorylation of K8 is associated with reduced apoptosis (Arentz et al., 2012), which would correlate with the behaviour of malignant cells rather than adenoma cells. There is evidence to show the soluble form of K8 protects damaged cells from apoptosis by acting as a phosphate 'sponge' to inhibit phosphokinase activation of pro-apoptotic substrates (Ku and Omary, 2006). It is unknown if the insoluble fraction behaves in a similar manner. There is also evidence that phosphorylation of K8 results in increased K8 solubility and intracellular distribution (Omary et al., 1998). Therefore, one explanation for my findings is that there are reduced amounts of insoluble K8 due to redistribution into the soluble compartment. The protective mechanism may have been overcome in adenoma tissue as decreased phosphorylation of K8 leads to insolubility and less intracellular distribution. Alternatively, this may not be a mechanism of protection but a feature of malignancy that does not apply to adenoma tissue. In cancer tissue phosphorylation of K8 rises again to prevent apoptosis, demonstrating phosphorylation interactions are complex and perhaps should not be examined in isolation. The relationship between K8 phosphorylation and butyrate and how K8 phosphorylation varies in solubility compartments with respect to the cancerized field should be examined in future research.

Acetylation

Keratin 8 is known to be acetylated in colon cancer cell lines (Leech et al., 2008) and the degree of acetylation increases in response to butyrate levels (Drake et al., 2009). Unfortunately, immunoreactive bands for acetylation could not be demonstrated. It is possible that this is due to a defective in-house antibody since K8 presence was subsequently demonstrated on the membrane and K8 is recognised as being highly acetylated (Leech et al., 2008). The alternative explanation is that the process of dissolving the insoluble K8 (protocol described in Chapter 4) has removed some post-translational modifications namely acetylation but preserved phosphorylation.

Keratin 8 isoforms

Ditzel et al., showed that K8 in cancer cells is N terminally truncated (Ditzel et al., 2002). I sought to investigate whether the lower molecular weight forms of K8 seen in adenoma samples (Figure 41) were N terminally truncated forms of K8. However, I was unable to demonstrate this. The lower molecular weight forms could represent K8 cleaved at alternative sites secondary to adenomagenesis and N terminus cleavage remains an exclusive feature of malignancy. The lack of immunoreactive bands for K8 N terminus is unlikely to be due to a defective antibody since bands were seen, as expected, in the MCF7 sample. The weak visible bands are likely due to contamination of MCF7 into other wells during gel loading as the bands were observed to get progressively weaker with distance from the MCF7 well.

Although I was unable to demonstrate the lower molecular weight forms of K8 were N terminally truncated forms of K8, the western blots clearly indicate the presence of K8 in the adenoma samples and not in the non-pathological tissue. This is consistent with the current literature (Arentz et al., 2012), where phosphorylated isoforms of K8 were up-regulated in cancer cells in comparison to matched normal. It could be that the isoforms identified in my adenoma samples were post-translationally altered isoforms, either by phosphorylation or another PTM that was not investigated in this study.

6.6 Summary

Validation:

- Keratin 8 iTRAQ fold changes were validated by western immunoblot densitometry.
- Keratin 18 iTRAQ fold changes were only partly validated by western imunoblot densitometry, however discrepancies in the differing results were marginal.
- Keratin 19 and vimentin iTRAQ fold changes could not be reliably validated.

Phosphorylation:
- Phosphorylation was reduced in adenoma samples compared with other samples in both butyrate groups.
- Phosphorylation did not appear to be influenced by butyrate status.

Acetylation:
- Immunoreactive bands for acetylation were not demonstrated; this may be due to accidental removal of acetylation during sample processing or faulty antibody.

Chapter 7

Field Effects – Orthogonal Validation:

Immunohistochemistry for Keratin 18 and 19

Expression

Chapter 7 Field Effects – Orthogonal Validation: Immunohistochemistry for Keratin 18 and 19 Expression Immunohistochemistry

7.1 Introduction

Data from chapter 5 demonstrated significant differences in keratin between biopsy sites and between butyrate environments. Independent orthogonal validation of these results using immunohistochemistry (IHC) will be explored in this chapter. Fujisaki and Shimoda defined K8, K18 and K19 expression differences between normal colonic mucosa and neoplastic mucosa using IHC (Fujisaki and Shimoda, 1993). Since then, few studies have investigated the distribution of keratins within the colonic crypt especially in relation to the cancerized field and butyrate exposure.

Immunohistochemistry for K8 was not performed in this study as a member of our group previously performed K8 IHC as part of their MD project. This work is now published (Khan et al., 2011). Khan et al., (2011) found an inverse relationship between K8 expression and butyrate in cancer tissue but a positive relationship between butyrate and K8 in adenoma tissue. K8 was also found to decrease with adenoma proximity but increase with cancer proximity (Khan et al., 2011). Increased K8 expression in colonic crypts from low butyrate environments was also reported (Khan et al., 2011). The same group also found patchy distribution of K8 in cancer tissue, where K8 expression was stronger at the mucosal surface than deeper cells within the colonic crypt (Khan et al., 2011). There are no studies examining the crypt distribution of K18 and K19 in relation to adenoma proximity and butyrate exposure.

Post-translational studies of keratins have demonstrated altered solubility thereby affecting cellular stability (Ku and Omary, 2006). It is possible that crypt distribution of keratins is equally as important for tissue stability and may help define pathological processes.

7.2 Hypotheses and Aims

Hypotheses:

- Keratin 18 and 19 expression or levels are altered in adenoma and field samples in comparison to normal samples
- If K18 and K19 expression levels are not representative of iTRAQ results then solubility of K18 and K19 could be altered in different stages of adenoma-carcinogenesis.
- Keratin distribution within the colonic crypt is affected by adenoma proximity and butyrate status.

Aims:

- To determine K18 and K19 expression levels in colonic adenoma, field and normal tissue in using immunohistochemistry
- To identify distribution differences between the sample groups and in relation to butyrate.

7.3 Materials and Methods

7.3.1 Materials

Hydrogen and methanol

30 mL of hydrogen peroxide was added to 270mL 100% methanol.

Phosphate Buffered Saline (PBS)

10 mM PBS was prepared by dissolving 1 PBS tablet in 200mL of distilled water (79382-50TAB, Sigma Aldrich, Dorset, UK).

Tris EDTA

Tris EDTA was prepared by dissolving 1.21g of Tris (Sigma Aldrich, Dorset, UK) and 0.37g EDTA (Sigma Aldrich, Dorset, UK) to 1000mL of distilled water and adjusted for use at pH 9.0.

Sodium Citrate

0.01M Sodium citrate was prepared by dissolving 2.94g of sodium citrate to 1000mL of distilled water and adjusted for use at pH 6.0.

Proteinase K

Proteinase K (Chemicon) 200µg/mL was diluted 1 in 10 using 50mM tris buffer and 0.15M NaCl.

10% Goat serum block

400µL of 10% goat serum (Vector Laboratories, Peterborough, UK) was diluted in 4mL of PBS with the addition of 40µL of x10 Casein (Vector Laboratories, Peterborough, UK).

2% goat serum solution was prepared from this solution by taking 1mL of 10% goat serum solution and diluted in 4mL PBS.

Primary antibody

Keratin 18 (raised in-house) used at a dilution of 1: 2000 in PBS.

Keratin 19 (ab7754, Abcam, Cambridge, UK) used at a dilution of 1: 1500 in PBS.

<u>Secondary antibody</u>

Biotinylated goat anti-mouse IgG (Vector Laboratories, Peterborough, UK) used at a dilution of 1: 200, 5µL in 1mL of 2% goat serum solution.

<u>ABC reagent kit</u>

ABC Vectastain Universal *elite* (Vector Laboratories, Peterborough, UK) was prepared by adding 2 drops of solution A and 2 drops of solution B to 5mL PBS.

<u>DAB peroxidase substrate kit (DAB)</u>

DAB (Vector Laboratories, Peterborough, UK) was prepared by adding 2 drops of buffer, 4 drops DAB and 2 drops hydrogen peroxide to 5mL of distilled water.

<u>Imaging</u>

Slides were viewed using a Nikon Eclipse TS100 microscope (Nikon, Surrey, UK) and captured using a Nikon DS-2MBWc camera (Nikon, Surrey, UK) at a resolution of 2560 x 1920 pixels. Images were stored and analysed using Nikon NIS Elements D (v2.30) software.

Protocol development

Prior to staining the entire slide series, a protocol was devised to determine the best antigen retrieval method and optimum primary antibody dilution for both K18 and K19. Briefly, sodium citrate 0.01M (Sigma Aldrich, Dorset, UK) and proteinase K (Millipore, Oxfordshire, UK) were used for antigen retrieval but found to be less effective compared with Tris EDTA. A negative control (omission of primary antibody) was used for each staining experiment to ensure staining had not occurred due to factors other than antibody. During protocol development Keratin 18 was tested at dilutions 1: 500, 1: 1000, 1: 1500, 1: 2000 and 1: 2500 to determine the optimum dilution for staining. Keratin 19 was tested at dilutions 1: 250, 1: 500, 1: 1000, 1: 1500 and 1: 2000 to determine the optimum dilution for staining (Figures 50 and 51).

Once the optimum antigen retrieval method and dilution was determined, slide staining for K18 and K19 were performed using the same protocol.

Biopsy sample characteristics

Colonic pinch biopsies (taken as previously described in Chapter 5), were sectioned, formalin fixed and paraffin mounted on slides.

A larger archive of tissue was available for IHC, in comparison to that available for iTRAQ and western immunoblot. To provide a more accurate representation of the population, all available tissue samples of the FACT series were analysed (Corfe et al., 2009). Biopsies were obtained from 20 adenoma patients: from the adenoma itself (AD); the contralateral wall of the adenoma (CO) and the mid-sigmoid (MS) (Table 18). Biopsies were obtained from the mid-sigmoid of 32 patients with no pathology (N) (Table 19).

Two slides containing three biopsies each (at 10 sections apart) were selected from each patient sample therefore each sample number was stained in duplicate.

Table 18. Slide sample numbers for pathological samples

Sample number	Biopsy sites	Butyrate level mmol/L	Sample number	Biopsy sites	Butyrate level mmol/L
186	AD, CO and MS	16	**105**	AD, CO and MS	5
125	AD, CO and MS	13	**111**	AD, CO and MS	3
108	AD, CO and MS	9	**188**	AD, CO and MS	2
214	AD, CO and MS	8	**167**	AD, CO and MS	1.6
168	AD, CO and MS	8	**139**	AD, CO and MS	1.5
164	AD, CO and MS	8	**179**	AD, CO and MS	1.3
170	AD, CO and MS	8	**148**	AD, CO and MS	1.3
210	AD, CO and MS	8	**123**	AD, CO and MS	1
181	AD, CO and MS	7	**163**	AD, CO and MS	0.7
136	AD, CO and MS	5	**174**	AD, CO and MS	0.6

(AD – adenoma, CO – contralateral and MS – mid-sigmoid) and corresponding butyrate level (obtained from faecal sampling).

Table 19. Slide sample numbers for normal samples

Sample number	Biopsy site	Butyrate level mmol/L	Sample number	Biopsy site	Butyrate level mmol/L
113	N	20	**142**	N	4.6
172	N	14	**109**	N	4
101	N	13	**149**	N	4
221	N	13	**112**	N	4
219	N	12	**114**	N	4
213	N	10	**161**	N	3.6
159	N	8	**140**	N	2.9
193	N	8	**182**	N	2.7
160	N	7	**110**	N	2.5
116	N	7	**165**	N	2.11
118	N	6	**141**	N	1.9
216	N	6	**135**	N	1.4
150	N	6	**133**	N	1.2
106	N	5	**157**	N	1
162	N	5	**153**	N	1
117	N	4.7	**156**	N	0.7

Normal samples – N and corresponding butyrate level (obtained from faecal sampling).

Removal of paraffin and rehydration of sections

25 slides were processed at a time by placing in a rack and performing the following washes:

Xylene: 2 x 5 minutes

100% ethanol: 2 x 3 minutes

95% ethanol: 3 minutes

90% ethanol: 3 minutes

Blocking of endogenous enzymes

The slides were immersed in hydrogen and methanol solution for 20 minutes before rinsing in distilled water and then in PBS.

Antigen retrieval

Slides were placed on stain trays and tissue samples encircled using ImEdge hydrophobic barrier pen. The slides were placed in Tris EDTA pH9, covered in cling film and microwaved at high setting for 9 minutes. The slides were left to cool in Tris EDTA for 10 minutes before rinsing in PBS: 1 x 1 minute and 2 x 5 minute washes.

Immunohistochemical staining

Slides (on stain trays) were blocked using 10% goat serum for 30 minutes. Following the block stage, the serum was tipped off and primary antibody (K18 at 1: 2000 [0.5μL/mL] or K19 at 1: 1500 [1μL/1.5mL]) pipetted onto the tissue sections and incubated at 4°C overnight.

Slides were transferred back into racks following primary antibody incubation and washed with PBS: 1 x 1 minute and 2 x 5 minute washes. Slides were placed back into stain trays and covered with biotinylated secondary goat anti-mouse antibody at room temperature for 30 minutes. During the 30 minute period ABC was prepared as described above and allowed to develop before use. Slides were washed with PBS (1 x 1 minute and 2 x 5 minute) and then covered with ABC for 30 minutes. Slides were washed again with PBS (1 x 1 minute and 2 x 5 minute). DAB was prepared as described above and pipetted onto the slides. Slides were incubated with DAB for 9 minutes before washing in tap water for 5 minutes.

Slides were immersed in Gills haematoxylin for 2 minutes before a further wash in running tap water until the water ran clear.

Dehydration and slide mounting

Slides were dehydrated by progressively immersing in ethanol at concentrations: 70%, 90%, 95%, 100% and 100% for 3 minutes each. Slides were then immersed in xylene until the ImEdge wax was removed. Slides were mounted in DPX mountant (Sigma Aldrich, Dorset, UK) and left to dry for 24 hours before imaging.

Semi-quantitative image scoring

The entire slide series was scored by a single observer and then validated by an independent second scorer. 6 well-orientated crypts per biopsy, showing the entire length of the crypt, were scored. A scoring system was devised based on previous descriptions in the literature (Fujisaki and Shimoda, 1993, Khan et al., 2011) and general observations of the appearance of the whole slide series. The general (most widespread pattern) staining intensity for the series was used as the standard for comparison. Scores for staining intensity were awarded in comparison to the standard.

Both K18 and K19 slides were scored based on three parameters:
1. Intensity of surface staining
2. Intensity of crypt base staining
3. Extent of crypt staining

Scores were awarded as follows:

0 - no staining

1 - weaker staining than standard

2 - same staining as standard

3 – stronger staining than standard

The same staining criteria were applied to both normal tissue and adenoma tissue. The magnitude of staining intensity was interpreted as the degree of keratin expression.

7.3.3 Statistics

SPSS (IBM SPSS Statistics for Windows, Version 20.0. Armonk, NY) was used for statistical analysis. The same tests were performed for both K18 and K19 slide series:

1. Spearman's rank correlation coefficient was performed to relate butyrate level and keratin expression (a p value of <0.01 was considered significant). Spearman's rank was chosen since the dataset is non parametric (not normally distributed). Graphs were plotted to reveal correlation and R^2 coefficient (a determination of how well the regression line approximates the real data points). Only graphs demonstrating good correlation, statistical significance or good R2 coefficient are shown in the main body of the thesis but the remainder are available in Appendix 7.

2. Comparison of keratin expression between normal, mid-sigmoid and contralateral sites was performed using confidence intervals and unpaired t test. A p value of <0.01 was considered significant.

7.4 Results

7.4.1 Optimum antigen retrieval method

Sodium citrate and proteinase K were found to be suboptimal in comparison to Tris EDTA for antigen retrieval (Figure 49).
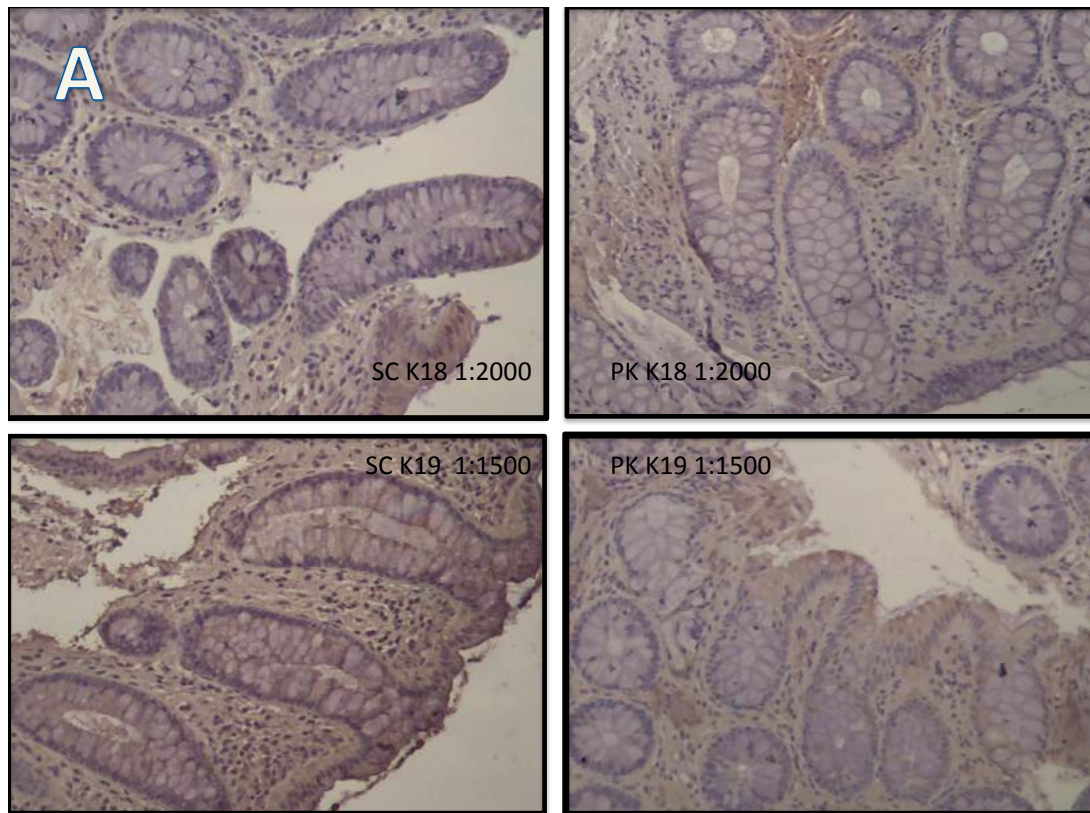
Figure 49. Immunohisochemistry slides for optimum retrieval method

A selection of slides showing IHC using sodium citrate (SC) and proteinase K (PK) and K18 antibody used at optimum dilution of 1:2000 and K19 antibody used at optimum dilution of 1:1500. In comparison to figures 50 and 51 poor staining of the crypts is indicated in the figure above signifying suboptimum antigen retrieval using sodium citrate and proteinase K.

7.4 Results

7.4.2 Optimum dilutions of K18 antibody for staining

Optimum staining was found at 1:2000 dilution of primary K18 antibody following antigen retrieval with Tris EDTA. Stronger dilutions (1:1000 and 1:1500) resulted in indiscriminate heavy staining of all cells within the crypts. Weaker dilutions revealed patching staining of cells, which was not representative of the staining characteristics of the entire crypt.
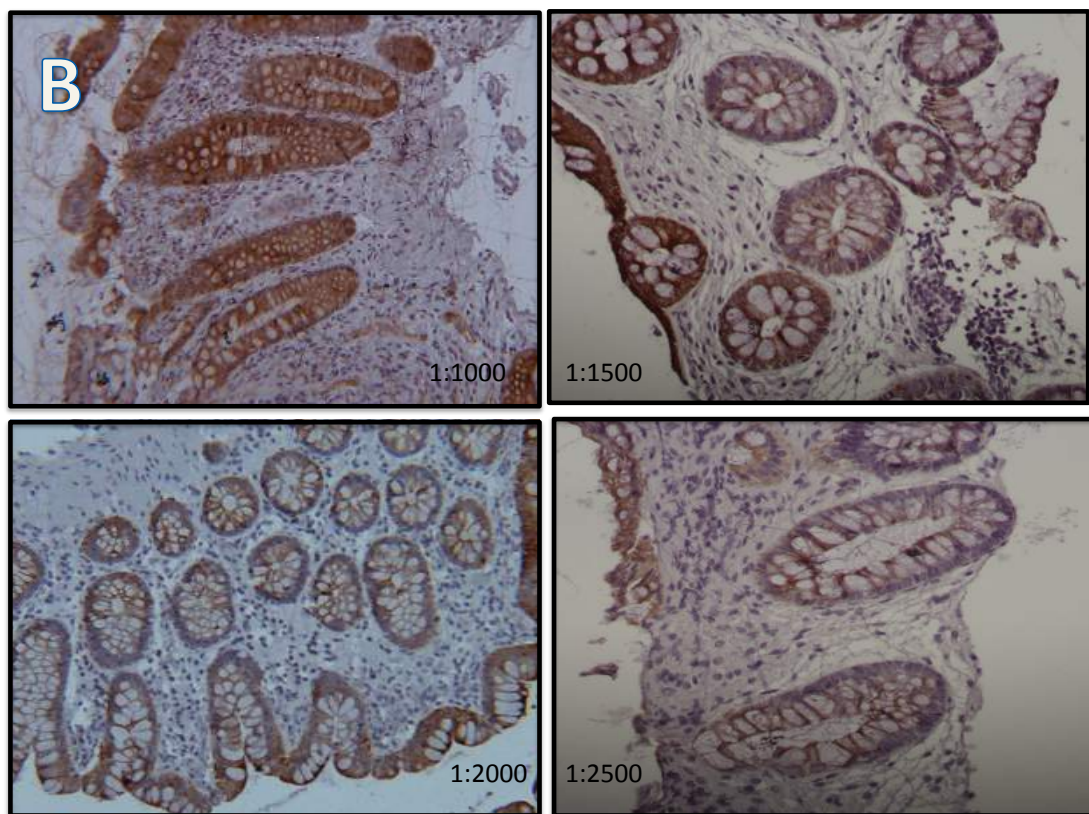
Figure 50. Immunohistochemistry slides for optimum K18 dilution

K18 stained IHC slides taken at x 20 magnification. Antigen retrieval was performed using Tris EDTA. Dilutions 1:1000, 1:1500, 1:2000 and 1:2500 as indicted on the figure. Slides at K18 dilution 1:1000 were too heavily stained. Slides at 1:1500 were slightly better but dark staining was seen at the mucosal border. The optimum staining was seen at dilution 1:2000; further dilution of K18 to 1:2500 revealed deficient staining of crypts.

7.4 Results

7.4.3 Optimum dilutions of K19 antibody for staining

Optimum staining was found at 1:1500 dilution of primary K19 antibody following antigen retrieval with Tris EDTA. Stronger dilutions (1:500 and 1:1000) resulted in indiscriminate heavy staining of all cells within the crypts. Weaker dilutions revealed insufficient staining of cells, which would not be able to demonstrate characteristics of the crypt.
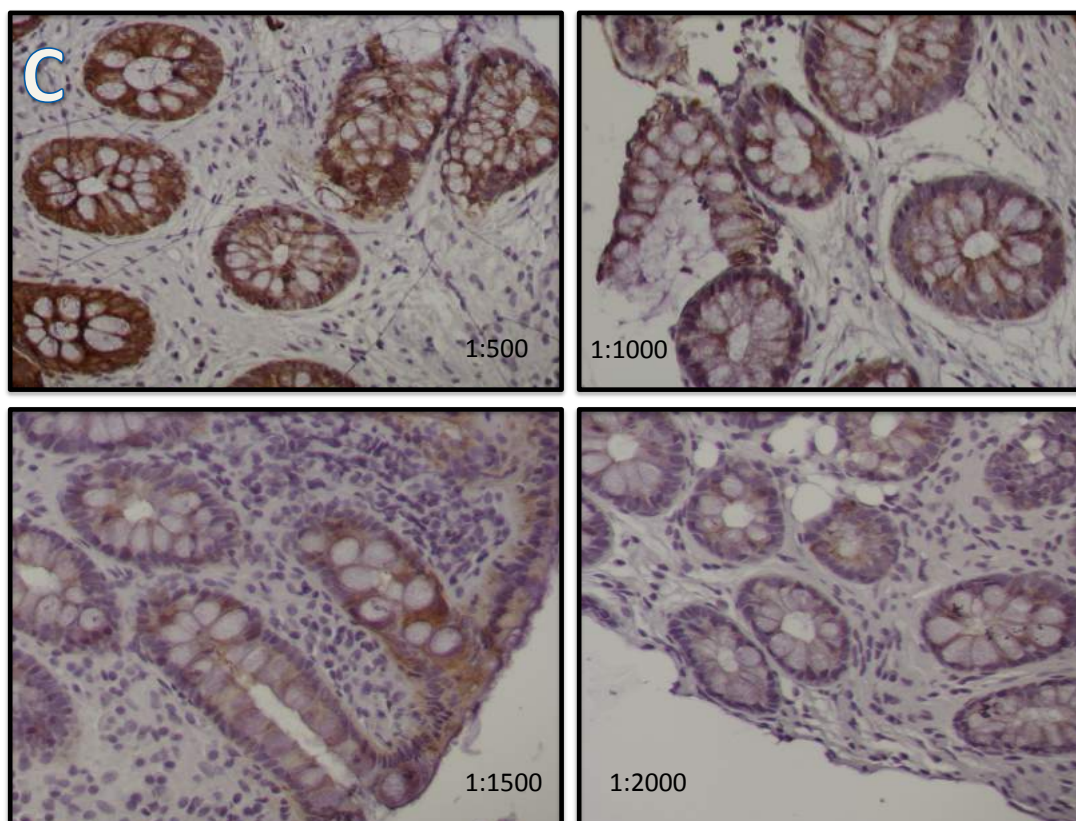
Figure 51. Immunohistochemistry slides for optimum K19 dilution

K19 stained IHC slides taken at x 20 magnification. Dilutions 1:500, 1:1000, 1:1500 and 1:2000 as indicted on the figure. Slides at K19 dilution 1:500 showed uniform strong staining of the crypts. Slides at 1:1000 were slightly better but dark staining was evident in some cells of the crypt. The optimum staining was seen at dilution 1:1500, further dilution of K19 to 1:2000 revealed deficient staining of crypts.

7.4 Results

7.4.4 Keratin 18 and 19 expression in relation to butyrate

Normal crypts

Figure 52 illustrate normal crypts and cells that were considered to have strong or weak staining in different areas of the crypt. There were no significant correlations between K18 or K19 expression in relation to butyrate level in any of the histologically normal (CO, MS or N) samples (Tables 20 and 21).
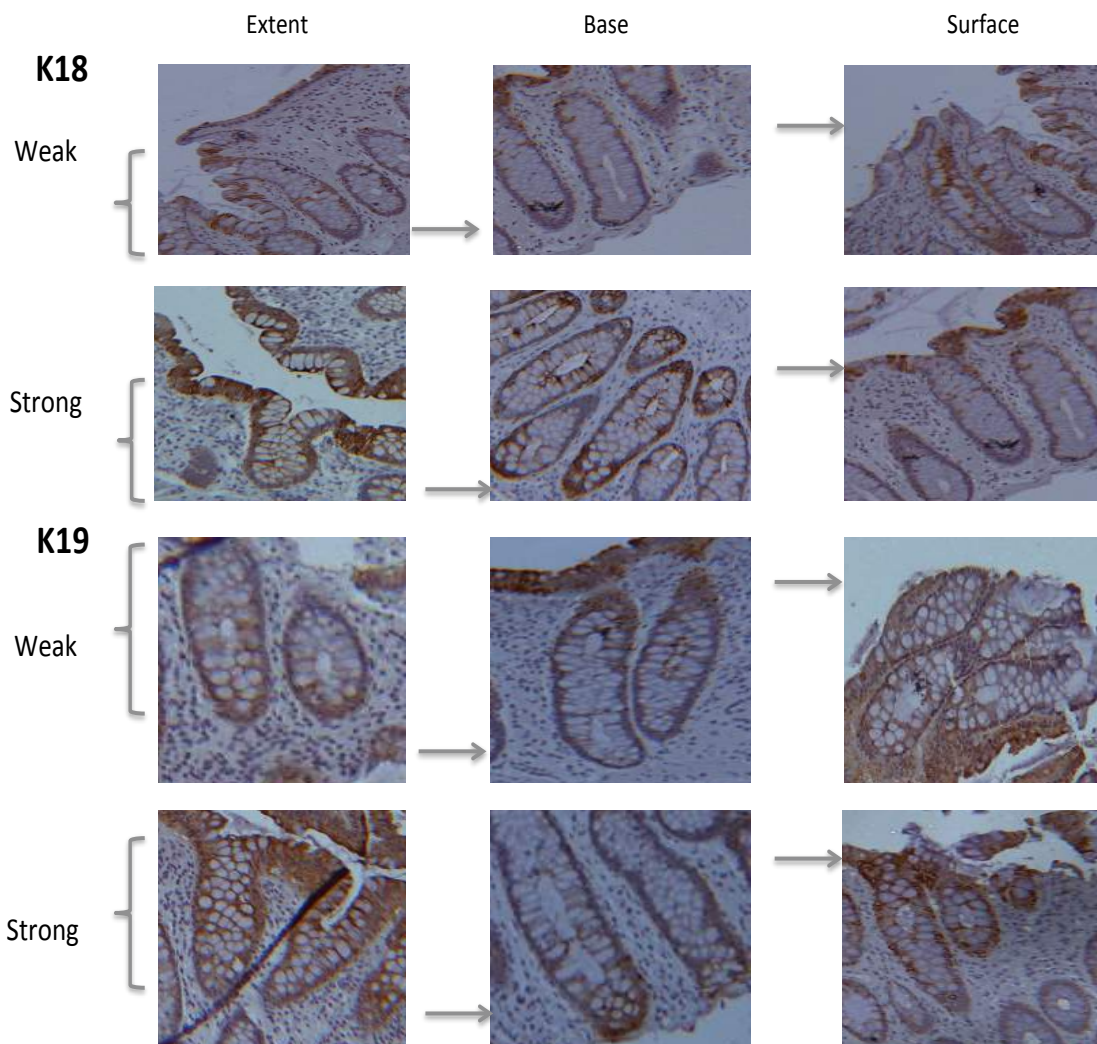
Figure 52. Normal crypt samples demonstrating the contrast between strong and weak K18 and K19

Staining at extent, base and surface indicated by grey arrows.

7.4 Results

Keratin 18 and 19 expression in relation to butyrate

Adenoma samples

Figure 53 illustrate adenomatous crypts with cells that were considered to have strong or weak staining in different areas of the crypt. Although histological appearance is not directly investigated in this study of note is the loss of crypt architecture in comparison to slides in Figure 52. There were no significant correlations between K18 or K19 in relation to butyrate level in adenoma samples (Tables 20 and 21).
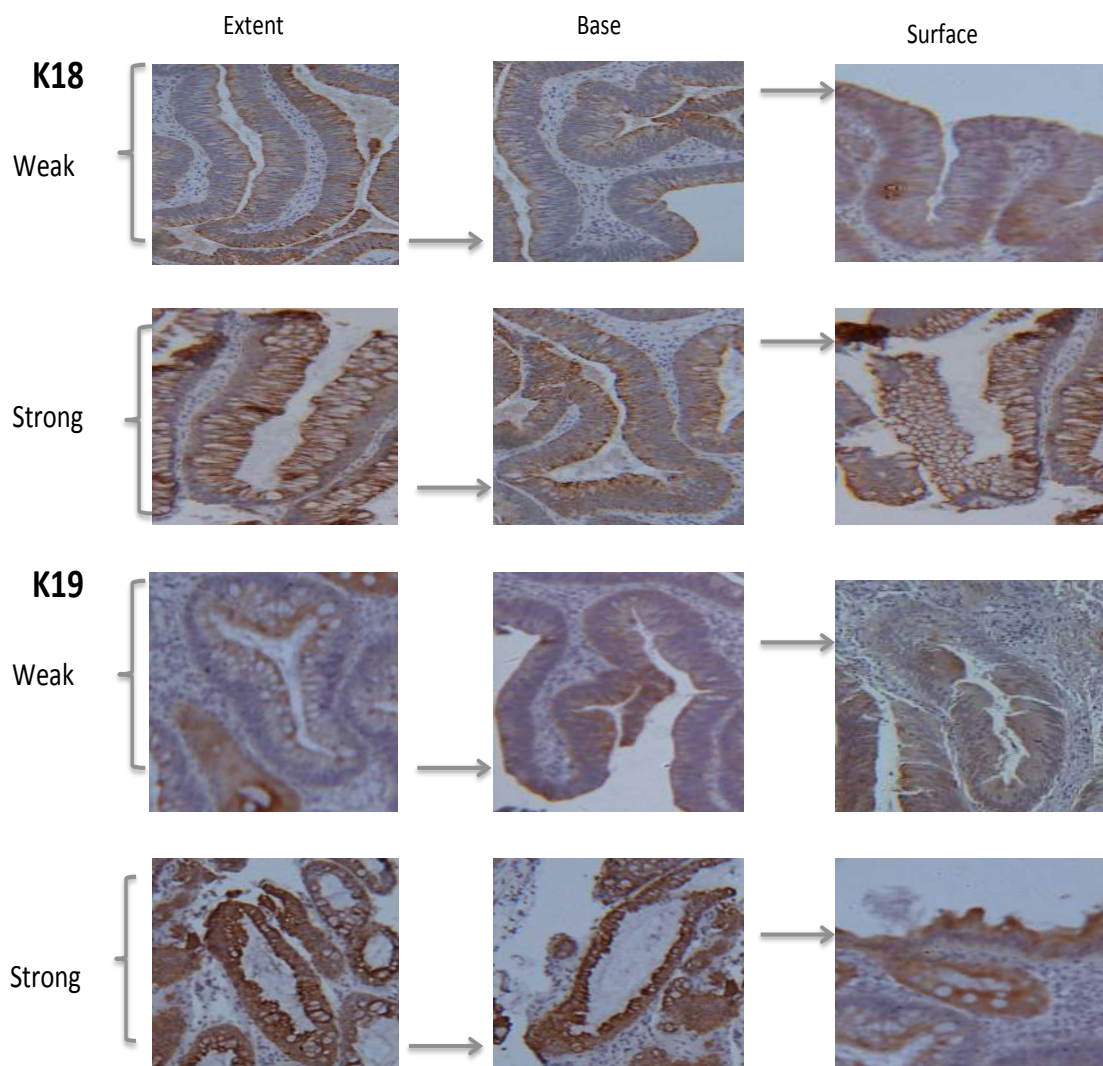
Figure 53. Adenoma samples demonstrating the contrast between strong and weak K18 and K19

Staining at extent, base and surface indicated by grey arrows.

7.4 Results

Keratin 18 expression in relation to butyrate

There were no significant associations (all p values > 0.01) between butyrate level and K18 expression.

Keratin 18

Table 20. Spearman's rank – correlation between K18 expression and butyrate level

Biopsy site	Crypt site	Spearman's rho	Correlation strength*	P value	R^2
Adenoma	Surface	-0.044	Weak	0.852	0.012
	Base	0.130	Weak	0.585	0.002
	Extent	0.070	Weak	0.769	0.006
Contralateral	Surface	0.022	Weak	0.927	0.004
	Base	-0.193	Weak	0.416	0.013
	Extent	-0.159	Weak	0.503	0.002
Mid-sigmoid	Surface	-0.347	Moderate	0.146	0.104
	Base	-0.308	Moderate	0.200	0.107
	Extent	-0.187	Weak	0.444	0.020
Normal	Surface	0.102	Weak	0.577	0.001
	Base	-0.090	Weak	0.624	0.007
	Extent	-0.040	Weak	0.828	0.001

*Correlation strength derived from Cohen J (1998) Statistical Power Analysis for Behavioural Sciences. Lawrence Erlbaum. R^2 is the determination of how well the regression line approximates the real data points.

There were no significant associations (all p values > 0.01) between butyrate level and K18 expression.

See appendix 7 for the graphs from which the data in table 20 are derived.

7.4 Results

Keratin 19 expression in relation to butyrate

No association was found between K19 expression and butyrate level.

Keratin 19

Table 21. Spearman's rank – correlation between K19 expression and butyrate level

Biopsy site	Crypt site	Spearman's rho	Correlation strength*	P value	R^2
Adenoma	Surface	0.287	moderate	0.219	0.077
	Base	0.321	moderate	0.168	0.059
	Extent	0.237	weak	0.314	0.023
Contralateral	Surface	-0.279	weak	0.234	0.113
	Base	0.095	weak	0.692	0.009
	Extent	0.128	weak	0.591	0.002
Mid-sigmoid	Surface	0.015	weak	0.948	0.001
	Base	0.107	weak	0.673	0.001
	Extent	-0.088	weak	0.728	0.042
Normal	Surface	0.062	weak	0.737	<0.001
	Base	0.016	weak	0.929	0.050
	Extent	0.090	weak	0.625	0.020

*Correlation strength derived from Cohen J (1998) Statistical Power Analysis for Behavioural Sciences. Lawrence Erlbaum. R^2 is the determination of how well the regression line approximates the real data points. There were no significant associations (all p values > 0.01) between butyrate level and K19 expression.

See appendix 7 for the graphs from which the data in table 21 are derived.

7.4 Results

7.4.5 Comparison of keratin 18 expression between sites

Surface

K18 expression at the surface of the crypt was seen to be lower in adenoma samples in comparison to the macroscopically normal samples (Figure 54A). If the samples from pathological colons were considered separately a progressive decrease in K18 expression can be seen with adenoma proximity. The decrease in K18 expression with adenoma proximity contrasts with iTRAQ findings. Only surface staining analyses for adenoma samples were performed. Analysis using base expression and extent of expression in adenoma samples was not possible since tissue architecture in the majority of adenoma samples was lost (Figure 53).

Base

K18 expression at the base of crypts from tissue of pathological colons (CO and MS) was significantly lower than tissue from disease free colons (N) (Figure 54B). This contrast with the results from iTRAQ where normal tissue exhibited lower K18 levels. No significant difference between the CO and MS sample could be demonstrated to suggest a progressive field change with adenoma proximity.

Extent

K18 extent expression from tissue of pathological colons (CO and MS) was significantly lower than tissue from disease free colons (N) (Figure 54C). Again, no significant difference could be demonstrated for extent of crypt staining between CO and MS to demonstrate a progressive field change for adenoma proximity. These results also contrast with iTRAQ findings where normal tissue exhibited lower K18 levels.

7.4 Results

7.4.6 Comparison of keratin 19 expression between sites

Surface

At the surface, a progressive decrease in K19 expression was seen with adenoma proximity, if the pathological samples are considered independently (Figure 54D). This result is in accordance to iTRAQ findings from the low butyrate group only. Only surface staining in adenoma samples were possible due to loss of crypt architecture.

Base

At the crypt base, a progressive decrease in K19 expression was seen with distance from the adenoma (Figure 54E). Significant differences between the field (CO) and mid-sigmoid and normal tissue were identified, this is in line with iTRAQ results from the high butyrate group, however, the iTRAQ findings were non significant.

Extent

The extent of expression mirrors the expression pattern at the base where K19 expression decreases with distance away from the adenoma (Figure 54F). Significant K19 expression differences were seen between the field (CO) and mid-sigmoid and normal. This relationship was also seen in iTRAQ results of the high butyrate group as K19 levels decreased with distance from the adenoma, however the iTRAQ results were non significant.

7.4 Results

Comparison of K18 and K19 expression between sites
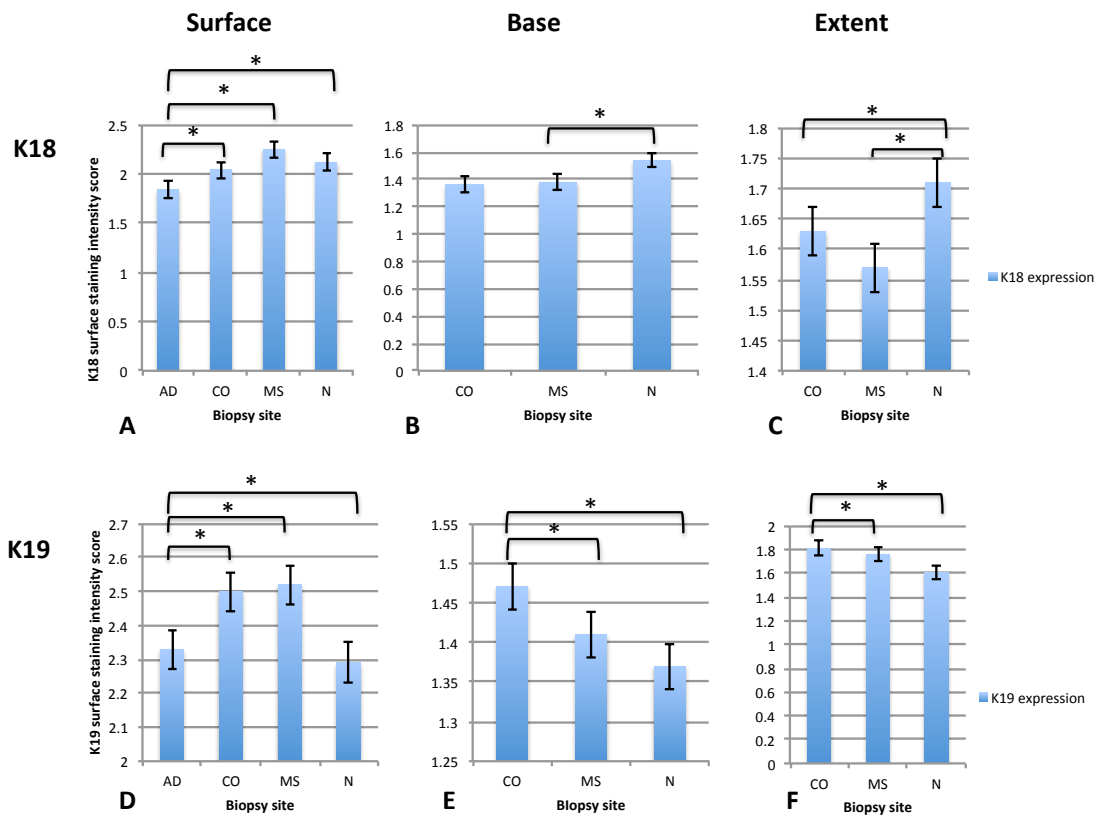
Figure 54. Comparison of mean K18 and K19 staining scores across biopsy sites

Figures A-C Comparison of mean K18 expression scores at the surface, base and extent between biopsy sites using unpaired t test. Values are expressed as mean score ± standard error.

At the surface AD = 1.84, CO = 2.04, MS = 2.25, N = 2.12.

At the base CO = 1.36, MS = 1.38, N = 1.54.

In crypt extent CO = 1.63, MS = 1.57, N = 1.71.

Figures D-F Comparison of mean K19 expression scores at the surface, base and extent between biopsy sites using unpaired t test.

At the surface AD = 2.33, CO = 2.50, MS = 2.52, N = 2.29.

At the base CO = 1.47, MS = 1.41, N = 1.37.

In crypt extent CO = 1.81, MS = 1.76, N = 1.61.

* = significant difference P value = <0.01.

7.4 Results

Comparison of total keratin 18 expression between sites

The values for surface, base and extent were added together to investigate if total K18 expression level within a crypt reveals a relationship between K18 expression and adenoma proximity. A relationship between K18 expression and adenoma proximity was not demonstrated to support field cancerization. A non-significant increase in K18 expression was noted with increasing distance from adenoma (Figure 55). This is contrary to the iTRAQ findings where higher levels of K18 were found with proximity to adenoma.
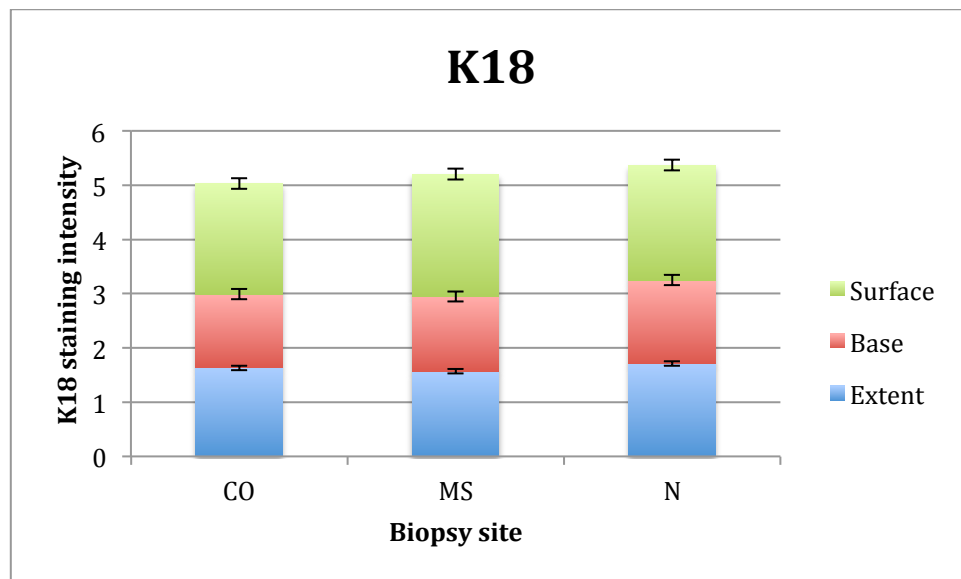
Figure 55. Total K18 expression at biopsy sites

Total K18 expression at biopsy sites contralateral (CO), mid-sigmoid (MS) and normal (N) for surface, base and extent of crypt. Values are expressed as mean ± standard error. Additions of the surface, base and extent values reveal the total K18 expression difference between sample sites were not significant (P = 0.87 between CO and MS; P = 0.87 between MS and N and P= 0.68 between CO and N). Suggesting distribution of K18 may be more important in identifying differences between sites.

7.4 Results

Comparison of total keratin 19 expression between sites

The values for surface, base and extent were added together to investigate whether total K19 expression within a crypt reveals a relationship between K19 and adenoma proximity. Total K19 expression appears to decrease with distance away from adenoma suggesting a field of lower K19 around the adenoma (Figure 56). This association varies according to butyrate level: in a high butyrate environment iTRAQ demonstrated a higher level of K19 with proximity to adenoma (contrary to IHC results) and in low butyrate samples K19 expression levels decrease with proximity to the adenoma (supported by IHC results).
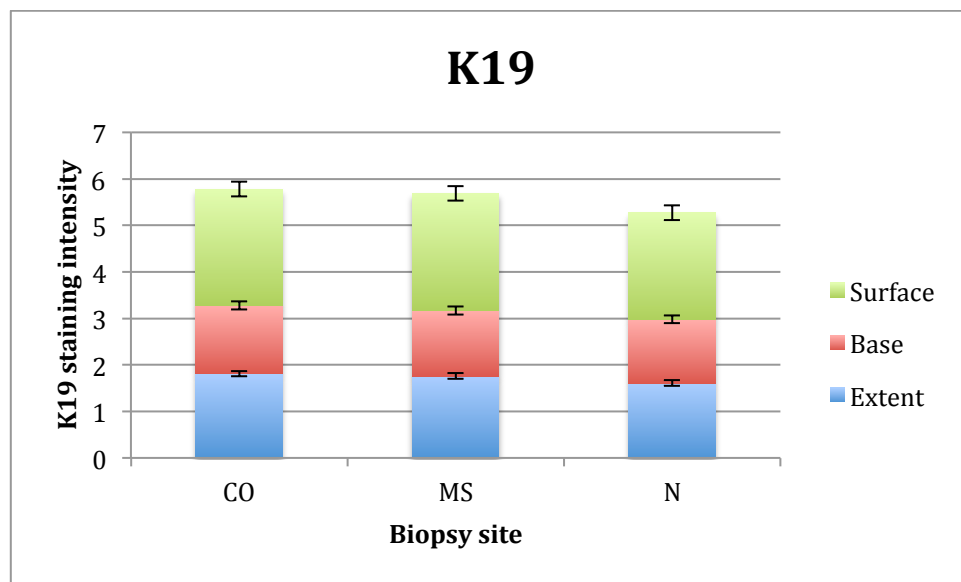
Figure 56. Total K19 expression at biopsy sites

Total K19 expression at biopsy sites contralateral (CO), mid-sigmoid (MS) and normal (N) for surface, base and extent of crypt. Values are expressed as mean ± standard error. Addition of the surface, base and extent values indicate that K19 expression increases with adenoma proximity. Comparisons between the sites using unpaired t test did not reveal any significant differences (P=0.91 between CO and MS; P=0.76 between MS and N and P=0.70 between CO and N).

7.4 Results

7.4.7 IHC results compared with iTRAQ results

iTRAQ fold change and mean IHC scores according to high and low butyrate for K18 and K19 do not seem to follow the same trend.

IHC and iTRAQ results for K18 again demonstrate samples from high butyrate environments have greater K18 fold changes and greater K18 expression levels than samples from low butyrate environments (Figure 57).
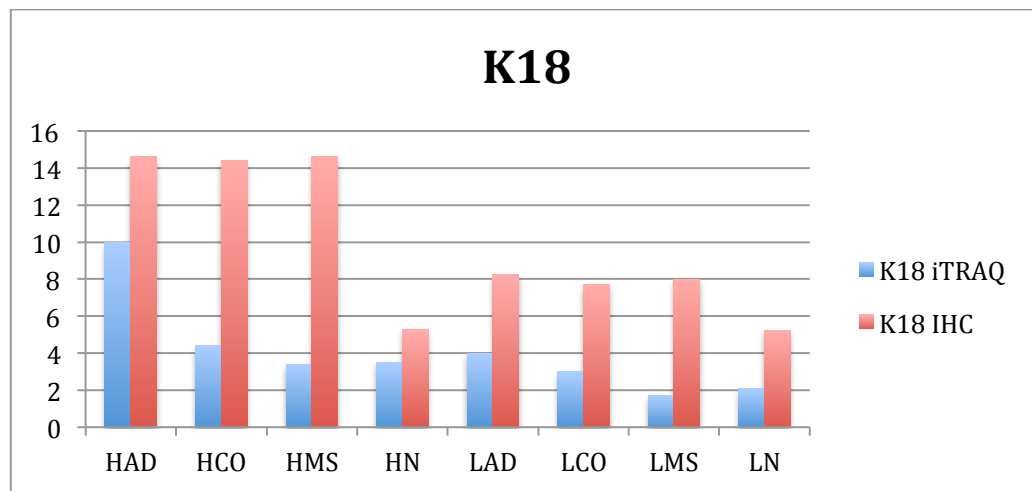
Figure 57. K18 iTRAQ results compared with IHC scores

iTRAQ fold change values have been multiplied by a factor of 10 so that the graphs can be represented on the same figure.

A trend could not be demonstrated in K19 samples. iTRAQ fold changes and IHC scores seemed to behave in a contrasting manner (Figure 58).
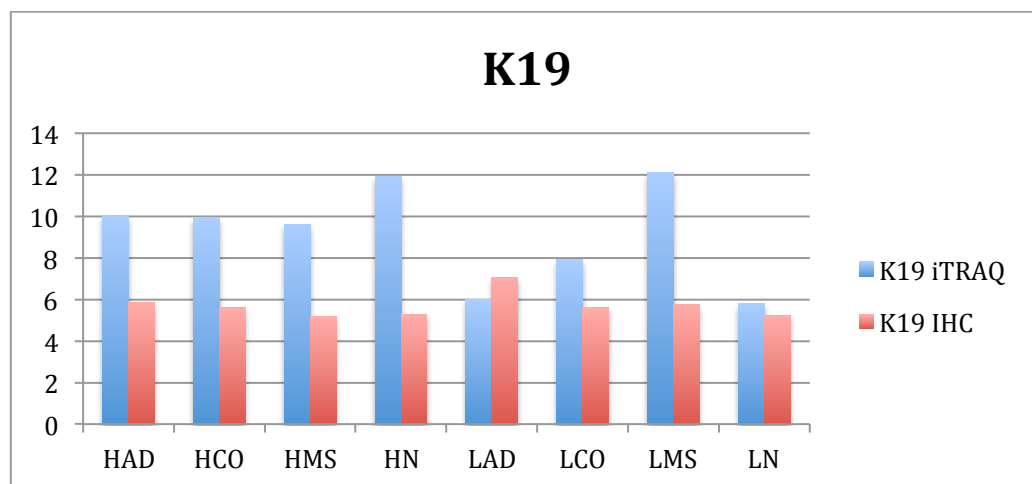
Figure 58. K19 iTRAQ results compared with IHC scores

iTRAQ fold change values have been multiplied by a factor of 10 so that the graphs can be represented on the same figure.

7.4 Results

Keratin 18

- Significant expression differences were only seen at the surface of the crypt, where K18 increased with distance from the adenoma. This is in contrast to the results from iTRAQ.

- There were no significant differences between expression of K18 between sites in either the base or the extent of the crypt.

- A non-significant trend of increased total K18 expression with increasing distance from the adenoma was seen. The findings are opposite to iTRAQ results.

Keratin 19

- K19 expression decreased with adenoma proximity at the surface of the crypt, this correlation was significant and was consistent with the iTRAQ findings in a low butyrate environment.

- Total K19 expression increased with adenoma proximity, this association was also demonstrated in the base and extent of the crypt. This correlation was significant and also consistent with iTRAQ findings in a high butyrate environment.

7.5 Discussion

7.5.1 Keratin 18

Influence of butyrate

Significant trends between K18 expression and butyrate levels could not be demonstrated. Results from IHC studies could not validate the iTRAQ findings where samples from high butyrate environments were found to have higher levels of K18. It is likely that the findings from immunohistochemistry are not representative of the true K18 level pattern. The reasons for this assertion are three fold: the R^2 coefficient for pathological samples and normal samples indicate the linear correlation only pass through 2% and 0.1% (respectively) of the total data points; both Spearman's coefficients were weak correlations and furthermore, did not reach statistical significance. The technique of IHC itself also has inherent weaknesses such as difficulties in standardising antigen retrieval will result in variable staining intensities. Quantification of staining intensities is both difficult and subjective and therefore 'expression' of K18 and K19 should be interpreted with caution. The main use of IHC is for localisation of proteins and is relatively weak at measuring keratin expression levels. As a result, there are many methodological and interpretation limitations in this part of the study.

Commercially available equipment could be used in future studies in order to standardise antigen retrieval, especially when large numbers of slides are processed. Although, positive and negative controls were used during the experiments for optimum staining and retrieval they were not used during when staining for K18 or K19. This was an oversight and limitation to this study and should not be repeated for future experiments. Although two independent observers scored the slide series, the final score is still open to subjective bias. For future studies, perhaps an automated system for scoring could be employed, in addition to the observers, to ensure reproducibility.

Influence of biopsy site

Comparison of K18 expression between biopsy sites was inconsistent with iTRAQ results. K18 expression at cryptal surface of adenoma samples was found to be lower than other pathological sites and normal tissue, the opposite of iTRAQ findings. The method for K18 expression quantification can be criticised since cellular atypia for adenoma samples was not taken into consideration during scoring. The IHC scoring was carried out by two non pathologically trained scorers. Other authors have found differing scores for crypts with different degrees of atypia (Fujisaki and Shimoda, 1993). If samples were classified into different degrees of atypia the results may be more consistent with the iTRAQ findings. The results from this study confirm the findings of Fujisaki and Shimoda (1993), where distributions for K18 were similar between cancer, adenoma and normal samples.

When K18 expression levels for surface, base and extent were plotted together (Figure 55) total K18 expression levels between biopsy sites were very similar and not reflective of iTRAQ findings, where adenoma samples demonstrated greater expression than normal samples. These findings suggest the distribution of K18 may be more important in defining the pathology of different samples than total expression levels. The surface, base and extent expression is similar in the adenoma group but as proximity from adenoma increases the surface expression increases with a reciprocal decrease in extent expression. It is possible, that during the transformation from normal mucosa to adenoma surface K18 is redistributed to the rest of the crypt (base and extent). This may represent an effort to stabilise the whole crypt prior to malignant transformation or characterise malignancy once transformation has taken place. The former hypothesis is more likely, since other studies have identified less staining for other keratins in deep cells of cancer tissue (Khan et al., 2011). It is possible the process of migration can alter keratin properties and as a result lower molecular weight forms of K18 were identified on western blot (Figure 41).

Results from this study are comparable to a similar study where adenoma, contralateral and mid-sigmoid samples were stained for keratin 8. Khan et al., (2011) also found decreased surface and base expression of K8 with proximity to the adenoma (Khan et al., 2011).

7.5.2 Keratin 19

Influence of butyrate

A significant association between K19 expression and butyrate levels could not be demonstrated. According to iTRAQ findings (Table 10) samples from high butyrate environments were found to have higher levels of K19, this was the trend seen in IHC but the results should be interpreted with caution since the correlation was weak and did not reach statistical significance. The influence of butyrate on normal samples attained a strong correlation but unfortunately, did not reach significance.

Influence of biopsy site

Surface expression of K19 followed the pattern of K18 where adenoma samples exhibited lower K19 expression. A progressive field change was apparent as surface K19 was lowest at adenoma sites and increased from adenoma to field and distant tissue. With respect to base and extent, the opposite trend was seen but a progressive field effect was demonstrated as K19 expression at base and extent decreased with distance from the pathological tissue, this equates to the trend seen in iTRAQ for the high butyrate group. The fluctuation of keratin distribution demonstrated in Figure 56 resembles that seen with K18 and reiterates the potential impact of keratin distribution on crypt pathology. This pattern of distribution could either reflect a resistance to malignant change or indicate the process of malignant change forces K18 and K19 migration to the base and general extent of the crypt.

These results mimic some of the K19 fold changes revealed in iTRAQ; all high butyrate pathological samples (AD, CO and MS) were found to have lower fold changes of K19 when compared to normal.

Keratin 18 and keratin 19 appear to behave differently as evidenced by iTRAQ and IHC findings. It is possible that different keratins are affected in different stages of adenoma-carcinomagenesis. A previous study has shown decreased K8 expression in adenoma and the field around it but when tissue has progressed into cancer K8 expression increases in the cancer itself and field around (Khan et al., 2011). It could be that K19 behaves in a similar manner to K8 but is an earlier marker for carcinogenesis; K19 expression begins to fall before progression to cancer. There is evidence to show decreased K19 expression is related to increased cell proliferation in colonic adenomas and carcinomas (Stammberger and Baczako, 1999). The mechanism for progression from adenoma to carcinoma could involve an initial decrease in K19 expression to allow increased cellular proliferation necessary for carcinoma growth.

Results from iTRAQ were observed to vary greatly to IHC results. This may be explained as keratins from the insoluble part of the proteome were investigated using iTRAQ but keratins in the whole cell and crypt were investigate using IHC. As discussed in chapter 6, it is possible that at different stages of adenoma-carcinogenesis keratins vary in solubility and are their intracellular distribution is altered.

The sample set used for IHC was much larger in comparison to that used for iTRAQ, however the results from IHC are open to observer bias, whereas iTRAQ quantifications are more precise. Efforts were made to reduce observer bias by employing a second scorer. A further criticism is that butyrate levels were determined via faecal sampling at one time point and may not be representative of the habitual butyrate environment from which the biopsies were obtained.

7.6 Summary

Keratin 18

- There was no significant trend between K18 expression and butyrate level - iTRAQ results could not be validated.

- Differences in total K18 expression between sample sites were not significant – iTRAQ results could not be validated.

- Significant differences between surface expression were found between pathological sites and normal suggesting crypt distribution of K18 is a marker of pathology.

Keratin 19

- A positive correlation between K19 and butyrate level was identified but this was not significant – iTRAQ results could not be validated.

- Differences in total K19 expression between sample sites were not significant – iTRAQ results could not be validated.

- Significant differences between surface expression were found between adenoma and normal sites suggesting crypt distribution of K19 is a marker of pathology.

Chapter 8

Summary

Chapter 8 Summary

8 Summary

Field Effects

Results from the adenoma recurrence data suggest field effects may exist. The absolute figures indicate more metachronous adenomas occur proximal to an index adenoma. Sub-analyses indicate up to 73% of metachronous adenomas occur within two segments of the removed index adenoma. This would support the theory of a predisposed field from which the index adenoma arose and which remains following polypectomy, influencing the development of further adenomas. Further literature to support this comes from clonality studies (Novelli et al., 1996, Merritt et al., 1997). Formation of polyclonal adenomas may be due to interactions with neighbouring crypts (Thirlwell et al., 2010). If this is indeed the case, the altered stromal field around neighbouring crypts would be left *in situ* following removal of an adenoma leaving a predisposed cancerized field. This might explain why metachronous adenomas continue to appear in similar areas to which an index adenoma has been removed. However, it must taken into consideration that this observation could be due to incomplete resection or an initially missed lesion.

One expectation is that the characteristics of a field should bear more resemblance to adenoma tissue than normal tissue of pathology free colons. This expectation was fulfilled as iTRAQ demonstrated K8 and K18 levels to be higher in adenoma, contralateral and mid-sigmoid samples when compared with normal tissue. K8 and K18 were found to increase progressively with proximity to the adenoma. There are numerous studies investigating differences between cancer, field and normal tissue such as methylation, CEA and Bcl-XL anti-apoptotic protein expression (Ahuja et al., 1998, Jothy et al., 1996, Badvie et al., 2006), theses studies demonstrate quantitative changes between normal and cancer tissue to increase progressively with proximity to cancer tissue, indicating a field of characteristically similar tissue around cancers. These findings, together with results from my iTRAQ data, not only demonstrate that fields around cancer and adenomas exist but also that fields display similar properties to neoplastic tissue and these properties become more pronounced

with proximity to the pathological tissue. Western blot validated iTRAQ findings, by demonstrating a progressive increase in densitometry of K8 and K18 with proximity to adenoma samples. However, IHC validation of K18 and K19 only partially supports the iTRAQ findings. The value of IHC over iTRAQ is the ability to characterize keratin distribution within a crypt but unlike iTRAQ it is subject to observer bias, especially when variable cryptal architecture is involved. Nevertheless, results from this study suggest distribution of keratin within the crypt is important and may be related to keratin solubility. This study of K18 and K19 and a study of K8 by Khan et al., 2011 found associations between surface expression of keratins and proximity to lesions but not in extent or base (Khan et al., 2011). Khan et al., (2011) found increased staining at the surface of K8 during progression towards cancer tissue (Khan et al., 2011). This study demonstrated an inverse relationship; in adenoma tissue surface staining decreased as neoplastic tissue progressed towards the adenoma. There are some explanations for these contrasting observations: the distributions of keratins in adenoma and cancer tissue are dissimilar as demonstrated by Fujisaki and Shimoda (1993)(Fujisaki and Shimoda, 1993). One explanation for this is that, the process of carcinogenesis drives keratins toward the surface of the crypt. Alternatively, a mechanism to resist transition from adenoma to carcinoma may involve redistributing keratins away from the surface. If keratins are reallocated to the base, adenomas may benefit from keratins stabilising colonocytes at the base, and following the 'bottom up' theory for histogenesis of adenomas (Preston et al., 2003), this would confer the most advantage. Further study of the expression of K18 and K19 variations within the crypt in cancer tissue in comparison to the adenoma findings from this study might allude to the role of keratins in adenoma-carcinogenesis. Samples were scored in relationship to other samples in the study: for this study it was adenoma and field tissue and for Khan et al. 2011 it was cancer and field tissue. In order to compare accurately the correlation between cancer, adenoma, field and pathology free tissue, IHC should be performed together and staining intensities should be analysed simultaneously.

An encouraging finding is that all the investigation modalities (iTRAQ, Western blot and IHC) show the paired keratins K8 and K18 behaving in a coordinated

manner. K19 was observed to behave differently to K8 and K18; generally K19 expression in this study has decreased with proximity to adenomas. There is evidence to show that K19 may be involved in an alternate pathological process (Stammberger and Baczako, 1999). Stammberger and Baczako found increased K19 to be associated with a decrease in proliferative activity and greater K19 immunoreactivity in adenoma than carcinomas of the colon, suggesting pathology free tissue produces a greater expression of K19 than neoplastic tissue.

Adenoma

Contralateral

Mid-sigmoid

Normal

- iTRAQ demonstrates progressive increase in K8 and K18 expression from normal to adenoma

- Western blot demonstrates progressive increase in K8 and K18 expression from normal to adenoma

Normal

Contralateral

Mid-sigmoid

Adenoma

- IHC demonstrates progressive decrease of K18 and K19 at colonic crypt surface from normal to adenoma

- Western blot demonstrates general decrease in phosphorylation from normal to adenoma

Figure 59. Illustration of how keratins vary according to adenoma proximity

Butyrate

In this study iTRAQ demonstrated high butyrate environments were associated with increased keratin (K8, 18 and 19) expression in all tissues regardless of pathology. iTRAQ findings for butyrate were appropriately validated by Western blot for K8 and K18 and by IHC for K19. Butyrate, a fermentation product of fibre is thought to protect against colorectal cancer by encouraging apoptosis of cancer and adenoma cells (Hague et al., 1995). The influence of butyrate on keratins is different between cancer and benign tissue. In this study high butyrate was associated with increased K8, K18 and K19 expression but the inverse association was found in a previous study by Khan et al., (2011) where high butyrate exposure resulted in decreased K8 expression in cancer tissue. In cancer, high butyrate results in less keratin and also structurally more disorganised keratin. It is possible that butyrate impedes cancer cells through interference with their cellular structure.

Since butyrate, in this study, was associated with a universal increase in keratin expression it is possible that the anti-carcinogenic effect is influenced, in part, by keratins. The mechanisms could be two fold: through augmentation of stability or the regulatory function of non-malignant colonocytes. It is possible that high butyrate exposure in benign tissue (adenoma, field and normal) increases keratins to protect against malignant change but once malignant change has taken place the protective function alters to become pro-apoptotic. The 'butyrate paradox' is well reported in the literature; butyrate inhibits cell proliferation and increases apoptosis in cancer cell lines (Comalada et al., 2006) but is also the main source of nutrition for normal colonocytes (Roediger, 1982). The paradox is incompletely understood but the capacity of butyrate to regulate gene expression by inhibition of histone deacetylases has been proposed (Gibson et al., 1999). The process by which butyrate distinguishes how to treat cancer cells differently is not known. Polley et al., identified several isoforms of K8 in cancer tissue and this study also found K8 of different molecular weights in adenoma samples, exposing a difference between pathological and non pathological tissues. Since acetylatyion of K8 is butyrate responsive (Leech et al., 2008) and the various isoforms of K8 are differentially acetylated (Khan et al.,

202

2011), this association could be the mechanism by which butyrate differentially affects cancer cells. Acetylation of K8 at different sites (in different tissues) could affect the cells predisposition to become more stable, proliferate or undergo apoptosis.

An alternative mode in which tissue can be selectively treated is due to mitosis. Cancer cells undergo mitosis at an increased rate in comparison to benign tissue. Khan et al., found mitotic cells have a fivefold increase in acetylation in comparison to a non-mitotic cell (Khan et al., 2011). The increased acetylation could be due to increased uptake of butyrate as an energy source for cell division. However, there is some evidence that during colorectal carcinogenesis colonocytes switch from aerobic to anaerobic metabolism (Jass, 1985) and therefore become less dependent on butyrate as a fuel source. The resulting unused butyrate could accumulate within the cell and this could further explain why malignant cells are susceptible to the distinguishing effects of butyrate. Results from the principal component analysis revealed clustering of high and low butyrate samples independently suggesting the effects of butyrate exposure assert a stronger influence on the characteristics of tissues samples than the location from which the samples were obtained.

Post-translational modifications

With respect to keratin acetylation via western blot, analysis did not demonstrate any significant results. Keratin phosphorylation was decreased in adenoma samples and increased in contralateral and mid-sigmoid. Again adenoma samples were found not to behave like cancer samples. K8 appeared to be less phosphorylated at serine 23 in adenoma samples but the converse was found by Arentz et al., (2012) where K8 phosphorylation was significantly increased in tumour tissue in comparison to matched normal.

Liao et al., (1995) found stress associated hyperphosphorylation of K8 and K18 in colon cancer cells when they were exposed to heat or rotavirus infection (Liao et al., 1995). Liao et al., (1995) and other studies have demonstrated increased solubility of K8 following hyperphosphorylation (Liao et al., 1995) and (Omary et

al., 1998) The stress response of cancer tissue to increase K8 solubility could be an effort to sustain the cell through cellular redistribution of K8 to the soluble compartment. In this study, the insoluble part of the proteome was examined; perhaps K8 from the adenoma sample was hyperphosphorylated and redistributed into the soluble part of the proteome prior to our analysis and hence seemingly lower phosphorylation of K8 when it came to our analysis. It is possible that adenoma tissues disperse more phosphorylated keratins to the soluble part of the colonocyte, so as to defend the cell from the stress of carcinogenic insult, leading to malignant change or the stress of malignant change itself.

Although adenoma samples in this study were not purposely submitted to stress we consistently found decreased phosphorylation in comparison to normal tissue. Perhaps the carcinogenic insult initiating adenomagenesis was a sufficient stressor to cause phosphorylation. When the adenoma biopsies were sampled hyperphosphorylated K8 had already been distributed to the soluble part. This was not part of my analysis but the stable histologically normal contralateral and mid-sigmoid tissue had no reason to redistribute K8 to the soluble part of the proteome and hence display seemingly greater amounts of phosphorylated K8. Collective results from this study indicate the behaviour of adenoma tissue is different to cancer tissue. There was consistent evidence of adenoma tissue behaving in the exact opposite manner of cancer and surprisingly their characteristics are sometimes more dissimilar to cancer than normal tissue. This may be due to the type of studies in which comparisons have been made. The majority of them have used cancer cells without separating the soluble and insoluble compartments, whereas in this study only the insoluble component was studied. Another explanation is that adenoma cells are actively resisting malignant change, instigating changes including PTMs almost paradoxical to that of cancer. In adenoma tissue there is a general increase in keratins which is opposite to that of cancer (Khan et al., 2011), and a decrease in phosphorylation which is also opposite to findings in cancer (Arentz et al., 2012). This tremendous effort of resistance could explain why a large proportion of adenomas do not progress to cancer.
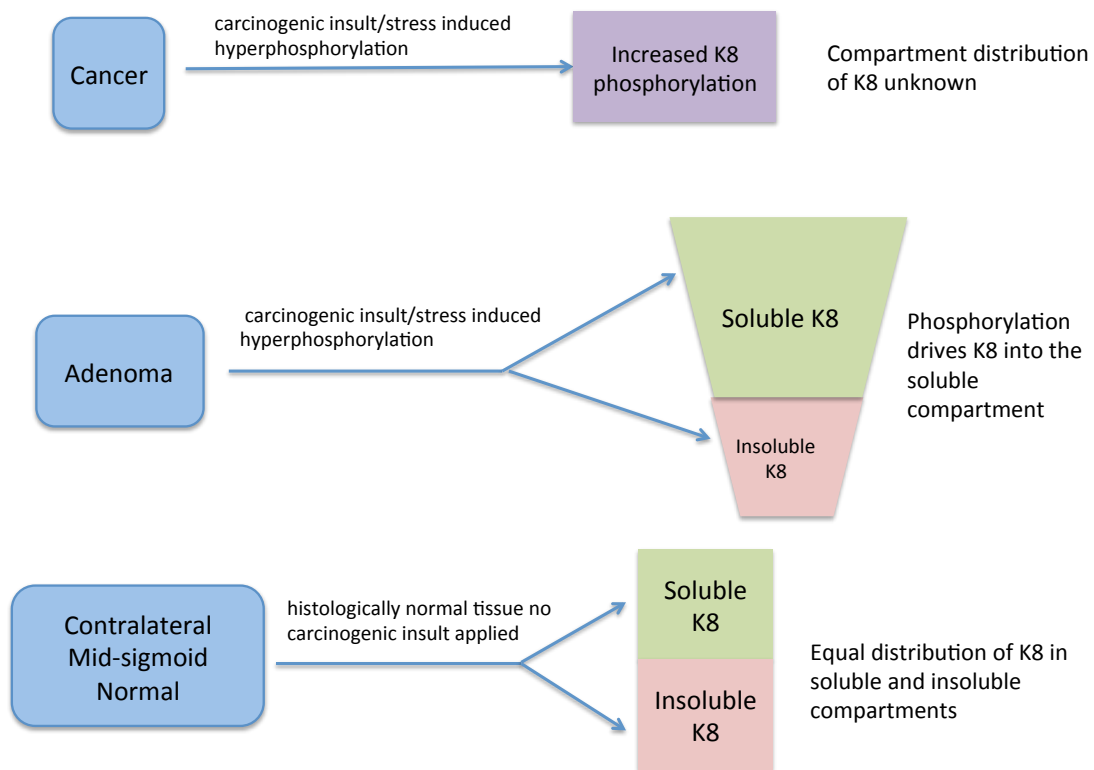
Figure 60. K8 phosphorylation differences between tissue types

This study has demonstrated a field of characteristically similar tissue exists around adenomas but has also demonstrated adenomas do not necessarily mimic cancer tissue. Reasons for this could be due to unmatched comparisons or active resistance to malignant change. A recurring theme that has emerged from this study, revealed through IHC and PTMs, is that the distribution of keratins is important in defining tissue pathology and its behaviour. This area of research should be expanded to compare cancer, adenoma, field and non-pathological tissue under matched conditions.

8.1 Conclusion

- Altered fields exist in the macroscopically normal tissue around adenomatous polyps.
- Keratins changes are identified as one of the alteration in fields around adenomas.

8.2 Future work

- Future work to strengthen results from this study should include performing a larger study with greater numbers of patients and samples.
- Future research studies could use colorectal cancer specimens with synchronous adenomas *in situ* to investigate relationships between thei fields but from one genetic background..
- Further K8 isoform analysis of adenoma tissue and the tissue around it may identify further field effects.

Publications and presentations

- Evans CA, <u>Rosser R</u>, Waby JS, Noirel J, Lai D, Wright PC, Williams EA, Riley SA, Bury JP and Corfe BM. Reduced keratin expression in colorectal neoplasia and associated fields is reversible by both diet and resection. BMJ Open Gastroenterology. May 2015.

- <u>Rosser R,</u> Corfe BM and Chapple KS. Analysis of metachronous adenoma sites suggest proximal occurrence is more probable. Short paper for oral presentation. International Surgical Congress of the Association of Surgeons of Great Britain and Ireland. April 2015.

- <u>Rosser R,</u> Evans CE, Chapple KS and Corfe BM. Identification of Altered Keratin in Cancerized Colonic Fields using Isobaric Tags for Relative and Absolute Quantification (iTRAQ) for protein profiling. Short paper for oral presentation. International Surgical Congress of the Association of Surgeons of Great Britain and Ireland. April 2015.

- <u>Rosser R</u>, Evans, CE, Corfe, BM and Chapple KS. Analysis of metachronous colorectal adenoma sites suggests proximal occurrence is more probable. Poster Presentation: Winner of the Endoscopy Section at British Society of Gastroenterology Annual meeting June 2013.

- <u>Rosser R</u>, Evans CE, Chapple KS and Corfe BM. Identification of Altered Keratin in Cancerized Colonic Fields using iTRAQ. Poster of Distinction at British Society of Gastroenterology Annual meeting June 2013.

- <u>Rosser R</u>, Evans CE, Chapple KS and Corfe BM. Up regulation of keratin 8 in cancerized colonic fields. Poster presented at Yorkshire and Humber Academic Day. Weetwood Hall, Leeds. May 2013.

- <u>Rosser R</u>, Evans CE, Chapple KS and Corfe BM. Identification of altered keratin levels in cancerized colonic fields using isobaric tags for relative and absolute quantification. Poster presented at ChELSI conference - Chemical Engineering at the Life Science Interface, Sheffield. November 2012.

- Majumdar D, <u>Rosser R</u>, Harvard S, Lobo AJ, Wright PC, Evans CA and Corfe BM. An integrated workflow for extraction and solubilization of intermediate filaments from colorectal biopsies for proteomic analysis. Electrophoresis. 2012 Jul; 33(13): 1967-74.

References

1. Achtstaetter, T., Hatzfeld, M., Quinlan, R. A., Parmelee, D. C. & Franke, W. W. 1986. Separation Of Cytokeratin Polypeptides By Gel Electrophoretic And Chromatographic Techniques And Their Identification By Immunoblotting. *Methods In Enzymology,* 134**,** 355-71.

2. Adam, I. J., Ali, Z. & Shorthouse, A. J. 2001. Inadequacy Of Colonoscopy Revealed By Three-Dimensional Electromagnetic Imaging. *Diseaes of the Colon And Rectum,* 44**,** 978-83.

3. Ahuja, N., Li, Q., Mohan, A. L., Baylin, S. B. & Issa, J. P. 1998. Aging And DNA Methylation In Colorectal Mucosa And Cancer. *Cancer Research,* 58**,** 5489-94.

4. Alfonso, P., Nunez, A., Madoz-Gurpide, J., Lombardia, L., Sanchez, L. & Casal, J. I. 2005. Proteomic Expression Analysis Of Colorectal Cancer By Two-Dimensional Differential Gel Electrophoresis. *Proteomics,* 5**,** 2602-11.

5. Arentz, G., Chataway, T., Condina, M.R., Price, T.J., Hoffman, P. & Hardingham, J.E. 2012. Increased Phospho-Keratin 8 Isoforms in Colorectal Tumours Associated with EGFR Pathway Activation And Reduced Apoptosis. Molecular Biology, 2012, 1-8.

6. Atkin, W. S., Saunders, B. P., British Society For, Gastroenterology. Association Of Coloproctology For Great Britian & Ireland 2002. Surveillance Guidelines After Removal Of Colorectal Adenomatous Polyps. *Gut,* 51 Suppl 5**,** V6-9.

7. Badvie, S., Hanna-Morris, A., Andreyev, H. J., Cohen, P., Saini, S. & Allen-Mersh, T. G. 2006. A "Field Change" Of Inhibited Apoptosis Occurs In Colorectal Mucosa Adjacent To Colorectal Adenocarcinoma. *Journal Of Clinical Pathology,* 59**,** 942-6.

8. Balkwill, F. 2002. Tumor Necrosis Factor Or Tumor Promoting Factor? *Cytokine & Growth Factor Reviews,* 13**,** 135-41.

9. Baribault, H., Penner, J., Iozzo, R. V. & Wilson-Heiner, M. 1994. Colorectal Hyperplasia And Inflammation In Keratin 8-Deficient FVB/N Mice. *Genes & Development,* 8**,** 2964-73.

10. Basford, P. J., George, R., Nixon, E., Chaudhuri, T., Mead, R. & Bhandari, P. 2014. Endoscopic Resection Of Sporadic Duodenal Adenomas: Comparison Of Endoscopic Mucosal Resection (EMR) With Hybrid Endoscopic Submucosal Dissection (ESD) Techniques And The Risks Of Late Delayed Bleeding. *Surgical Endoscopy,* 28**,** 1594-600.

11. Bauer, V. P. & Papaconstantinou, H. T. 2008. Management Of Serrated Adenomas And Hyperplastic Polyps. *Clinics In Colon And Rectal Surgery,* 21**,** 273-9.

12. Bauman, P. A., Dalton, W. S., Anderson, J. M. & Cress, A. E. 1994. Expression Of Cytokeratin Confers Multiple Drug Resistance. *Proceedings of the National Academy of Sciences of the United States of America,* 91**,** 5311-4.

13. Bergink, S. & Jentsch, S. 2009. Principles Of Ubiquitin And SUMO Modifications In DNA Repair. *Nature,* 458**,** 461-7.

14. Bernstein, C., Bernstein, H., Payne, C. M., Dvorak, K. & Garewal, H. 2008. Field Defects In Progression To Gastrointestinal Tract Cancers. *Cancer Letters,* 260**,** 1-10.

15. Beutler, E. 1984. Multicentric Origin Of Colon Carcinoma. *Science,* 224**,** 630.

16. Bingham, S. A., Day, N. E., Luben, R., Ferrari, P., Slimani, N., Norat, T., Clavel-Chapelon, F., Kesse, E., Nieters, A., Boeing, H., Tjonneland, A., Overvad, K., Martinez, C., Dorronsoro, M., Gonzalez, C. A., Key, T. J., Trichopoulou, A., Naska, A., Vineis, P., Tumino, R., Krogh, V., Bueno-De-Mesquita, H. B., Peeters, P. H., Berglund, G., Hallmans, G., Lund, E., Skeie, G., Kaaks, R. & Riboli, E. 2003. Dietary Fibre In Food And Protection Against Colorectal Cancer In The European Prospective Investigation Into Cancer And Nutrition (EPIC): An Observational Study. *Lancet,* 361**,** 1496-501.

17. Birkenkamp-Demtroder, K., Olesen, S. H., Sorensen, F. B., Laurberg, S., Laiho, P., Aaltonen, L. A. & Orntoft, T. F. 2005. Differential Gene

Expression In Colon Cancer Of The Caecum Versus The Sigmoid And Rectosigmoid. *Gut,* 54**,** 374-84.

18. Bond, J. H. 2000. Polyp Guideline: Diagnosis, Treatment, And Surveillance For Patients With Colorectal Polyps. Practice Parameters Committee Of The American College Of Gastroenterology. *The American Journal Of Gastroenterology,* 95**,** 3053-63.

19. Bonithon-Kopp, C., Piard, F., Fenger, C., Cabeza, E., O'morain, C., Kronborg, O. & Faivre, J. 2004. Colorectal Adenoma Characteristics As Predictors Of Recurrence. *Diseases Of The Colon And Rectum,* 47**,** 323-33.

20. Braakhuis, B. J., Tabor, M. P., Kummer, J. A., Leemans, C. R. & Brakenhoff, R. H. 2003. A Genetic Explanation Of Slaughter's Concept Of Field Cancerization: Evidence And Clinical Implications. *Cancer Research,* 63**,** 1727-30.

21. Bujanda, L., Cosme, A., Gil, I. & Arenas-Mirave, J. I. 2010. Malignant Colorectal Polyps. *World Journal Of Gastroenterol,* 16**,** 3103-11.

22. Burn, J., Mathers, J. & Bishop, D. T. 2013. Genetics, Inheritance And Strategies For Prevention In Populations At High Risk Of Colorectal Cancer (CRC). *Recent Results in Cancer Research,* 191**,** 157-83.

23. Busch, T., Armacki, M., Eiseler, T., Joodi, G., Temme, C., Jansen, J., Von Wichert, G., Omary, M. B., Spatz, J. & Seufferlein, T. 2012. Keratin 8 Phosphorylation Regulates Keratin Reorganization And Migration Of Epithelial Tumor Cells. *Journal Of Cell Science,* 125**,** 2148-59.

24. Cairns, J. 1975. Mutation Selection And The Natural History Of Cancer. *Nature,* 255**,** 197-200.

25. Cairns, S. R., Scholefield, J. H., Steele, R. J., Dunlop, M. G., Thomas, H. J., Evans, G. D., Eaden, J. A., Rutter, M. D., Atkin, W. P., Saunders, B. P., Lucassen, A., Jenkins, P., Fairclough, P. D. & Woodhouse, C. R. 2010. Guidelines For Colorectal Cancer Screening And Surveillance In Moderate And High Risk Groups (Update From 2002). *Gut,* 59**,** 666-89.

26. Carlsson, G., Petrelli, N. J., Nava, H., Herrera, L. & Mittelman, A. 1987. The Value Of Colonoscopic Surveillance After Curative Resection For Colorectal Cancer Or Synchronous Adenomatous Polyps. *Archives Of Surgery,* 122**,** 1261-3.

27. Castells, A., Marzo-Castillejo, M., Mascort, J. J., Amador, F. J., Andreu, M., Bellas, B., Ferrandez, A., Ferrandiz, J., Giraldez, M., Gonzalo, V., Jover, R., Quintero, E., Alonso-Coello, P., Bonfill, X., Lanas, A., Pinol, V. & Pique, J. 2009. Clinical Practice Guideline. Prevention Of Colorectal Cancer. 2009 Update. Asociacion Espanola De Gastroenterologia. Journal Of *Gastroenterology and Hepatology,* 32**,** 717 E1-58.

28. Chen, C. C., Lin, W. C., Kong, M. S., Shi, H. N., Walker, W. A., Lin, C. Y., Huang, C. T., Lin, Y. C., Jung, S. M. & Lin, T. Y. 2012. Oral Inoculation Of Probiotics Lactobacillus Acidophilus NCFM Suppresses Tumour Growth Both In Segmental Orthotopic Colon Cancer And Extra-Intestinal Tissue. *The British Journal Of Nutrition,* 107**,** 1623-34.

29. Chevallet, M., Luche, S. & Rabilloud, T. 2006. Silver Staining Of Proteins In Polyacrylamide Gels. *Nature Protocols,* 1**,** 1852-8.

30. Chirakkal, H., Leech, S. H., Brookes, K. E., Prais, A. L., Waby, J. S. & Corfe, B. M. 2006. Upregulation Of BAK By Butyrate In The Colon Is Associated With Increased Sp3 Binding. *Oncogene,* 25**,** 7192-200.

31. Cho, K. H., Lee, H. S. & Ku, S. K. 2008. Decrease In Intestinal Endocrine Cells In Balb/C Mice With CT-26 Carcinoma Cells. *Journal Of Veterinary Science,* 9**,** 9-14.

32. Cho, W. C. 2007. Proteomics Technologies And Challenges. *Genomics, Proteomics & Bioinformatics,* 5**,** 77-85.

33. Chou, C. F., Riopel, C. L., Rott, L. S. & Omary, M. B. 1993. A Significant Soluble Keratin Fraction In 'Simple' Epithelial Cells. Lack Of An Apparent Phosphorylation And Glycosylation Role In Keratin Solubility. *Journal Of Cell Science,* 105 (Pt 2)**,** 433-44.

34. Chou, C. F., Smith, A. J. & Omary, M. B. 1992. Characterization And Dynamics Of O-Linked Glycosylation Of Human Cytokeratin 8 And 18. *The Journal Of Biological Chemistry,* 267**,** 3901-6.

35. Clarke, J. M., Young, G. P., Topping, D. L., Bird, A. R., Cobiac, L., Scherer, B. L., Winkler, J. G. & Lockett, T. J. 2012. Butyrate Delivered By Butyrylated Starch Increases Distal Colonic Epithelial Apoptosis In Carcinogen-Treated Rats. *Carcinogenesis,* 33**,** 197-202.

36. Comalada, M., Bailon, E., De Haro, O., Lara-Villoslada, F., Xaus, J., Zarzuelo, A. & Galvez, J. 2006. The Effects Of Short-Chain Fatty Acids On Colon Epithelial Proliferation And Survival Depend On The Cellular Phenotype. *Journal Of Cancer Research And Clinical Oncology,* 132**,** 487-97.

37. Corfe, B. M. 2012. Hypothesis: Butyrate Is Not An HDAC Inhibitor, But A Product Inhibitor Of Deacetylation. *Molecular Biosystems,* 8**,** 1609-12.

38. Corfe, B. M., Williams, E. A., Bury, J. P., Riley, S. A., Croucher, L. J., Lai, D. Y. & Evans, C. A. 2009. A Study Protocol To Investigate The Relationship Between Dietary Fibre Intake And Fermentation, Colon Cell Turnover, Global Protein Acetylation And Early Carcinogenesis: The Fact Study. *Bmc Cancer,* 9**,** 332.

39. Couchie, D., Holic, N., Chobert, M. N., Corlu, A. & Laperche, Y. 2002. In Vitro Differentiation Of WB-F344 Rat Liver Epithelial Cells Into The Biliary Lineage. *Differentiation; Research In Biological Diversity,* 69**,** 209-15.

40. Dakubo, G. D., Jakupciak, J. P., Birch-Machin, M. A. & Parr, R. L. 2007. Clinical Implications And Utility Of Field Cancerization. *Cancer Cell International,* 7**,** 2.

41. Demarque, M. D., Nacerddine, K., Neyret-Kahn, H., Andrieux, A., Danenberg, E., Jouvion, G., Bomme, P., Hamard, G., Romagnolo, B., Terris, B., Cumano, A., Barker, N., Clevers, H. & Dejean, A. 2011. Sumoylation By Ubc9 Regulates The Stem Cell Compartment And Structure And Function Of The Intestinal Epithelium In Mice. *Gastroenterology,* 140**,** 286-96.

42. Ditzel, H. J., Strik, M. C., Larsen, M. K., Willis, A. C., Waseem, A., Kejling, K. & Jensenius, J. C. 2002. Cancer-Associated Cleavage Of Cytokeratin 8/18 Heterotypic Complexes Exposes A Neoepitope In Human Adenocarcinomas. *The Journal Of Biological Chemistry,* 277**,** 21712-22.

43. Drake, P. J., Griffiths, G. J., Shaw, L., Benson, R. P. & Corfe, B. M. 2009. Application Of High-Content Analysis To The Study Of Post-Translational Modifications Of The Cytoskeleton. *Journal Of Proteome Research,* 8**,** 28-34.

44. Enker, W. E., Laffer, U. T. & Block, G. E. 1979. Enhanced Survival Of Patients With Colon And Rectal Cancer Is Based Upon Wide Anatomic Resection. *Annals Of Surgery,* 190**,** 350-60.

45. Evans, C., Noirel, J., Ow, S. Y., Salim, M., Pereira-Medrano, A. G., Couto, N., Pandhal, J., Smith, D., Pham, T. K., Karunakaran, E., Zou, X., Biggs, C. A. & Wright, P. C. 2012. An Insight Into Itraq: Where Do We Stand Now? *Analitical And Bioanalytical Chemistry,* 404**,** 1011-27.

46. Farley, A. R. & Link, A. J. 2009. Identification And Quantification Of Protein Posttranslational Modifications. *Methods In Enzymology,* 463**,** 725-63.

47. Fearon, E. R. & Vogelstein, B. 1990. A Genetic Model For Colorectal Tumorigenesis. *Cell,* 61**,** 759-67.

48. Feinberg, A. P., Ohlsson, R. & Henikoff, S. 2006. The Epigenetic Progenitor Origin Of Human Cancer. *Nature Reviews. Genetics,* 7**,** 21-33.

49. Feinberg, A. P. & Tycko, B. 2004. The History Of Cancer Epigenetics. *Nature Reviews. Cancer,* 4**,** 143-53.

50. Feinberg, A. P. & Vogelstein, B. 1983. Hypomethylation Distinguishes Genes Of Some Human Cancers From Their Normal Counterparts. *Nature,* 301**,** 89-92.

51. Filipe, M. I. & Branfoot, A. C. 1974. Abnormal Patterns Of Mucus Secretion In Apparently Normal Mucosa Of Large Intestine With Carcinoma. *Cancer,* 34**,** 282-90.

52. Finch, P. W., He, X., Kelley, M. J., Uren, A., Schaudies, R. P., Popescu, N. C., Rudikoff, S., Aaronson, S. A., Varmus, H. E. & Rubin, J. S. 1997. Purification And Molecular Cloning Of A Secreted, Frizzled-Related Antagonist Of WNT Action. *Proceedings Of The National Academy Of Sciences Of The United States Of America,* 94**,** 6770-5.

53. Fodde, R., Smits, R. & Clevers, H. 2001. APC, Signal Transduction And Genetic Instability In Colorectal Cancer. *Nature Reviews. Cancer,* 1**,** 55-67.

54. Friedman, D. B., Hill, S., Keller, J. W., Merchant, N. B., Levy, S. E., Coffey, R. J. & Caprioli, R. M. 2004. Proteome Analysis Of Human Colon Cancer By Two-Dimensional Difference Gel Electrophoresis And Mass Spectrometry. *Proteomics,* 4**,** 793-811.

55. Fujisaki, J. & Shimoda, T. 1993. Expression Of Cytokeratin Subtypes In Colorectal Mucosa, Adenoma, And Carcinoma. *Gastroenterologia Japonica,* 28**,** 647-56.

56. Gertsch, P., Baer, H. U., Kraft, R., Maddern, G. J. & Altermatt, H. J. 1992. Malignant Cells Are Collected On Circular Staplers. *Diseases Of The Colon And Rectum,* 35**,** 238-41.

57. Gibson, P. R., Rosella, O., Wilson, A. J., Mariadason, J. M., Rickard, K., Byron, K. & Barkla, D. H. 1999. Colonic Epithelial Cell Activation And The Paradoxical Effects Of Butyrate. *Carcinogenesis,* 20**,** 539-44.

58. Gold, P. & Freedman, S. O. 1965. Demonstration Of Tumor-Specific Antigens In Human Colonic Carcinomata By Immunological Tolerance And Absorption Techniques. *The Journal Of Experimental Medicine,* 121**,** 439-62.

59. Graham, T. A., Mcdonald, S. A. & Wright, N. A. 2011. Field Cancerization In The GI Tract. *Future Oncology,* 7**,** 981-93.

60. Greaves, L. C., Preston, S. L., Tadrous, P. J., Taylor, R. W., Barron, M. J., Oukrif, D., Leedham, S. J., Deheragoda, M., Sasieni, P., Novelli, M. R., Jankowski, J. A., Turnbull, D. M., Wright, N. A. & Mcdonald, S. A. 2006. Mitochondrial DNA Mutations Are Established In Human Colonic Stem Cells, And Mutated Clones Expand By Crypt Fission. *Proceedings Of The National Academy Of Sciences Of The United States Of America,* 103**,** 714-9.

61. Habtezion, A., Toivola, D. M., Asghar, M. N., Kronmal, G. S., Brooks, J. D., Butcher, E. C. & Omary, M. B. 2011. Absence Of Keratin 8 Confers A Paradoxical Microflora-Dependent Resistance To Apoptosis In The Colon. *Proceedings Of The National Academy Of Sciences Of The United States Of America,* 108**,** 1445-50.

62. Hague, A., Elder, D. J., Hicks, D. J. & Paraskeva, C. 1995. Apoptosis In Colorectal Tumour Cells: Induction By The Short Chain Fatty Acids Butyrate, Propionate And Acetate And By The Bile Salt Deoxycholate. *International Journal Of Cancer. Journal International Du Cancer,* 60**,** 400-6.

63. Hampel, H. & Peltomaki, P. 2000. Hereditary Colorectal Cancer: Risk Assessment And Management. *Clinical Genetics,* 58**,** 89-97.

64. Holt, B. A. & Bourke, M. J. 2012. Wide Field Endoscopic Resection For Advanced Colonic Mucosal Neoplasia: Current Status And Future Directions. *Clinical Gastroenterology And Hepatol,* 10**,** 969-79.

65. Humphries, A. & Wright, N. A. 2008. Colonic Crypt Organization And Tumorigenesis. *Nature Reviews. Cancer,* 8**,** 415-24.

66. Ishiguro, K., Yoshida, T., Yagishita, H., Numata, Y. & Okayasu, T. 2006. Epithelial And Stromal Genetic Instability Contributes To Genesis Of Colorectal Adenomas. *Gut,* 55**,** 695-702.

67. Issa, J. P., Ottaviano, Y. L., Celano, P., Hamilton, S. R., Davidson, N. E. & Baylin, S. B. 1994. Methylation Of The Oestrogen Receptor CpG Island Links Ageing And Neoplasia In Human Colon. *Nature Genetics,* 7**,** 536-40.

68. Janke, C. & Bulinski, J. C. 2011. Post-Translational Regulation Of The Microtubule Cytoskeleton: Mechanisms And Functions. *Nature Reviews. Molecular Cell Biology,* 12**,** 773-86.

69. Jass, J. R. 1985. Diet, Butyric Acid And Differentiation Of Gastrointestinal Tract Tumours. *Medical Hypotheses,* 18**,** 113-8.

70. Johnson, H., Jr., Margolis, I. & Wise, L. 1988. Site-Specific Distribution Of Large-Bowel Adenomatous Polyps. Emphasis On Ethnic Differences. *Diseases Of The Colon And Rectum,* 31**,** 258-60.

71. Jothy, S., Slesak, B., Harlozinska, A., Lapinska, J., Adamiak, J. & Rabczynski, J. 1996. Field Effect Of Human Colon Carcinoma On Normal Mucosa: Relevance Of Carcinoembryonic Antigen Expression. *Tumour Biology : The Journal Of The International Society For Oncodevelopmental Biology And Medicine,* 17**,** 58-64.

72. Khan, A. Q., Bury, J. P., Brown, S. R., Riley, S. A. & Corfe, B. M. 2011. Keratin 8 Expression In Colon Cancer Associates With Low Faecal Butyrate Levels. *BMC Gastroenterology,* 11**,** 2.

73. Kinzler, K. W. & Vogelstein, B. 1996. Lessons From Hereditary Colorectal Cancer. *Cell,* 87**,** 159-70.

74. Knosel, T., Emde, V., Schluns, K., Schlag, P. M., Dietel, M. & Petersen, I. 2006. Cytokeratin Profiles Identify Diagnostic Signatures In Colorectal Cancer Using Multiplex Analysis Of Tissue Microarrays. *Cell Oncol,* 28**,** 167-75.

75. Ku, N. O., Liao, J. & Omary, M. B. 1998. Phosphorylation Of Human Keratin 18 Serine 33 Regulates Binding To 14-3-3 Proteins. *The EMBO Journal,* 17**,** 1892-906.

76. Ku, N. O., Michie, S. A., Soetikno, R. M., Resurreccion, E. Z., Broome, R. L., Oshima, R. G. & Omary, M. B. 1996. Susceptibility To Hepatotoxicity In Transgenic Mice That Express A Dominant-Negative Human Keratin 18 Mutant. *The Journal Of Clinical Investigation,* 98**,** 1034-46.

77. Ku, N. O. & Omary, M. B. 1995. Identification And Mutational Analysis Of The Glycosylation Sites Of Human Keratin 18. *The Journal Of Biological Chemistry,* 270**,** 11820-7.

78. Ku, N. O. & Omary, M. B. 2001. Effect Of Mutation And Phosphorylation Of Type I Keratins On Their Caspase-Mediated Degradation. *The Journal Of Biological Chemistry,* 276**,** 26792-8.

79. Ku, N. O. & Omary, M. B. 2006. A Disease- And Phosphorylation-Related Nonmechanical Function For Keratin 8. *The Journal Of Cell Biology,* 174**,** 115-25.

80. Ku, N. O., Toivola, D. M., Strnad, P. & Omary, M. B. 2010. Cytoskeletal Keratin Glycosylation Protects Epithelial Tissue From Injury. *Nature Cell Biology,* 12**,** 876-85.

81. Laemmli, U. K. 1970. Cleavage Of Structural Proteins During The Assembly Of The Head Of Bacteriophage T4. *Nature,* 227**,** 680-5.

82. Laiyemo, A. O., Doubeni, C., Sanderson, A. K., 2nd, Pinsky, P. F., Badurdeen, D. S., Doria-Rose, V. P., Marcus, P. M., Schoen, R. E., Lanza, E., Schatzkin, A. & Cross, A. J. 2011. Likelihood Of Missed And Recurrent Adenomas In The Proximal Versus The Distal Colon. *Gastrointestinal Endoscopy,* 74**,** 253-61.

83. Lamlum, H., Papadopoulou, A., Ilyas, M., Rowan, A., Gillet, C., Hanby, A., Talbot, I., Bodmer, W. & Tomlinson, I. 2000. APC Mutations Are Sufficient For The Growth Of Early Colorectal Adenomas. *Proceedings Of The National Academy Of Sciences Of The United States Of America,* 97**,** 2225-8.

84. Lanza, G., Jr., Altavilla, G., Cavazzini, L. & Negrini, R. 1985. Colonic Mucosa Adjacent To Adenomas And Hyperplastic Polyps -A Morphological And Histochemical Study. *Histopathology,* 9**,** 857-73.

85. Leech, S. H., Evans, C. A., Shaw, L., Wong, C. H., Connolly, J., Griffiths, J. R., Whetton, A. D. & Corfe, B. M. 2008. Proteomic Analyses Of Intermediate Filaments Reveals Cytokeratin 8 Is Highly Acetylated-Implications For Colorectal Epithelial Homeostasis. *Proteomics,* 8**,** 279-88.

86. Leedham, S. J. & Wright, N. A. 2008. Expansion Of A Mutated Clone: From Stem Cell To Tumour. *Journal Of Clinical Pathology,* 61**,** 164-71.

87. Levine, J. S. & Ahnen, D. J. 2006. Clinical Practice. Adenomatous Polyps Of The Colon. *The New England Journal Of Medicine,* 355**,** 2551-7.

88. Liao, J., Lowthert, L. A. & Omary, M. B. 1995. Heat Stress Or Rotavirus Infection Of Human Epithelial Cells Generates A Distinct Hyperphosphorylated Form Of Keratin 8. *Experimental Cell Research,* 219**,** 348-57.

89. Lokman, N. A., Ween, M. P., Oehler, M. K. & Ricciardelli, C. 2011. The Role Of Annexin A2 In Tumorigenesis And Cancer Progression. *Cancer Microenvironment : Official Journal Of The International Cancer Microenvironment Society,* 4**,** 199-208.

90. Magin, T. M., Vijayaraj, P. & Leube, R. E. 2007. Structural And Regulatory Functions Of Keratins. *Experimental Cell Research,* 313**,** 2021-32.

91. Majumdar, D., Rosser, R., Havard, S., Lobo, A. J., Wright, P. C., Evans, C. A. & Corfe, B. M. 2012a. An Integrated Workflow For Extraction And Solubilization Of Intermediate Filaments From Colorectal Biopsies For Proteomic Analysis. *Electrophoresis,* 33**,** 1967-74.

92. Majumdar, D., Tiernan, J. P., Lobo, A. J., Evans, C. A. & Corfe, B. M. 2012b. Keratins In Colorectal Epithelial Function And Disease. *International Journal Of Experimental Pathology,* 93**,** 305-18.

93. Martinez, M. E., Sampliner, R., Marshall, J. R., Bhattacharyya, A. K., Reid, M. E. & Alberts, D. S. 2001. Adenoma Characteristics As Risk Factors For Recurrence Of Advanced Adenomas. *Gastroenterology,* 120**,** 1077-83.

94. Matek, W., Guggenmoos-Holzmann, I. & Demling, L. 1985. Follow-Up Of Patients With Colorectal Adenomas. *Endoscopy,* 17**,** 175-81.

95. McGarrity, T. J. & Peiffer, L. P. 1994. Protein Kinase C Activity As A Potential Marker For Colorectal Neoplasia. *Digestive Diseases And Sciences,* 39**,** 458-63.

96. McInroy, L. & Maatta, A. 2007. Down-Regulation Of Vimentin Expression Inhibits Carcinoma Cell Migration And Adhesion. *Biochemical And Biophysical Research Communications,* 360**,** 109-14.

97. McIntyre, A., Gibson, P. R. & Young, G. P. 1993. Butyrate Production From Dietary Fibre And Protection Against Large Bowel Cancer In A Rat Model. *Gut,* 34**,** 386-91.

98. Merritt, A. J., Gould, K. A. & Dove, W. F. 1997a. Polyclonal Structure Of Intestinal Adenomas In Apcmin/+ Mice With Concomitant Loss Of Apc+ From All Tumor Lineages. *Proceedings Of The National Academy Of Sciences Of The United States Of America,* 94**,** 13927-31.

99. Mizuuchi, E., Semba, S., Kodama, Y. & Yokozaki, H. 2009. Down-Modulation Of Keratin 8 Phosphorylation Levels By PRL-3 Contributes To Colorectal Carcinoma Progression. *International Journal Of Cancer. Journal International Du Cancer,* 124**,** 1802-10.

100. Moll, R., Divo, M. & Langbein, L. 2008. The Human Keratins: Biology And Pathology. *Histochemistry And Cell Biology,* 129**,** 705-33.

101. Moll, R., Franke, W. W., Schiller, D. L., Geiger, B. & Krepler, R. 1982. The Catalog Of Human Cytokeratins: Patterns Of Expression In Normal Epithelia, Tumors And Cultured Cells. *Cell,* 31**,** 11-24.

102. Mueller, M. M. & Fusenig, N. E. 2004. Friends Or Foes - Bipolar Effects Of The Tumour Stroma In Cancer. *Nature Reviews. Cancer,* 4**,** 839-49.

103. Myzak, M. C., Ho, E. & Dashwood, R. H. 2006. Dietary Agents As Histone Deacetylase Inhibitors. *Molecular Carcinogenesis,* 45**,** 443-6.

104. Nakamura, S. & Kino, I. 1984. Morphogenesis Of Minute Adenomas In Familial Polyposis Coli. *Journal Of The National Cancer Institute,* 73**,** 41-9.

105. Nava, H., Carlsson, G., Petrelli, N. J., Herrera, L. & Mittelman, A. 1987. Follow-Up Colonoscopy In Patients With Colorectal Adenomatous Polyps. *Diseases Of The Colon And Rectum,* 30**,** 465-8.

106. Neugut, A. I., Jacobson, J. S., Ahsan, H., Santos, J., Garbowski, G. C., Forde, K. A., Treat, M. R. & Waye, J. 1995. Incidence And Recurrence Rates Of Colorectal Adenomas: A Prospective Study. *Gastroenterology,* 108**,** 402-8.

107. Neugut, A. I., Jacobson, J. S. & De Vivo, I. 1993. Epidemiology Of Colorectal Adenomatous Polyps. *Cancer Epidemiology, Biomarkers & Prevention : A Publication Of The American Association For Cancer Research, Co-sponsored By The American Society Of Preventive Oncology,* 2**,** 159-76.

108. Neugut, A. I., Johnsen, C. M., Forde, K. A. & Treat, M. R. 1985. Recurrence Rates For Colorectal Polyps. *Cancer,* 55**,** 1586-9.

109. Newton, M. A., Clipson, L., Thliveris, A. T. & Halberg, R. B. 2006. A Statistical Test Of The Hypothesis That Polyclonal Intestinal Tumors Arise By Random Collision Of Initiated Clones. *Biometrics,* 62**,** 721-7.

110. Noshirwani, K. C., Van Stolk, R. U., Rybicki, L. A. & Beck, G. J. 2000. Adenoma Size And Number Are Predictive Of Adenoma Recurrence: Implications For Surveillance Colonoscopy. *Gastrointestinal Endoscopy,* 51**,** 433-7.

111. Novelli, M. R., Williamson, J. A., Tomlinson, I. P., Elia, G., Hodgson, S. V., Talbot, I. C., Bodmer, W. F. & Wright, N. A. 1996. Polyclonal Origin Of Colonic Adenomas In An XO/XY Patient With FAP. *Science,* 272**,** 1187-90.

112. O'Callaghan, N. J., Toden, S., Bird, A. R., Topping, D. L., Fenech, M. & Conlon, M. A. 2012. Colonocyte Telomere Shortening Is Greater With Dietary Red Meat Than White Meat And Is Attenuated By Resistant Starch. *Clinical Nutrition,* 31**,** 60-4.

113. Omary, M. B., Ku, N. O., Liao, J. & Price, D. 1998. Keratin Modifications And Solubility Properties In Epithelial Cells And In Vitro. *Sub-Cellular Biochemistry,* 31**,** 105-40.

114. Otchy, D. P., Ransohoff, D. F., Wolff, B. G., Weaver, A., Ilstrup, D., Carlson, H. & Rademacher, D. 1996. Metachronous Colon Cancer In Persons Who Have Had A Large Adenomatous Polyp. *The American Journal Of Gastroenterology,* 91**,** 448-54.

115. Owen, D. A. & Reid, P. E. 1995. Histochemical Alterations Of Mucin In Normal Colon, Inflammatory Bowel Disease And Colonic Adenocarcinoma. *The Histochemical Journal,* 27**,** 882-9.

116. Owens, D. W., Wilson, N. J., Hill, A. J., Rugg, E. L., Porter, R. M., Hutcheson, A. M., Quinlan, R. A., Van Heel, D., Parkes, M., Jewell, D. P., Campbell, S. S., Ghosh, S., Satsangi, J. & Lane, E. B. 2004. Human Keratin 8 Mutations That Disturb Filament Assembly Observed In Inflammatory Bowel Disease Patients. *Journal Of Cell Science,* 117**,** 1989-99.

117. Pajak, B., Gajkowska, B. & Orzechowski, A. 2009. Sodium Butyrate Sensitizes Human Colon Adenocarcinoma COLO 205 Cells To Both

Intrinsic And TNF-Alpha-Dependent Extrinsic Apoptosis. *Apoptosis : An International Journal On Programmed Cell Death,* 14**,** 203-17.

118. Parikh, A. A., Fan, F., Liu, W. B., Ahmad, S. A., Stoeltzing, O., Reinmuth, N., Bielenberg, D., Bucana, C. D., Klagsbrun, M. & Ellis, L. M. 2004. Neuropilin-1 In Human Colon Cancer: Expression, Regulation, And Role In Induction Of Angiogenesis. *The American Journal Of Pathology,* 164**,** 2139-51.

119. Perrin, P., Pierre, F., Patry, Y., Champ, M., Berreur, M., Pradal, G., Bornet, F., Meflah, K. & Menanteau, J. 2001. Only Fibres Promoting A Stable Butyrate Producing Colonic Ecosystem Decrease The Rate Of Aberrant Crypt Foci In Rats. *Gut,* 48**,** 53-61.

120. Pham, T. K., Roy, S., Noirel, J., Douglas, I., Wright, P. C. & Stafford, G. P. 2010. A Quantitative Proteomic Analysis Of Biofilm Adaptation By The Periodontal Pathogen Tannerella Forsythia. *Proteomics,* 10**,** 3130-41.

121. Polley, A. C., Mulholland, F., Pin, C., Williams, E. A., Bradburn, D. M., Mills, S. J., Mathers, J. C. & Johnson, I. T. 2006. Proteomic Analysis Reveals Field-Wide Changes In Protein Expression In The Morphologically Normal Mucosa Of Patients With Colorectal Neoplasia. *Cancer Research,* 66**,** 6553-62.

122. Preston, S. L., Wong, W. M., Chan, A. O., Poulsom, R., Jeffery, R., Goodlad, R. A., Mandir, N., Elia, G., Novelli, M., Bodmer, W. F., Tomlinson, I. P. & Wright, N. A. 2003. Bottom-Up Histogenesis Of Colorectal Adenomas: Origin In The Monocryptal Adenoma And Initial Expansion By Crypt Fission. *Cancer Research,* 63**,** 3819-25.

123. Rex, D. K., Cutler, C. S., Lemmel, G. T., Rahmani, E. Y., Clark, D. W., Helper, D. J., Lehman, G. A. & Mark, D. G. 1997. Colonoscopic Miss Rates Of Adenomas Determined By Back-To-Back Colonoscopies. *Gastroenterology,* 112**,** 24-8.

124. Roediger, W. E. 1982. Utilization Of Nutrients By Isolated Epithelial Cells Of The Rat Colon. *Gastroenterology,* 83**,** 424-9.

125. Sack, T. L., Gum, J. R., Low, M. G. & Kim, Y. S. 1988. Release Of Carcinoembryonic Antigen From Human Colon Cancer Cells By Phosphatidylinositol-Specific Phospholipase C. *The Journal Of Clinical Investigation,* 82**,** 586-93.

126. Saini, S. D., Kim, H. M. & Schoenfeld, P. 2006. Incidence Of Advanced Adenomas At Surveillance Colonoscopy In Patients With A Personal History Of Colon Adenomas: A Meta-Analysis And Systematic Review. *Gastrointestinal Endoscopy,* 64**,** 614-26.

127. Sasaki, M., Watanabe, H., Jass, J. R., Ajioka, Y., Kobayashi, M., Matsuda, K. & Hatakeyama, K. 1997. Occult Lymph Node Metastases Detected By Cytokeratin Immunohistochemistry Predict Recurrence In "Node-Negative" Colorectal Cancer. *J Gastroenterol,* 32**,** 758-64.

128. Satelli, A. & Li, S. 2011. Vimentin In Cancer And Its Potential As A Molecular Target For Cancer Therapy. *Cellular And Molecular Life Sciences,* 68**,** 3033-46.

129. Sealy, L. & Chalkley, R. 1978. The Effect Of Sodium Butyrate On Histone Modification. *Cell,* 14**,** 115-21.

130. Shen, L., Kondo, Y., Rosner, G. L., Xiao, L., Hernandez, N. S., Vilaythong, J., Houlihan, P. S., Krouse, R. S., Prasad, A. R., Einspahr, J. G., Buckmeier, J., Alberts, D. S., Hamilton, S. R. & Issa, J. P. 2005. MGMT Promoter Methylation And Field Defect In Sporadic Colorectal Cancer. *Journal Of The National Cancer Institute,* 97**,** 1330-8.

131. Shih, I. M., Wang, T. L., Traverso, G., Romans, K., Hamilton, S. R., Ben-Sasson, S., Kinzler, K. W. & Vogelstein, B. 2001. Top-Down Morphogenesis Of Colorectal Tumors. *Proceedings Of The National Academy Of Sciences Of The United States Of America,* 98**,** 2640-5.

132. Shussman, N. & Wexner, S. D. 2014. Colorectal Polyps And Polyposis Syndromes. *Gastroenterology Report - Oxford Journals,* 2**,** 1-15.

133. Snider, N. T., Leonard, J. M., Kwan, R., Griggs, N. W., Rui, L. & Omary, M. B. 2013. Glucose And SIRT2 Reciprocally Mediate The Regulation Of Keratin 8 By Lysine Acetylation. *The Journal Of Cell Biology,* 200**,** 241-7.

134. Snider, N. T. & Omary, M. B. 2014. Post-Translational Modifications Of Intermediate Filament Proteins: Mechanisms And Functions. *Nature Reviews Molecular Cell Biology,* 15**,** 163-77.

135. Snider, N. T., Weerasinghe, S. V., Iniguez-Lluhi, J. A., Herrmann, H. & Omary, M. B. 2011. Keratin Hypersumoylation Alters Filament Dynamics

And Is A Marker For Human Liver Disease And Keratin Mutation. *The Journal Of Biological Chemistry,* 286**,** 2273-84.

136. Soellner, P., Quinlan, R. A. & Franke, W. W. 1985. Identification Of A Distinct Soluble Subunit Of An Intermediate Filament Protein: Tetrameric Vimentin From Living Cells. *Proceedings Of The National Academy Of Sciences Of The United States Of America,* 82**,** 7929-33.

137. Stammberger, P. & Baczako, K. 1999. Cytokeratin 19 Expression In Human Gastrointestinal Mucosa During Human Prenatal Development And In Gastrointestinal Tumours: Relation To Cell Proliferation. *Cell And Tissue Research,* 298**,** 377-81.

138. Suzuki, H., Watkins, D. N., Jair, K. W., Schuebel, K. E., Markowitz, S. D., Chen, W. D., Pretlow, T. P., Yang, B., Akiyama, Y., Van Engeland, M., Toyota, M., Tokino, T., Hinoda, Y., Imai, K., Herman, J. G. & Baylin, S. B. 2004. Epigenetic Inactivation Of SFRP Genes Allows Constitutive WNT Signaling In Colorectal Cancer. *Nature Genetics,* 36**,** 417-22.

139. Tajika, M., Niwa, Y., Bhatia, V., Kondo, S., Tanaka, T., Mizuno, N., Hara, K., Hijioka, S., Imaoka, H., Ogura, T., Haba, S. & Yamao, K. 2011. Comparison Of Endoscopic Submucosal Dissection And Endoscopic Mucosal Resection For Large Colorectal Tumors. *European Journal Of Gastroenterology And Hepatology,* 23**,** 1042-9.

140. Tan, H. T., Tan, S., Lin, Q., Lim, T. K., Hew, C. L. & Chung, M. C. 2008. Quantitative And Temporal Proteome Analysis Of Butyrate-Treated Colorectal Cancer Cells. *Molecular & Cellular Proteomics,* 7**,** 1174-85.

141. Taniguchi, L., Higurashi, T., Uchiyama, T., Kondo, Y., Uchida, E., Uchiyama, S., Jono, F., Hamanaka, J., Kuriyama, H., Hata, Y., Endo, H., Takahashi, H., Nagase, H., Matsuhashi, N. & Nakajima, A. 2014. Metabolic Factors Accelerate Colorectal Adenoma Recurrence. *BMC Gastroenterology,* 14**,** 187.

142. Thiery, J. P. 2002. Epithelial-Mesenchymal Transitions In Tumour Progression. *Nature Reviews. Cancer,* 2**,** 442-54.

143. Thirlwell, C., Will, O. C., Domingo, E., Graham, T. A., Mcdonald, S. A., Oukrif, D., Jeffrey, R., Gorman, M., Rodriguez-Justo, M., Chin-Aleong, J., Clark, S. K., Novelli, M. R., Jankowski, J. A., Wright, N. A., Tomlinson, I. P. & Leedham, S.

J. 2010. Clonality Assessment And Clonal Ordering Of Individual Neoplastic Crypts Shows Polyclonality Of Colorectal Adenomas. *Gastroenterology,* 138**,** 1441-54, 1454 E1-7.

144. Thliveris, A. T., Clipson, L., White, A., Waggoner, J., Plesh, L., Skinner, B. L., Zahm, C. D., Sullivan, R., Dove, W. F., Newton, M. A. & Halberg, R. B. 2011. Clonal Structure Of Carcinogen-Induced Intestinal Tumors In Mice. *Cancer Prevention Research,* 4**,** 916-23.

145. Thliveris, A. T., Halberg, R. B., Clipson, L., Dove, W. F., Sullivan, R., Washington, M. K., Stanhope, S. & Newton, M. A. 2005. Polyclonality Of Familial Murine Adenomas: Analyses Of Mouse Chimeras With Low Tumor Multiplicity Suggest Short-Range Interactions. *Proceedings Of The National Academy Of Sciences Of The United States Of America,* 102**,** 6960-5.

146. Toden, S., Bird, A. R., Topping, D. L. & Conlon, M. A. 2007. Differential Effects Of Dietary Whey, Casein And Soya On Colonic DNA Damage And Large Bowel SCFA In Rats Fed Diets Low And High In Resistant Starch. *British Journal Of Nutrition,* 97**,** 535-43.

147. Toivola, D. M., Krishnan, S., Binder, H. J., Singh, S. K. & Omary, M. B. 2004. Keratins Modulate Colonocyte Electrolyte Transport Via Protein Mistargeting. *The Journal Of Cell Biology,* 164**,** 911-21.

148. Trujillo, K. A., Heaphy, C. M., Mai, M., Vargas, K. M., Jones, A. C., Vo, P., Butler, K. S., Joste, N. E., Bisoffi, M. & Griffith, J. K. 2011. Markers Of Fibrosis And Epithelial To Mesenchymal Transition Demonstrate Field Cancerization In Histologically Normal Tissue Adjacent To Breast Tumors. *International Journal of Cancer,* 129**,** 1310-21.

149. Umpleby, H. C., Fermor, B., Symes, M. O. & Williamson, R. C. 1984. Viability Of Exfoliated Colorectal Carcinoma Cells. *The British Journal Of Surgery,* 71**,** 659-63.

150. Van Den Brink, G. R. & Offerhaus, G. J. 2007. The Morphogenetic Code And Colon Cancer Development. *Cancer Cell,* 11**,** 109-17.

151. Van Rijn, J. C., Reitsma, J. B., Stoker, J., Bossuyt, P. M., Van Deventer, S. J. & Dekker, E. 2006. Polyp Miss Rate Determined By Tandem Colonoscopy: A

Systematic Review. *The American Journal Of Gastroenterology,* 101**,** 343-50.

152. Vanhoutvin, S. A., Troost, F. J., Hamer, H. M., Lindsey, P. J., Koek, G. H., Jonkers, D. M., Kodde, A., Venema, K. & Brummer, R. J. 2009. Butyrate-Induced Transcriptional Changes In Human Colonic Mucosa. *Public Library Of Science One,* 4**,** E6759.

153. Vasen, H. F., Mecklin, J. P., Khan, P. M. & Lynch, H. T. 1991. The International Collaborative Group On Hereditary Non-Polyposis Colorectal Cancer (ICG-HNPCC). *Diseases Of The Colon And Rectum,* 34**,** 424-5.

154. Vogelstein, B., Fearon, E. R., Hamilton, S. R., Kern, S. E., Preisinger, A. C., Leppert, M., Nakamura, Y., White, R., Smits, A. M. & Bos, J. L. 1988. Genetic Alterations During Colorectal-Tumor Development. *The New England Journal Of Medicine,* 319**,** 525-32.

155. Vucenik, I., Gotovac, J., Druzijanic, N. & Shamsuddin, A. M. 2001. Usefulness Of Galactose Oxidase-Schiff Test In Rectal Mucus For Screening Of Colorectal Malignancy. *Anti-cancer Research,* 21**,** 1247-55.

156. Wakabayashi, K., Saito, H., Kaneko, F., Nakamoto, N., Tada, S. & Hibi, T. 2005. Gene Expression Associated With The Decrease In Malignant Phenotype Of Human Liver Cancer Cells Following Stimulation With A Histone Deacetylase Inhibitor. *International Journal Of Oncology,* 26**,** 233-9.

157. Wang, T. L., Rago, C., Silliman, N., Ptak, J., Markowitz, S., Willson, J. K., Parmigiani, G., Kinzler, K. W., Vogelstein, B. & Velculescu, V. E. 2002. Prevalence Of Somatic Alterations In The Colorectal Cancer Cell Genome. *Proceedings Of The National Academy Of Sciences Of The United States Of America,* 99**,** 3076-80.

158. Waye, J. D. & Braunfeld, S. 1982. Surveillance Intervals After Colonoscopic Polypectomy. *Endoscopy,* 14**,** 79-81.

159. Wilkinson, K. A. & Henley, J. M. 2010. Mechanisms, Regulation And Consequences Of Protein Sumoylation. *The Biochemical Journal,* 428**,** 133-45.

160. Winawer, S. J., Zauber, A. G., Ho, M. N., O'brien, M. J., Gottlieb, L. S., Sternberg, S. S., Stewart, E. T., Bond, J. H., Schapiro, M., Panish, J. F. & Et Al. 1993a. The National Polyp Study. *European Journal Of Cancer Prevention,* 2 Suppl 2**,** 83-7.

161. Winawer, S. J., Zauber, A. G., Ho, M. N., O'brien, M. J., Gottlieb, L. S., Sternberg, S. S., Waye, J. D., Schapiro, M., Bond, J. H., Panish, J. F. & Et Al. 1993b. Prevention Of Colorectal Cancer By Colonoscopic Polypectomy. The National Polyp Study Workgroup. *The New England Journal Of Medicine,* 329**,** 1977-81.

162. Wu, W. W., Wang, G., Baek, S. J. & Shen, R. F. 2006. Comparative Study Of Three Proteomic Quantitative Methods, DIGE, cICAT, And iTraq, Using 2D Gel- Or LC-Maldi TOF/TOF. *Journal Of Proteome Research,* 5**,** 651-8.

163. Xu, H., Sakamoto, K. & Shamsuddin, A. M. 1992. Detection Of The Tumor Marker D-Galactose-Beta-(1-->3)-N-Acetyl-D-Galactosamine In Colonic Cancer And Precancer. *Archives Of Pathology & Laboratory Medicine,* 116**,** 1234-8.

164. Yu, D. C., Bury, J. P., Tiernan, J., Waby, J. S., Staton, C. A. & Corfe, B. M. 2011a. Short-Chain Fatty Acid Level And Field Cancerization Show Opposing Associations With Enteroendocrine Cell Number And Neuropilin Expression In Patients With Colorectal Adenoma. *Molecular Cancer,* 10**,** 27.

165. Zafar, A., Mustafa, M. & Chapman, M. 2012. Colorectal Polyps: When Should We Tattoo? *Surgical Endoscopy,* 26**,** 3264-6.

Appendices

Appendix 1 Service evaluation approval form

Sheffield Teaching Hospitals **NHS**
NHS Foundation Trust

Investigator Site File

Principal Investigator: Ria Rosser	
Service Evaluation Title: Incidence of Adenoma Recurrence Following Endoscopic Removal	
Service Evaluation Reference No:	**4124**
Service Evaluation Manager: Janet Turner	
Date approved:	**15/08/2011**

Clinical Effectiveness Unit
Sheffield Teaching Hospitals NHS Foundation Trust
Northern General Hospital
Sheffield S5 7AU
0114 27 15115
CAEU@sth.nhs.uk
October 2010

Appendix 2 Data collection tool

Adenoma Recurrence Data Collection Tool

Patient number: DOB/Age:

Initial colonoscopy date: Adenoma-
                                                                    Date removed:

                                                                    Number of adenomas:

Site:	R	S	RSJ	D	SF	T	HF	A	C	ICV	TI
No:											
Size:											
Adequacy of excision:											
Histology:											

Follow up colonoscopy date:

Adenoma recurrence-

        Date identified:

Number of adenomas:

Site:	R	S	RSJ	D	SF	T	HF	A	C	ICV	TI
No:											
Size:											
Adequacy of excision:											
Histology:											

Key:

Colon site   Excision
R- rectum   EF – excised fully
S – sigmoid   UnC – unable to comment
RSJ – rectosigmoid junction   I - incomplete
D – descending
SF – splenic flexure
T – transverse
HF – hepatic flexure
A – ascending
C – caecum
ICV – ileocaecal valve
TI – terminal ileum

Appendix 3 Probability calculation

Calculation for proximal movements

<u>Caecum</u>
Number of index polyps at caecum = 77
Maximum number of possible proximal segments (caecum to caecum) = 0
Number of proximal polyp movements 77 x 0 = 0

<u>Ascending</u>
Number of index polyps at ascending colon = 85
Maximum number of possible proximal segments (ascending to caecum) = 1
Number of polyps multiplied by possible proximal movements = 85 x 1 = **85**
Number of proximal polyp movements taken:
     14 polyps moved from ascending to caecum – 14 x 1 = **14**
Number of polyps occurring in same segment = 71

<u>Hepatic Flexure</u>
Number of index polyps at hepatic flexure = 33
Maximum number of possible proximal segments (hepatic flexure to caecum) = 2
Number of polyps multiplied by possible proximal movements = 33 x 2 = **66**
Number of proximal polyp movements taken:
     4 polyps moved from hepatic flexure to caecum – 4 x 2 = 8
     4 polyps moved from hepatic flexure to ascending – 4 x 1 = 4
                                      sum = **12**
Number of polyps occurring in the same segment = 25

<u>Transverse</u>
Number of index polyps at transverse = 79
Maximum number of possible proximal segments (transverse to caecum) = 3
Number of polyps multiplied by possible proximal movements = 79 x 3 = **237**
Number of proximal polyp movements taken:
     12 polyps moved from transverse to caecum – 12 x 3 = 36
     9 polyps moved from transverse to ascending – 9 x 2 = 18
     10 polyps moved from transverse to hepatic flexure – 10 x 1 = 10
                                      sum = **64**
Number of polyps occurring in the same segment = 31

Appendix 3 Probability calculation

Splenic flexure
Number of index polyps at splenic flexure = 17
Maximum number of possible proximal segments (splenic flexure to caecum) = 4
Number of polyps multiplied by possible proximal movements = 17 x 4 = **68**
Number of proximal polyp movements taken:

      2 polyps moved from splenic flexure to caecum – 2 x 4 = 8
      5 polyps moved from splenic flexure to ascending – 5 x 3 = 15
      1 polyps moved from splenic flexure to hepatic flexure – 1 x 2 = 2
      3 polyps moved from splenic flexure to transverse – 3 x 1 = 3
                                                    sum = **28**
Number of polyps occurring in the same segment = 6

Descending
Number of index polyps at descending = 57
Maximum number of possible proximal segments (descending to caecum) = 5
Number of polyps multiplied by possible proximal movements = 57 x 5 = **285**
Number of proximal polyp movements taken:

      7 polyps moved from descending to caecum – 7 x 5 = 35
      10 polyps moved from descending to ascending – 10 x 4 = 40
      2 polyps moved from descending to hepatic flexure – 2 x 3 = 6
      16 polyps moved from descending to transverse – 16 x 2 = 32
      0 polyps moved from descending to splenic flexure – 0 x 1 = 0
                                                    sum = **113**
Number of polyps occurring in the same segment = 22

Sigmoid
Number of index polyps at sigmoid = 194
Maximum number of possible proximal segments (sigmoid to caecum) = 6
Number of polyps multiplied by possible proximal movements = 194 x 6 = **1164**
Number of proximal polyp movements taken:

      22 polyps moved from sigmoid to caecum – 22 x 6 = 132
      12 polyps moved from sigmoid to ascending – 12 x 5 = 60
      8 polyps moved from sigmoid to hepatic flexure – 8 x 4 = 36
      24 polyps moved from sigmoid to transverse – 24 x 3 = 72
      5 polyps moved from sigmoid to splenic flexure – 5 x 2 = 10
      17 polyps moved from sigmoid to descending – 17x 1 = 17
                                                    sum = **327**
Number of polyps occurring in the same segment = 106

Appendix 3 Probability calculation

Rectosigmoid junction
Number of index polyps at rectosigmoid junction = 29
Maximum number of possible proximal segments (rectosigmoid to caecum) = 7
Number of polyps multiplied by possible proximal movements = 29 x 7 = **203**
Number of proximal polyp movements taken:

       4 polyps moved from rectosigmoid to caecum – 4 x 7 = 28
       2 polyps moved from rectosigmoid to ascending – 2 x 6 = 12
       0 polyps moved from rectosigmoid to hepatic flexure – 0 x 5 = 0
       4 polyps moved from rectosigmoid to transverse – 4 x 4 = 16
       0 polyps moved from rectosigmoid to splenic flexure – 0 x 3 = 3
       0 polyps moved from rectosigmoid to descending – 0 x 2 = 0
       15 polyps moved from rectosigmoid to sigmoid – 15 x 1 = 15

                                                                    sum = **71**
Number of polyps occurring in the same segment = 4

Rectum
Number of index polyps at rectum = 63
Maximum number of possible proximal segments (rectum to caecum) = 8
Number of polyps multiplied by possible proximal movements = 63 x 8 = **504**
Number of proximal polyp movements taken:

       19 polyps moved from rectum to caecum – 19 x 8 = 152
       18 polyps moved from rectum to ascending – 18 x 7= 126
       5 polyps moved from rectum to hepatic flexure – 5 x 6 = 30
       11 polyps moved from rectum to transverse– 11 x 5 = 55
       3 polyps moved from rectum to splenic flexure – 3 x 4 = 12
       11 polyps moved from rectum to descending – 11 x 3 = 33
       32 polyps moved from rectum to sigmoid – 32 x 2 = 64
       12 polyps moved from rectum to rectosigmoid – 12 x 1 = 12

                                                              sum = **484**
Number of polyps occurring in the same segment = 48

Index adenoma segment	Proximal segment movements taken	Proximal segment movements possible
Caecum	0	0
Ascending	14	85
Splenic flexure	12	66
Transverse	64	237
Hepatic flexure	28	68
Descending	113	285
Sigmoid	327	1164
Rectosigmoid junction	71	203
Rectum	484	504
Total movements	**1113**	**2612**

Percentage of total segments taken out of segments available:

1113/2612 x 100 = 43%

Appendix 3 Probability calculation

Calculation for distal movements

Rectum
Number of index polyps at rectum = 63
Maximum number of possible distal segments (rectum to rectum) = 0
Number of rectum polyp movements 63 x 0 = 0

Rectosigmoid junction
Number of index polyps at rectosigmoid = 29
Maximum number of possible distal segments (rectosigmoid to rectum) = 1
Number of polyps multiplied by possible distal movements = 29 x 1 = **29**
Number of distal polyp movements:
      1 polyp moved from rectosigmoid to rectum – 1 x 1 = **1**
Number of polyps occurring in same segment = 28

Sigmoid
Number of index polyps at sigmoid = 194
Maximum number of possible distal segments (sigmoid to rectum) = 2
Number of polyps multiplied by possible distal movements = 194 x 2 = **388**
Number of distal polyp movements:
      36 polyps moved from sigmoid to rectum – 36 x 2 = 72
      5 polyps moved from sigmoid to rectosigmoid - 5 x 1 = 5
                                     sum = **77**
Number of polyps occurring in same segment = 153

Descending
Number of index polyps at descending = 57
Maximum number of possible distal segments (descending to rectum) = 3
Number of polyps multiplied by possible distal movements = 57 x 3 = **171**
Number of distal polyp movements:
      4 polyps moved from descending to rectum – 4 x 3 = 12
      0 polyps moved from descending to rectosigmoid–0 x 2 = 0
      11 polyps moved from descending to sigmoid - 11 x 1 = 11
                                     sum = **23**
Number of polyps occurring in same segment = 42

Appendix 3 Probability calculation

Splenic Flexure
Number of index polyps at splenic flexure = 17
Maximum number of possible distal segments (splenic flexure to rectum) = 4
Number of polyps multiplied by possible distal movements = 17 x 4 = **68**
Number of distal polyp movements:

      0 polyps moved from splenic flexure to rectum – 0 x 4 = 0
      1 polyp moved from splenic flexure to rectosigmoid– 1 x 3 = 3
      0 polyps moved from splenic flexure to sigmoid – 0 x 2 = 0
      3 polyps moved from splenic flexure to descending - 3 x 1 = 3
                                        sum = **6**

Number of polyps occurring in same segment = 9

Transverse
Number of index polyps at transverse flexure = 79
Maximum number of possible distal segments (transverse to rectum) = 5
Number of polyps multiplied by possible distal movements = 79 x 5 = **395**
Number of distal polyp movements:

      6 polyps moved from transverse to rectum – 6 x 5 = 30
      3 polyp moved from transverse to rectosigmoid– 3 x 4 = 12
      13 polyps moved from transverse to sigmoid – 13 x 3 = 39
      6 polyps moved from transverse to descending - 6 x 4 = 24
      4 polyps moved from transverse to splenic flexure – 4 x 1 = 4
                                        sum = **109**

Number of polyps occurring in same segment = 47

Hepatic flexure
Number of index polyps at hepatic flexure = 33
Maximum number of possible distal segments (hepatic flexure to rectum) = 6
Number of polyps multiplied by possible distal movements = 33 x 6 = **198**
Number of distal polyp movements:

      1 polyp moved from hepatic flexure to rectum – 1 x 6 = 6
      0 polyp moved from hepatic flexure to rectosigmoid– 0 x 5 = 0
      4 polyps moved from hepatic flexure to sigmoid – 4 x 4 = 16
      5 polyps moved from hepatic flexure to descending - 5 x 3 = 15
      2 polyps moved from hepatic flexure to splenic flexure – 2 x 2 = 4
      8 polyps moved from hepatic flexure to transverse – 8 x 1 = 8
                                        sum = **49**

Number of polyps occurring in same segment = 13

Appendix 3 Probability calculation

Ascending
Number of index polyps at ascending = 85
Maximum number of possible distal segments (ascending to rectum) = 7
Number of polyps multiplied by possible distal movements = 85 x 7 = **385**
Number of distal polyp movements:

       7 polyps moved from ascending to rectum – 7 x 7 = 49
       2 polyps moved from ascending to rectosigmoid– 2 x 6 = 12
       11 polyps moved from ascending to sigmoid – 11 x 5 = 55
       9 polyps moved from ascending to descending - 9 x 4 = 36
       3 polyps moved from ascending to splenic flexure – 3 x 3 = 9
       14 polyps moved from ascending to transverse – 14 x 2 = 28
       3 polyps moved from ascending to hepatic flexure -3 x 1 = 3
                                sum = **192**
Number of polyps occurring in same segment = 35

Caecum
Number of index polyps at caecum = 77
Maximum number of possible distal segments (caecum to rectum) = 8
Number of polyps multiplied by possible distal movements = 77 x 8 = **616**
Number of distal polyp movements:

       7 polyps moved from caecum to rectum – 7 x 8 = 56
       2 polyps moved from caecum to rectosigmoid– 2 x 7 = 14
       8 polyps moved from caecum to sigmoid – 8 x 6 = 48
       5 polyps moved from caecum to descending - 5 x 5 = 25
       5 polyps moved from caecum to splenic flexure – 5 x 4 = 20
       11 polyps moved from caecum to transverse – 11 x 3 = 33
       3 polyps moved from caecum to hepatic flexure - 3 x 2 = 6
       15 polyps moved from caecum to ascending – 15x 1 = 15
                                  sum = **217**
Number of polyps occurring in same segment = 21

Appendix 3 Probability calculation

Index adenoma segment	Proximal segment movements taken	Proximal segment movements possible
Rectum	0	0
Rectosigmoid junction	1	29
Sigmoid	77	388
Descending	23	171
Splenic flexure	6	68
Transverse	109	395
Hepatic flexure	49	198
Ascending	192	385
Caecum	217	616
Total movements	**674**	**2250**

Percentage of total segments taken out of segments available:

$$674/2250 \times 100 = 30\%$$

Appendix 4 Published protocol

Appendix 5 iTRAQ Standard operating procedure S.O.P

Peptide fractionation

Strong cation exchange (SCX) was achieved using a PolySULFOETHYL A Pre-Packed Column (PolyLC, Columbia, MD) with a 5 μm particle size and a column dimension of 100 mm.4.6 mm i.d., 200 Å pore size, on a BioLC HPLC (Dionex, Surrey, U.K.). Sample was loaded onto the column and washed for at least 60 minutes at a flow rate of 400 μL /min with 100 % SCX Buffer A (20 % acetonitrile, 0.1 % Formic Acid) to remove salts, TCEP and unincorporated iTRAQ reagent. Peptides were then separated using a gradient of SCX Buffer B (20% acetonitrile, 0.1% formic acid, 0.5 M KCl) at the same flow rate of 400 μL /min. Buffer B levels increased from 0% to 25% from 5 minutes to 30 minutes then from 25% to 100% over 5 minutes, followed by an increase from 26% to 100% over the next 15 min. Buffer B was held for another 5 min for isocratic washing prior to column re-equilibration with buffer A. The sample injection volume was 100 μL, and the liquid flow rate was 400 μL/min. The SCX chromatogram was monitored using UVD170U ultraviolet detector and Chromeleon software v. 6.50 (Dionex, LC Packings, The Netherlands). Fractions were collected using a Foxy Jr. (Dionex) fraction collector in 1 min intervals.

Sample desalting

Fractions were desalted using buffers: A (97% H_2O, 0.1% formic acid); B (97% acetonitrile, 0.1% formic acid) and C (3% acetonitrile, 0.1% trifluoroacetic acid) and MiniSpin™ columns according to the protocol outlined by The Nest Group (The Nest Group, MA, USA). Fractions were vacuum-concentration prior to LC-MS/MS analysis.

LC-MS/MS analysis

Fractions collected from offline separation techniques were eluted through the Famos-Ultimate 3000 nano-LC system (Dionex, LC Packings, The Netherlands) interfaced with a QSTAR® XL (Applied Biosystems; MDS-Sciex) tandem ESI-

QUAD-TOF MS. Vacuum dried fractions were resuspended in loading buffer (3% acetonitrile, 0.1% trifluoroacetic acid), injected and captured into a 0.3.5 mm trap column (3 µm C18 Dionex-LC Packings). Trapped samples were then eluted onto a 0.075.150 mm analytical column (3 µm C18 Dionex-LC Packings) using an automated binary gradient with a flow of 300 nL/min from 95% buffer A (3% acetonitrile, 0.1% formic acid), to 35% buffer B (97% acetonitrile, 0.1% formic acid) over 90 min, followed by a 5 min ramp to 95% buffer II (with isocratic washing for 10 min). Predefined 1 s 350–1600 m/z MS survey scans were acquired with up to two dynamically excluded precursors selected for a 3 s MS/MS (m/z 65–2000) scan. The collision energy range was increased by 20% as compared to the unlabeled peptides in order to overcome the stabilizing effect of the basic N-terminal derivatives, and to achieve equivalent fragmentation as recommended by Applied Biosystems.

Protein identification and relative quantification

The mass-spectrometric data was collected and analysed as previously described (Pham et al., 2010). Briefly, MS/MS data generated from the QSTAR® XL was converted to generic MGF peaklists using the mascot.dll embedded script (version 1.6 release no. 25) in Analyst QS v. 1.1 (Applied Biosystems, Sciex; Matrix Science). Further processing of the data was undertaken using an in-house Phenyx algorithm cluster (binary version 2.6; Geneva Bioinformatics SA) at the ChELSI Institute, University of Sheffield, against the *Homo sapiens* UniProt protein knowledgebase (SwissProt and Trembl (41070 and 71449 entries respectively downloaded 5th November 2010) to derive peptide sequence and hence protein identification. These data were then searched within the reversed *Homo sapiens* database to estimate the false-positive rate. Peptides identifications at 1% false discovery rate were accepted. The iTRAQ reporter ion intensities were exported. Protein quantifications were obtained by computing the geometric means of the reporters' intensities. Median correction was subsequently applied to every reporter in order to compensate for systematic errors, *e.g.* if a sample happened to have been loaded at a largely different total concentration. The reporters' intensities, in each individual MS/MS scan, were also median corrected using the same factors, with the rationale that if the total

concentration of a sample A was half that of another sample B, the intensities of sample A's reporter have to be doubled to allow for a fair comparison. *t*-tests applied to determine alterations in protein level between samples use these corrected intensities since these were carried out for every protein and because of the multiple times each test was performed, the threshold (α=5%) used for significance was corrected for data mining. The standard Bonferroni correction (α/P, where *P* is the number of proteins) was used to minimise false positive results. This workflow was developed in-house (Pham et al., 2010).

Appendix 6 Protein list for insoluble fraction

Protein list for insoluble fraction

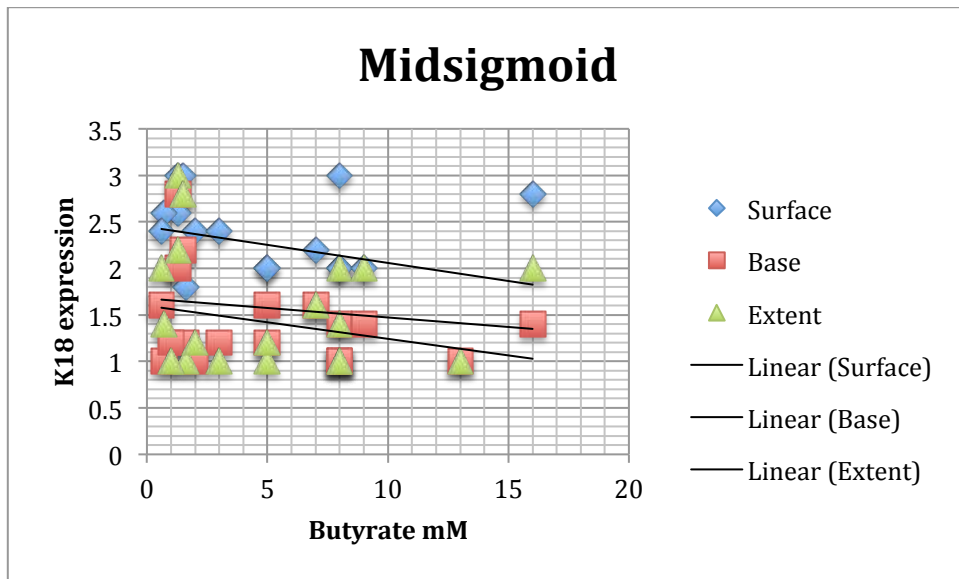| Ascension number	Number of peptides matched	Protein name
A2NUT2_CHAIN_0	1	Lambda chain
A4D1Z4	1	KIA00415 gene product
A6NN01	1	histone A2A
B0YJC4	1	vimentin
B3KSN3	1	C DNA (highly similar to ATP-binding cassette sub-family B member 8, mitochondrial)
B4DGF3	1	C DNA (highly similar to Talin-2)
B4DIK9	1	C DNA
B4DRV1	1	C DNA (highly similar to Protein-glutamine gamma-glutamyltransferase K)
B4DRX3	1	60S ribosomal protein
B4DU60	1	Citrate lyase subunit beta-like protein, mitochondrial
B4DUI9	1	C DNA (highly similar to Troponin C, skeletal muscle)
B5MEB8	1	obsolete
B7Z1I0	1	integrin linked protein kinase
B7Z2X4	1	C DNA (highly similar to Gelsolin)
B8ZZ37	1	obsolete
D2CFK5	1	somatostatin receptor 5C
D3YTB1	1	60S ribosomal protein
P05141_CHAIN_0	1	ADP/ATP translocase 2
P06733_CHAIN_0	1	Alphaenolase
P26599	1	Polypyrimidine tract binding protein
P35268_CHAIN_0	1	60S ribosomal protein
P50914_CHAIN_0	1	60S ribosomal protein
P51884_CHAIN_0	1	Lumican
P62269_CHAIN_0	1	40s ribosomal protein
P98160_CHAIN_0	1	basement membrane
Q15746_ISOFORM_3B	1	myosin light chain
Q3B7J3	1	ZCCHC3 protein
Q53S60	1	putatative uncharacterised protein
Q6IBG5	1	MYL6 protein
Q6NUK4_ISOFORM_2	1	Receptor expression-enhancing protein 3
Q71S07	1	Non-erythrocytic beta-spectrin 4
Q765P7_ISOFORM_2	1	Actin-bundling with BAIAP2 homology protein 1
Q8N7L7	1	C DNA (FLJ40893 fis, clone UTERU200160)
Q8WXQ3	1	putatative uncharacterised protein
Q96S66_ISOFORM_4	1	Chloride channel CLIC-like protein 1

Q9BYE0	1	Transcrition factor HES-7
Q9H0N0	1	Ras-related protein Rab-6C
Q9H6H4_ISOFORM_2	1	Receptor expression-enhancing protein 4
Q9NYP9	1	RER1 Protein
Q9UED0	1	amyloid like protein 2
A8K230	2	zinc finger protein
B4DJ98	2	C DNA (highly similar to Protein disulfide-isomerase A3)
B4DJC3	2	Histone H2A
B4DPR2	2	C DNA (highly similar to Serum albumin)
B4DRD6	2	Histone H1
B7Z3F2	2	C DNA
B7Z3U6	2	sodium pump subunit alpha 1
C9JA88	2	obsolete
C9JRX8	2	LYR motif containing protein 4
D3DP13	2	fibrinogen beta chain
P07355_CHAIN_0	2	Annexin A2
P07585_CHAIN_0	2	Decorin
P08727	2	K19
P11021_CHAIN_0	2	78 kDA glucose related protein
P15924	2	Desmoplakin
P54707	2	potassium transporting ATPase alpha 2
Q01082_ISOFORM_2	2	Spectrin beta chain
Q3MIV8	2	myosin heavy chain 11
Q59GW6	2	Acetyl-CoA acetyltransferase, cytosolic variant
Q6DD88	2	atlastin-3
Q9P0H9	2	Ribosome binding protein1
Q9P2E9_ISOFORM_1	2	Ribosome binding protein1
Q9Y4F5_ISOFORM_3	2	Protein KIAA0284
Q9Y6C2_CHAIN_0	2	Elastin microfibril interface-located protein 1
A6NKY3	3	obsolete
A8K092	3	ATP synthase subunit alpha
B2R4U6	3	C DNA
P02545_ISOFORM_ADelta10	3	Prelamin
P08572	3	collagen alpha 2 chain
P16401_CHAIN_0	3	Histone H1.5
P46782_CHAIN_1	3	40s ribosomal protein
P62851	3	40s ribosomal protein
B4E335	4	Actin
P62277_CHAIN_0	4	40s ribosomal protein
Q12959_ISOFORM_5	4	disks large homolg
P01857	5	Ig gamma chain region 1C
P05783_CHAIN_0	5	K18
P12111_ISOFORM_2	5	collagen alpha 3 chain

| P35579_ISOFORM_2	5	Myosin 9
B7Z9B0	7	C DNA growth arrest specific protein 8
P02461_CHAIN_0	8	collagen alpha 1 chain
Q53SW3	8	putatative uncharacterised protein
Q5HY54	8	filamin A
P05787_CHAIN_0	10	K8
Q702N8_ISOFORM_B	10	Xin actin-binding repeat-containing protein 1
Q9HAM5	10	C DNA (moderately similar to HYPOXIA-INDUCIBLE FACTOR 1 ALPHA)
Q9NRC6	10	Spectrin beta chain
P12109_CHAIN_0	11	collagen alpha 1 chain
Q14222	12	EEF1A
P58876_CHAIN_0	14	Histone H2B
P68431_CHAIN_0	18	histone H3.1
P50591	27	TNF superfamily lignd 10
P02452_CHAIN_0	37	collagen alpha 1 chain
P08123_CHAIN_0	60	collagen alpha 2 chain
P62805_CHAIN_0	119	histone

Uniprot accessed: 12th June 2013.

Appendix 7 Graphs

Spearman's correlation of faecal butyrate and keratin 18 expression of adenoma tissue.

Spearman's correlation coefficient of faecal butyrate level and keratin expression at surface, base and extent of adenoma colonic crypts (surface = -0.044 [p=0.852], base = 0.130 [p=0.585] and extent = 0.070 [p=0.769]).

Spearman's correlation of faecal butyrate and keratin 18 expression of contralateral tissue.

Spearman's correlation coefficient of faecal butyrate level and keratin expression at surface, base and extent of contralateral colonic crypts (surface = 0.022 [p=0.927], base = -0.193 [p=0.416] and extent = -0.159 [p=0.503]).

Appendix 7 Graphs

Spearman's correlation of faecal butyrate and keratin 18 expression of mid-sigmoid tissue.

Spearman's correlation coefficient of faecal butyrate level and keratin expression at surface, base and extent of mid-sigmoid colonic crypts (surface = -0.0347 [p=0.146], base = -0.308 [p=0.200] and extent = -0.187 [p=0.444]).
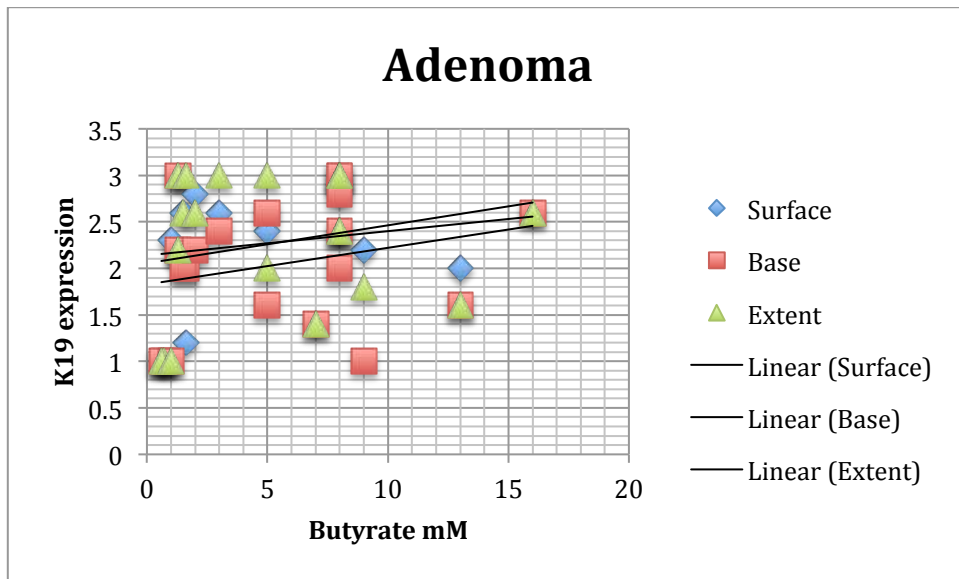
Spearman's correlation of faecal butyrate and keratin 18 expression of normal tissue.
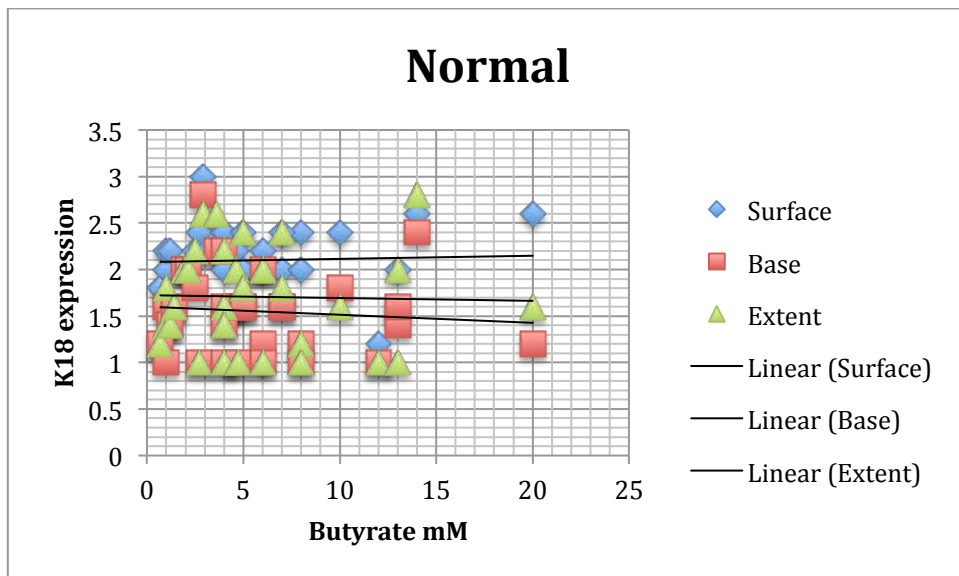
Spearman's correlation coefficient of faecal butyrate level and keratin expression at surface, base and extent of normal colonic crypts (surface = 0.102 [p=0.577], base = -0.090 [p=0.624] and extent = -0.040 [p=0.828]).
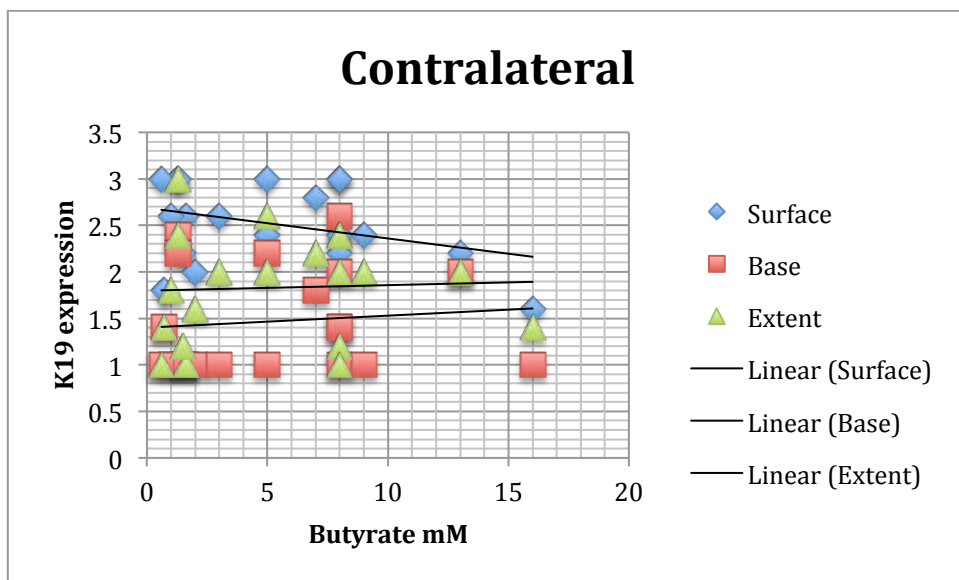
Appendix 7 Graphs

Spearman's correlation of faecal butyrate and keratin 19 expression of adenoma tissue.

Spearman's correlation coefficient of faecal butyrate level and keratin expression at surface, base and extent of adenoma colonic crypts (surface = 0.287 [p=0.219], base = 0.321 [p=0.168] and extent = 0.237 [p=0.314]).
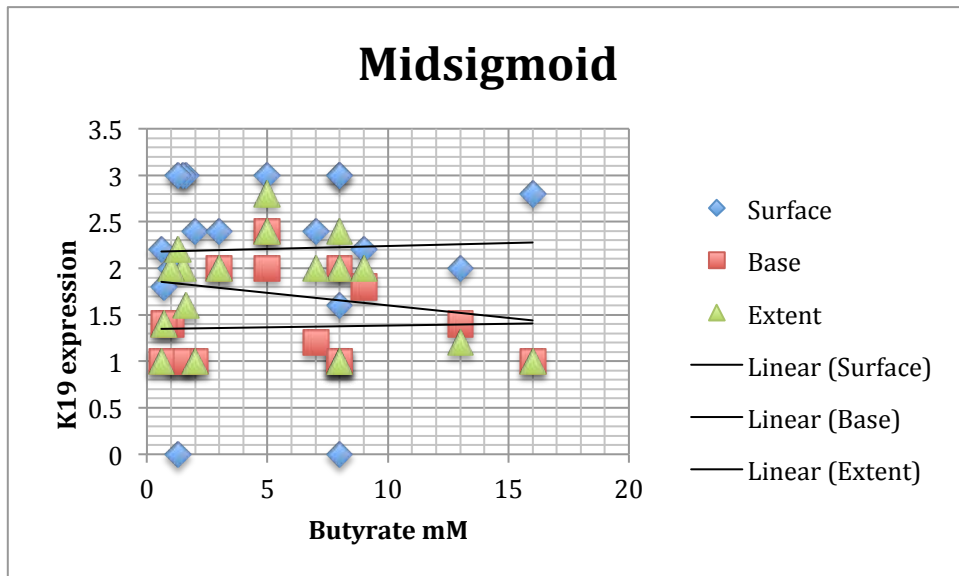
Spearman's correlation of faecal butyrate and keratin 19 expression of contralateral tissue.

Spearman's correlation coefficient of faecal butyrate level and keratin expression at surface, base and extent of contralateral colonic crypts (surface = -0.279 [p=0.234], base = 0.095 [p=0.692] and extent = 0.128 [p=0.591]).
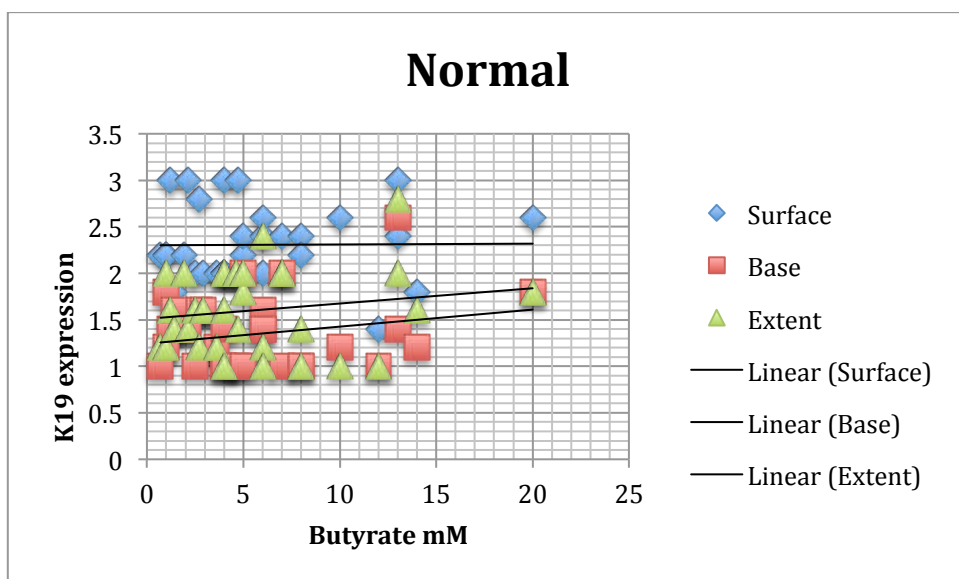
Appendix 7 Graphs

Spearman's correlation of faecal butyrate and keratin 19 expression of mid-sigmoid tissue.

Spearman's correlation coefficient of faecal butyrate level and keratin expression at surface, base and extent of mid-sigmoid colonic crypts (surface = 0.015 [p=0.948], base = 0.107 [p=0.673] and extent = -0.088 [p=0.728]).

Spearman's correlation of faecal butyrate and keratin 19 expression of normal tissue.

Spearman's correlation coefficient of faecal butyrate level and keratin expression at surface, base and extent of mid-sigmoid colonic crypts (surface = 0.062 [p=0.737], base = 0.016 [p=0.929] and extent = 0.090 [p=0.625]).